THE UNIVERSITY
of EDINBURGH

Studies of Macromolecular Trafficking Across Arabidopsis Homografts

Danaé Paultre

Doctor of Philosophy

The University of Edinburgh

2017

Table of contents

Declaration

I declare that the work presented in this thesis is my own. Any contribution from other parties is explicitly acknowledged. It has not been submitted in any previous application for a degree or qualification.

Acknowledgements

I have thoroughly enjoyed my time in Prof. Oparka's Laboratory. I have learnt that enthusiasm and enjoyment could be preserved despite the rigor of scientific research and frequent set-backs. I felt very privileged to contribute to the scientific debate by publishing in peer reviewed journals. This would not have been possible without the great people who helped me during the course of this PhD. I would like to thank my supervisor Prof. Karl Oparka for his guidance and support at both the personal and professional level; Karen Bell for her help in the lab; Dr. Kirsten Knox for her invaluable breadth of knowledge which she has always happily shared; and my family.

Abstract

Micrografting was used to study the restoration of symplasmic transport at the graft union and to examine the long-distance transport of macromolecules between scion and rootstock. New techniques were established, such as correlative imaging and single-cell analysis in microfluidic devices, to study graft development both *in vivo* and *in vitro*. Imaging of *Arabidopsis* homografts showed that a symplasmic domain develops in the callus stele whose function may be to contain the spread of auxin into the surrounding ground tissue. It was demonstrated, also, that recent reports of organelle transfer at the graft union cannot be explained by the formation of secondary plasmodesmata (PD) at the graft interface. While fused calli did not exchange organelles *in vitro*, large aggregates of the SIEVE-ELEMENT OCCLUSION RELATED protein fused to YFP (SEOR-YFP; 112 kDa) were unloaded from mature sieve tubes into living cells of the graft partner *in vivo*, suggesting that vascular remodelling may be a prerequisite for the exchange of organelles at the graft interface.

Fusion proteins expressing organelle-targeting signals were found to translocate across the graft junction, unloading into cell files adjacent to the root protophloem. The phloem mobility of a given fusion protein was assessed using bioinformatic and statistical analysis of publicly available data. The size of a protein and its relative abundance in CCs both emerged as defining factors for subsequent phloem transport. The recipient tissue for phloem-unloaded macromolecules was identified as the phloem-pole pericycle (PPP). This cell layer is required to remove macromolecules from the terminus of the protophloem. Induced callose deposition at the PD that connect protophloem SEs to the PPP caused a restriction in unloading and

a subsequent arrest in root growth. A non-cell autonomous protein of CC origin, NaKR1-1, is proposed to affect the unloading of macromolecules either by increasing the size exclusion limit (SEL) of PD within the PPP or by enabling a build-up in pressure at the protophloem terminus, due to SUC2 activity, thus allowing phloem unloading.

Abbreviations

ARF7	Auxin-response factor 7
At	Arabidopsis thaliana
BAP	6-Benzylaminopurine
CalS	Callose synthase
CC	Companion cell
CHER1	Choline transporter-like 1
CIM	Callus induction media
CmPP16	16-kD *Cucurbita maxima* phloem protein
CT	transit peptide of RecA homolog1
CTER	carboxytetraethylrhodamine
CP	transit peptide of Rubisco subunit 1a
dag	days after grafting
$DIOC_6$	3,3′-dihexyloxacarbocyanine iodide
DNA	Deoxyribonucleic acid
DT	Desmotubule
DTT	Dithiothreitol
EDTA	Ethylenediaminetetraacetic acid
EFP	extrafascicular phloem
eGFP	enhanced green fluorescent protein
EM	Electron microscopy
ER	Endoplasmic reticulum
FABD2	F-actin binding domain 2
FP	Fluorescent protein
FP	Fascicular phloem
FRAP	Fluorescence recovery after photobleaching
FT	FLOWER LOCUS T
FTIP1-1	FT-interacting protein 1
GEO	Gene expression omnibus

GFP	Green fluorescent protein
GSL8	Glucan synthase-like 8
H2B	Histone 2B
HPTS	8-acetoxypyrene-l,3,6, trisulphonic acid, trisodium salt
Hsc70	Heat shock 70 kDa protein 8
HSP70	70-kDa heat shock protein
iCalS	inducible Callose synthase
kDa	kilo Dalton
LB	Lysogeny broth
LD	Long day
LR white	London resin white
MBM	methyl methacrylate/n-butylmethacrylate
MES	2-(*N*-morpholino)ethanesulfonic acid
MGG	Maceration-glycine-glucose media
MP	Movement protein
MP17	Movement protein 17
mRNA	Messenger ribonucleic acid
Mr	relative molecular mass
MS	Murashige and Skoog
NAA	Naphthaleneacetic acid
NaKR1-1	Sodium potassium root defective 1
NCAP	Non-cell autonomous protein
PALM	Photoactivation localisation microscopy
PCBP1	Plasmodesmata-callose-binding protein 1
PCR	Polymerase chain reaction
PD	Plasmodesmata
PDLP1	Plasmodesmata-located protein 1
PDMS	Polydimethylsiloxane
PFS	Planar fenestrated sheet
PIM	Protoplasts-induction media
PIPES	1,4-piperazinediethanesulofonic acid

PM	Plasma membrane
PP1/2	Phloem protein 1/2
PPP	Phloem-pole pericycle cell
PPU	Pore-plasmodesma unit
Pt-spec	Plastid-spectynomicin
RBP	RNA binding protein
RFP	Red fluorescent protein
RM	Regenerative media
RNA	Ribonucleic acid
RTNLB	Reticulon-like protein B
3D-SIM	3D-Structured illumination microscopy
SE	Sieve element
SEL	Size exclusion limit
SEO	Sieve element occlusion
SEOR	Sieve element occlusion related
SER	Sieve element reticulum
sp	short peptide
STmd	sialyl transferase transmembrane domain
SUC2	Sucrose permease 2
SUT	Sucrose transporter family
TEM	Transmission electron microscopy
TMV	Tobacco mosaic virus
TNA	Total nucleic acid
tpFNR	transit peptide of ferredoxin-$NADP^+$ oxidoreductase
tpPC	transit peptide of plastocianin
tRNA	transfer ribonucleic acid
WT	Wild type
YFP	Yellow fluorescent protein

CHAPTER 1: Structure, Origin and Function of Plasmodesmata (PD)

Multicellularity arose several times and independently in most major lineages of eukaryotic organisms (Niklas, 2014). It entails the evolution of traits favouring cell adhesion, cell-cell communication, and cell differentiation (Ruiz-Trillo *et al*., 2007). Cytoplasmic bridges that enable the exchange of molecules between neighbouring cells are therefore a common occurrence amongst multicellular eukaryotes. These take the form of gap junction in animals, septal pores in fungi and PD in higher plants (Bloemendal and Kück, 2013).

It is however the PD of plants that stand out for their key role in sustaining complexity in these multicellular organisms. In higher plants, all cells are directly or indirectly connected by PD. They form the symplasm, continuous protoplasts loosely compartmentalized within the apoplast, the non-living parts of the plant (i.e. cell-walls, xylem and intercellular spaces; Münch, 1930). Symplasmic transport is essential to plant development and tissue differentiation. It relies extensively on PD conductivity between neighbouring or distant cells. PD are therefore structurally plastic and exert a high degree of control over intercellular transport. The molecular events, unfolding at PD to enable transport, are however poorly understood. Crucial questions remain on the rules that apply for selective transport and whether these rules can be generalised to all types of PD found in the plant body.

PD are small pores (~ 20-50 nm wide) found across the cell wall of plant cells where the plasma membrane (PM) of two or more adjacent cells are in contact. They can take multiple forms in plants from simple to complex PD, PD-derived sieve pores and pore-plasmodesma units (PPUs). Each type has a specialised function. While simple and complex PD are more relevant to close-range intercellular transport, sieve pores and PPUs are essential for long distance communication between symplasmic domains that would otherwise be isolated.

1.1. PD structure

1.1.a. Simple PD

Although biomolecular data have accumulated over the years, models describing the detailed structure of PD are still lacking. This is because PD are embedded in the cell wall and are not compliant to the usual isolation or purification protocols that would be necessary to complement precise tomographic techniques. The ultrastructure of PD was first drawn from EM studies in the 1960's (reviewed in Robards, 1971). PD were seen as PM-lined canals with a central rod with the endoplasmic reticulum (ER) emerging on either side (see Figure 1.1.A). Globular subunits could be observed in transverse sections of PD which were thought to be part of the central proteinaceous tubule (see Figure 1.1.B). Due to its similarity to a microtubule, this central rod was coined the desmotubule (DT), despite suggestions that this electron-dense area could be a strand of ER (Robards, 1968). The nature of the DT, either proteinaceous or phospholipidic, was long argued due to the unstable physical restriction that would be required on a bilayered membrane to fit in the PD channel. However, in recent years, studies on membrane curvature proved that some

proteins can shape and maintain membranes beyond their instability threshold (reviewed in Tilsner *et al.*, 2011). In particular, Yop1p and reticulons, both integral ER proteins, *in vitro* can induce the formation of tubules with a diameter as small as the one found for the DT, ~15-17 nm (Hu *et al.*, 2008). Moreover, dyes and/or peptide markers, when loaded on the membrane or in the lumen of the ER, can be transported without interruption across PD. The DT is now thought to be composed of 'appressed' ER with ~3nm subunits embedded within both the ER inner and outer leaflet (Lucas *et al.*, 1993).

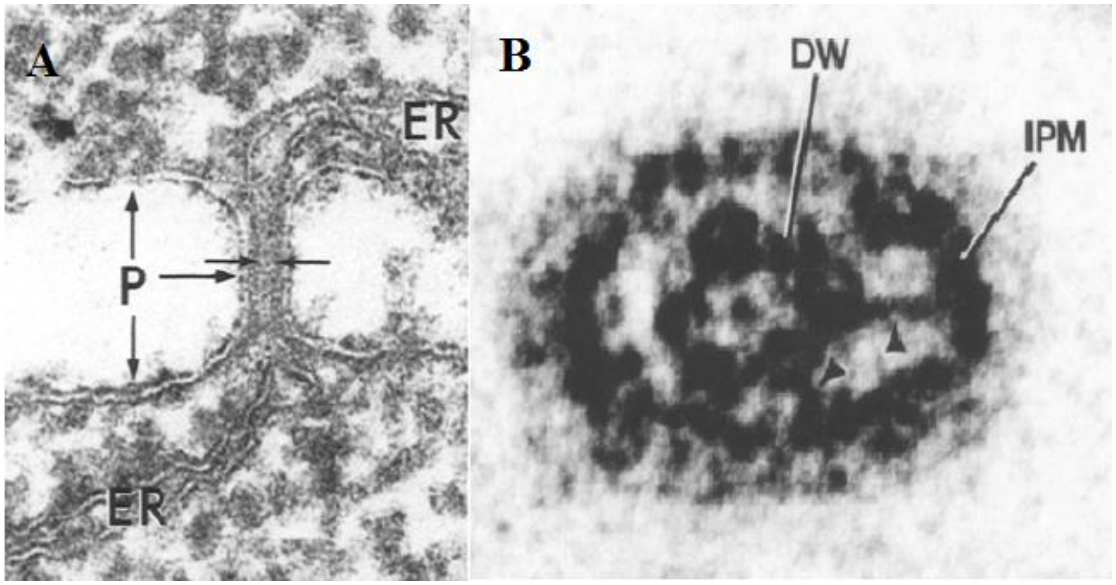

Figure 1: EM pictures showing **A.** Endoplasmic reticulum (ER) emerging from either side of PD and continuity of plasma membrane (P) in a longitudinal section of *Azolla* roots. Source: Overall et al.,1982.

B. Transverse view of PD between phloem parenchyma cells of *Nicotiana tabacum*, showing spoke-like extensions (arrowheads) between the desmotubule wall (DW) and the inner leaflet of the plasma membrane (PM). Source: Ding et al., 1992.

The composition of these globular subunits is still unknown. Their cytosolic domain creates the ~2.5-nm diameter microchannels observed in the cytoplasmic

sleeve (i.e. the electron-lucent space between the PM and the DT) by interacting with spokes and other globular particles coming from the inner leaflet of the PM (Ding *et al.*, 1992). Actin, myosin-like proteins and myosin VIII, which have all been localised by antibodies in the PD channel (White *et al.*, 1994; Radford and White, 1998; Reichelt *et al.*, 1999), are thought to be associated with these globular subunits. It is hypothesised that spiralling actin filaments along the DT with the action of myosin could enable the regulation of macromolecular traffic in two ways; either by narrowing the cytoplasmic sleeve, bringing the outer leaflet of the PM closer to the inner leaflet of the DT, or by offering a track for cargo transport along the length of PD. Centrin nanofilaments have also been located at the 'neck' of PD (Blackman *et al.*, 1999). PD channels have a constriction at either end forming a 'neck' that can be partially obstructed by the ER. Contractile proteins such as centrin could bring the ER membrane closer to the edge of PD closing their entrance (Overall and Blackman, 1996) (see Figure 1.2).

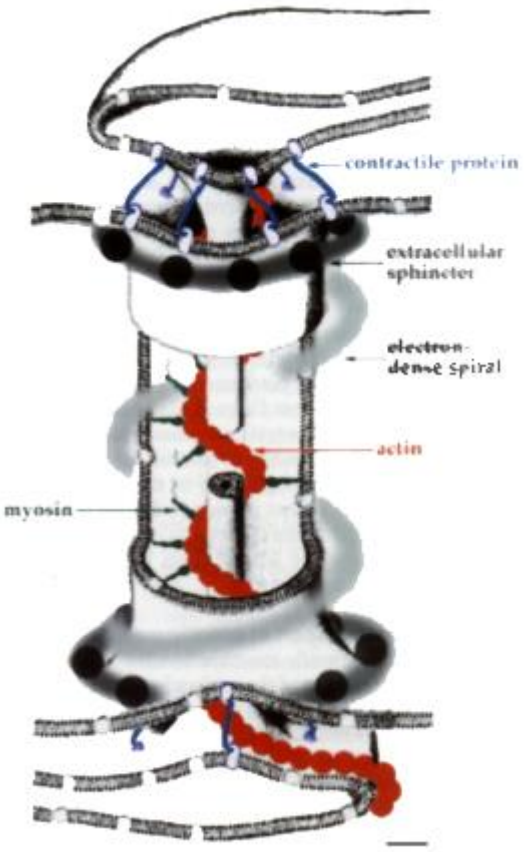

Figure 1.2: Model of a plasmodesma. Actin and myosin, which are helically arranged around the desmotubule, connect the plasma membrane to the desmotubule. Contractile proteins (possibly centrin) link the plasma membrane to the endoplasmic reticulum (ER) via anchoring proteins at the 'neck' of the plasmodesma. These anchoring proteins within the membrane may have a close association with the putative extracellular sphincter. These extracellular structures may provide anchoring points to the wall for the components of the plasmodesma. The extracellular sphincters at the neck and extracellular spiral could also be involved in modulating the outer dimensions of the plasmodesma. Transport of specific macromolecules could occur via the actin-myosin motile system or via a dilated ER.. The size exclusion limit for passive transport between cells would depend on the dimensions of the gap between the desmotubule and the plasma membrane as determined by contractile proteins, or by an *as* yet unidentified 'molecular sieve'. Scale: 10 nm. Source: Overall and Blackman, 1996.

The neck regions are caused by sphincter particles and 1-3-β glucan (callose) present in the extracellular space. The deposition of callose normally occurs at PD necks during development but it can also be stimulated by physical and physiological stresses that reduce the neck aperture and limit PD flux. The deposition of callose is believed to be controlled by diverse proteins (reviewed in Maule, 2008). So far, PD-callose-binding protein 1 (PCBP1) is the only protein that was found to locate exclusively at PD necks and influence callose accumulation (Simpson *et al.*, 2009). Other proteins were found to affect callose deposition, such as 1-3-β-glucanase and PD-located protein 1 (PDLP1), but although both GFP-tagged proteins locate to PD,

their exact position in PD has yet to be confirmed (Levy *et al.*, 2007; Thomas *et al.*, 2008). The emergence of super-resolution imaging techniques such as 3D-Structured Illumination Microscopy (SIM) or Photoactivation Localisation Microscopy (PALM) is expected to address this issue (Brown *et al*., 2010). These techniques work by limiting the interference of diffraction, allowing the resolution of structures in the nm range. Fitzgibbon *et al.* (2010) were able to resolve immuno-stained callose and GFP-tagged viral movement proteins, respectively, at the neck regions or in the central cavity of PD using 3D-SIM. This approach, if extended on most of the proteins identified in the PD-proteome (Fernandez-Calvino *et al*., 2011), could give a much finer picture of PD structure.

Biogenesis of simple PD

PD can be categorised into primary PD and secondary PD depending on how they form. Primary PD are laid down at the cell plate during cytokinesis, while secondary PD arise completely *de novo* across existing cell walls.

Formation of primary PD at cytokinesis

Early EM studies showed that ER strands could be 'entrapped' in the forming cell plate at cytokinesis (Hepler, 1982). This was proposed to initiate the synthesis of simple PD across the cell wall. Seguí-Simarro *et al.* (2004) gave a detailed description of cell plate formation and its association with the ER using electron tomography of high-pressure frozen/freeze-substituted samples. They observed that the ER was loosely associated with the phragmoplast, a precursor to the cell plate that is composed of microtubules, microfilaments, Golgi vesicles and ER. ER strands became

increasingly present across the forming cell plate once the phragmoplast matured to a planar fenestrated sheet (PFS), which occurs after callose synthesis in the tubular-vesicular cell wall (see Figure 1.3.A and B). They also noticed linkage between the ER and the newly formed PM (see Figure 1.3.C).

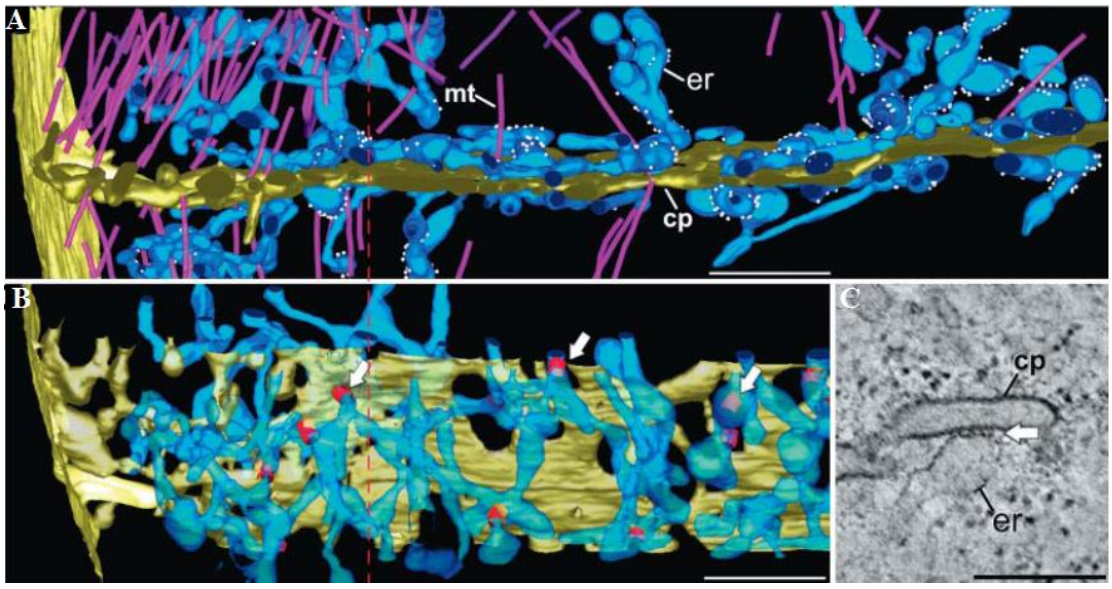

Figure 1.3: A. and B. Association of ER membranes with peripheral growth zone (PGZ) and PFS cell plate regions. Dashed line marks the transition between them.(B) Side view. Many cytoplasmic ER tubules are seen intermingled with MTs over the PGZ region (left side), but little direct interaction of ER tubules with cell plate (cp) membranes is observed. By contrast, in the PFS zone (right), numerous ER tubules appear closely associated with the cell plate. (B) 45° tilt view of (A). Scale: 500 nm

C. Detail of a contact site (arrow) between an ER tubule and a PFS-type cell plate (cp). Note the membrane-bridging elements. Scale: 200 nm. Source: Seguí-Simarro *et al*., 2004.

In light of this research and other studies of ER dynamics, Tilsner *et al.* (2011) have suggested that ER 'entrapment' is not random but actively regulated by the cellular machinery. It would involve membrane-curving proteins to insert narrow ER tubules in the PFS. The plant homologs of reticulons (RTNLBs) are likely to carry out this task. Indeed, Knox *et al.* (2015) showed that some of the Fluorescent Protein (FP)-RTNLBs, when expressed under the 35S promoter, were recruited at the cell plate of

Arabidopsis root cells during cytokinesis. The molecular events that lead to mature simple PD from 'entrapped' ER are however unknown.

Formation of secondary plasmodesmata post-cytokinesis

Secondary PD have been the subject of much debate because their structure cannot be distinguished from those of primary PD (Ehlers and Kollmann, 2001). Although most reports agree that secondary PD should occur, either to compensate for the dilution of primary PD during cell wall expansion, or to bridge the symplast separation of non-division walls, meticulous developmental analyses are needed to prove their existence.

Until a study by Seagull (1983), the frequency of PD per unit wall area was thought to decline during cell elongation, suggesting that new PD were not added into the growing cell wall. This was based on results obtained from cells of the maize root cap (Juniper and Barlow, 1969) and *Azolla* roots (Gunning, 1978), which both have a limited lifespan. However, in expanding walls of root cells exhibiting indeterminate growth, Seagull (1983) showed that the number of PD and their frequency could increase. His observations, on paired PD and the appearance of pit fields (i.e. pectin-rich areas of the wall showing a high number of PD), led him to the conclusion that secondary PD were inserted in close proximity to pre-existing PD, eventually forming pit fields (see Figure 6). This was confirmed by the results of Faulkner *et al.* (2008) who looked at the distribution of PD over time in the basal wall of trichomes using a GFP-marker and immuno-labelling. They proposed that secondary PD originate from the twinning of simple PD. They described how new PD could arise from the insertion of an ER strand in the cell wall using simple PD as a template or nucleation site (see

Figure 1.4). It is not known however if this ‘fission’ model of secondary PD is the only one applicable in division walls.

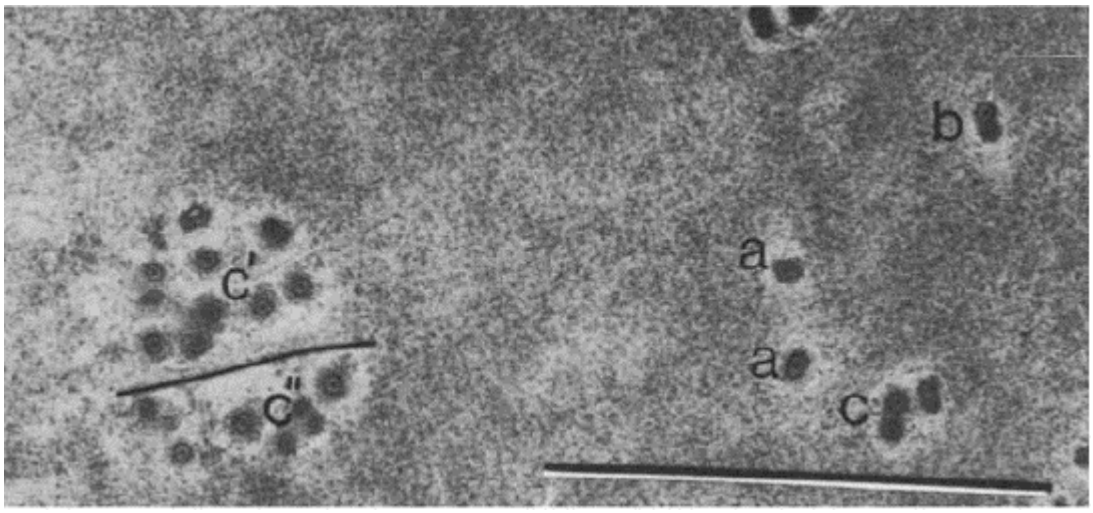

Figure 1.4: Section which grazes through the radial longitudinal cell wall and cortical cytoplasm of an isodiametric, radish root cell. Plasmodesmata can be seen individually (a), in pairs (b), or in clusters (c) which form pit-field. Source: Seagull, 1983.

An alternative is that cells have the ability to insert secondary PD entirely *de novo*, presumably either from the fusion of two half PD forming on either side of the cell wall, or from the insertion of an ER strand on one side across the wall (Jones, 1976). This could involve an altogether different signalling mechanism to coordinate cell wall perforation and eventually PD fusion (Jones, 1976). Most of the studies that try to prove the existence of secondary PD in division walls fail to make that distinction between the ‘fission’ model and the ‘fusion’ model. For instance, Ormenese *et al.* (2006), when looking at the shoot apical meristem, showed that cytokinin treatment increased the frequency of simple PD per unit wall area. They inferred that these PD were of secondary origin because ‘old’ periclinal walls, that had formed prior to

treatment, were also found with more PD. Their data however do not indicate if PD were then randomly spaced or in discrete clusters. To show that PD could form entirely *de novo*, studies have therefore focused on the formation of secondary PD between non-division walls of ontogenically-unrelated cells, which by definition lack primary PD.

During plant development, some tissues can undergo postgenital fusions and form secondary PD. A well-known example occurs during floral development when carpel primordia coalesce to form the gynoecium. In *Catharanthus roseus*, diffusible molecules (morphogens) were shown to be exchanged when growing carpel primordia begin to touch. This is shortly followed by the re-differentiation of the epidermal cells in the contact zone into parenchymatous cells. Secondary PD were proposed to enable the symplasmic transport of these morphogens because functional secondary PD, both simple and branched, were found across the non-division wall before any detectable epidermal re-differentiaton (Van der Schoot *et al.,* 1995). So far, no intermediate phases of PD development have been recognised in non-division walls of the plant, preventing further description of the formation of *de novo* secondary PD. This has however been achieved in interspecies studies, in particular those looking at the graft interface (covered in Chapter 3 of this thesis).

1.1.b. Complex plasmodesmata

The overall structure of complex PD is the same as for simple PD; a PM-lined canal with a central DT and necks at the apertures. It differs by the presence of a central cavity in the region of the middle lamella and branching arms. Faulkner *et al.* (2008) suggested that complex PD emerge from either the fission of simple PD or the *de novo*

DT insertion at a PD site (see Figure 1.4.C and B). They would not occur entirely *de novo*. This was confirmed by Fitzgibbon *et al.* (2013) who observed that, when fluorescent markers specific to simple and complex PD were simultaneously used, the appearance of many GFP-labelled complex PD co-localised with existing RFP-labelled simple PD. The occurrence of complex PD should therefore increase during normal plant development (Fitzgibbon *et al*., 2013; Oparka *et al*., 1999). In particular, complex PD are more apparent in leaves after the sink-source transition. Looking at this developmental stage, Kraner *et al.* (2017) identified a mutant lacking complex PD in developed *Arabidopsis* leaves. The mutation was found to affect a choline transporter family protein (CHER1). Interestingly, the formation of secondary PD, as well as the maturation of simple to complex PD, were impaired in the *cher1-4* mutants. Because choline is a precursor for the synthesis of phosphatidylcholine, the main phospholipids in eukaryotic membranes, the authors suggested that lipid remodelling might be necessary for both processes. This might provide some of the first molecular descriptions for these events.

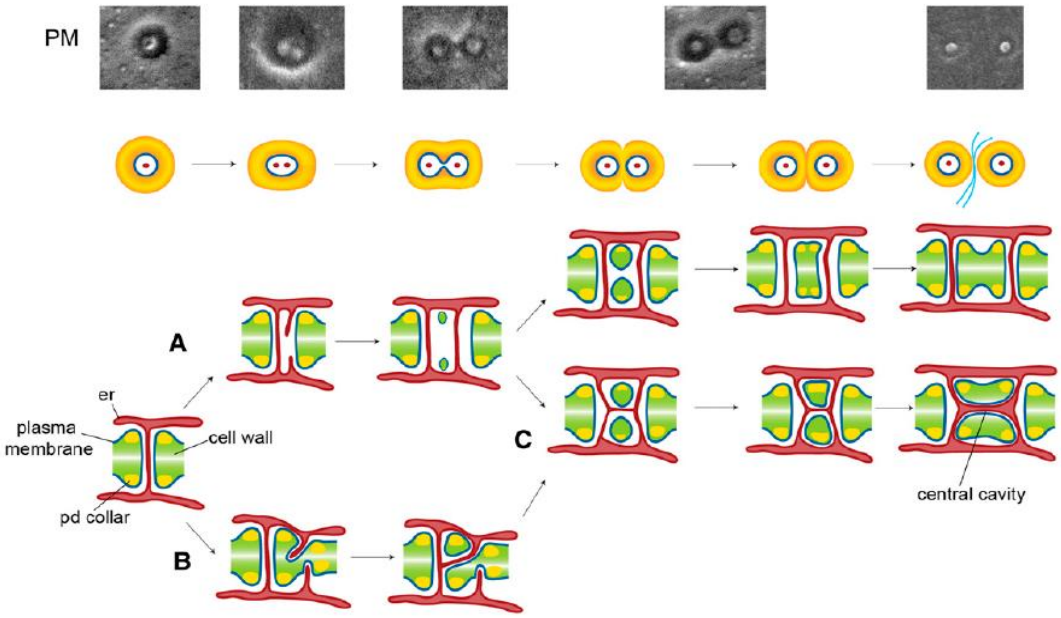

Figure 1.4: Models of Secondary PD Formation. The top images show the PM fracture plane for putative stages in the formation of secondary PD pores.

A. Fission model. The diagram depicts the insertion of a second desmotubule into an elongated PD pore, creating two desmotubules within a shared pore orifice. With increasing wall extension, the new PD becomes separated from the original by increasing deposition of new wall microfibrils between the two pores. Central cavities may or may not form between the two pores. **B.** De novo pore formation. The new PD pore is inserted immediately adjacent to the template pore by localised erosion of the cell wall. Two new desmotubules, each originating from a different cell, merge in the middle lamella region of the wall to form a complex structure. **C.** Branched PD formation may result from either the fission model (A) or de novo pore formation (B). Twinned pores may or may not remain connected by ER in the middle lamella region of wall. Central cavities develop between interconnected PD as new pores are being formed. Source: Faulkner *et al*., 2008.

1.2. Role of PD in local transport and development

PD allow intercellular continuity, or symplasm formation, in the plant and have a function analogous to gap junctions in animals. They were originally thought only to facilitate the passive transport of nutrients and growth regulators. However, the

discovery of non-cell autonomous macromolecules (either proteins or RNA), that travel via PD, revealed PD transport to be a highly regulated process necessary for adequate cell-cell communication during the life of the plant (Zambryski and Crawford, 2000).

The transport of molecules is set by the size exclusion limit (SEL) of the PD pores (i.e. the space available in the cytoplasmic sleeve either for cytosolic or membrane-mediated transport). PD were proposed to exist in four dynamic states: blocked, rested, dilated and gated by non-cell autonomous proteins (NCAPs) (i.e. proteins that act away from their site of synthesis) (see Figure1.5) (Lucas *et al.*, 2009).

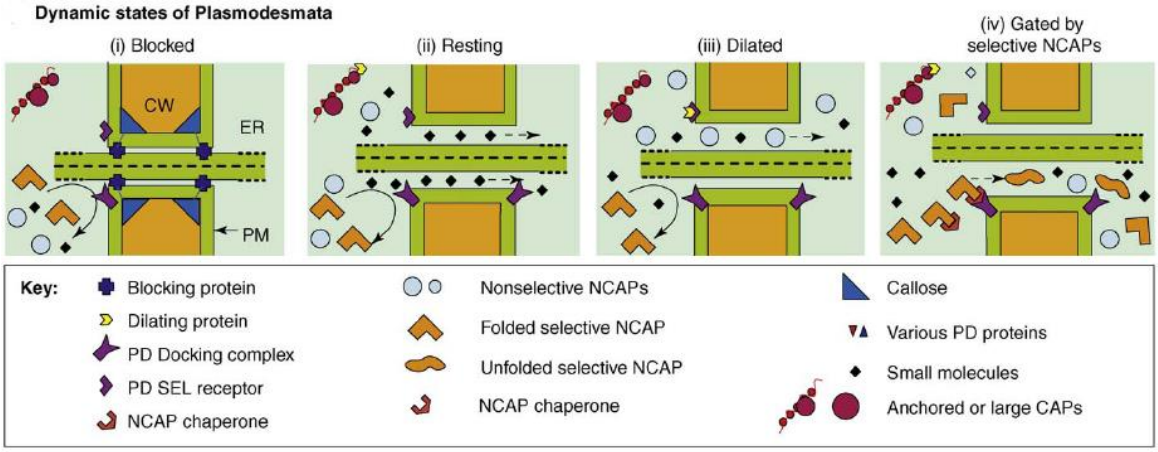

Figure 1.5: Functional states of PD. (i) Blocked state: symplasmic isolation of cells can be achieved by occlusion of PD microchannels by PD blocking proteins and/or upregulation of callose deposition at the neck region, which constricts the cytoplasmic sleeve. (ii) Resting state: PD microchannels have an SEL of <1 kDa, permitting only small molecules to diffuse to neighbouring cells. Regarding the movement of non-cell autonomous proteins (NCAPs), two mechanisms appear to operate. (iii) General PD dilation might take place through removal of callose or by the binding of a protein to a microchannel-dilating/SEL receptor. The ability to diffuse through the PD would be governed by the physical dimensions of protein and the extent to which the microchannel was dilated. (iv) Selective trafficking of NCAPs involves the binding of an NCAP-chaperone complex to a PD docking complex. This interaction causes gating of the PD microchannel, with a resultant increase in SEL. During the passage of the NCAP, other molecules that are free to diffuse into the dilated microchannel can pass into the cytoplasm of the neighboring cell. Exit of the NCAP allows the microchannel to relax back to the resting state. Source: Lucas *et al.*, 2009.

Rested PD represent PD with a basal SEL. This basal SEL determines the passive diffusion or non-targeted transport of molecules. It tends to be < 1 kDa which is large enough to let small solutes, such as micronutrients, photo-assimilates and growth factors, pass through. However, different tissues can display different SELs depending on their nature or developmental stage. This is crucial for the creation of symplasmic boundaries that contribute to the fine-tuning of cell differentiation, plant development and environmental responses (Oparka and Roberts, 2001). Guard cells, for instance, can fully differentiate from epidermal leaf cells once their PD have been truncated (Palevitz and Hepler, 1985). During the development of *Arabidopsis thaliana* embryos (i.e. from the heart stage to the torpedo stage), a reduction in the SEL of PD was also shown to be responsible for the formation of four symplasmic subdomains: the cotyledons, the shoot apical meristem, the hypocotyl and the root, which are necessary for plant viability (Kim *et al.*, 2005). It is not known whether these subdomains are a consequence of PD dilation or an increase in PD SEL ('gating'). The formation of lateral roots and the tropic response of hypocotyls, which are both controlled by auxin, seem also to depend on the callose-mediated permeability of PD. This is because PD closure can facilitate the formation of local auxin gradients, necessary for signalling. Auxin is indeed a small solute, even smaller than sucrose, (~200 Da) that can therefore freely diffuse through PD. When Han *et al.* (2014) silenced mRNA transcripts of Glucan Synthase Like 8, an enzyme responsible for callose deposition at PD, they effectively prevented the photo- and gravitropism of the hypocotyl in *Arabidopsis*. Moreover, they showed that the expression of GLS8 was directly dependent on the auxin responsive pathway via ARF7. Similarly, in roots, extensive callose deposition was shown to accompany the emergence of lateral roots,

a phenomenon known to occur at sites of high auxin concentration (Benitez-Alfonso *et al*., 2013).

The gating of PD was first proved by studying viral infection of Tobacco Mosaic Virus (TMV) in which the expression of its 30-kD movement protein (MP) in leaves, which normally display a SEL < 1kD, was shown to enable traffic of dextran, a 10-kD glucan (Oparka et al, 1997). Viruses such as TMV that take advantage of the symplasm to spread systemically possess MPs that facilitate transport of the viral genome through PD. This is achieved by transiently increasing the SEL of PD in a way that is not fully understood. Since the study by Wolf *et al.* (1989), numerous plant proteins, important for local cell-fate determination or long-range signalling, were also shown to gate PD. These include transcription factors (especially homeobox proteins), chaperones (e.g. HSP70 from phloem exudate), mRNA trafficking proteins (e.g. *Curcubita maxima* CmPP16; reviewed in Oparka, 2004).

Other mechanisms exist to prevent the free diffusion of macromolecules without interfering with the PD SEL. Subcellular targeting and sequestration, also referred to as 'nuclear trapping', can both prevent leaking of proteins into neighbouring cells (Brunkard *et al*., 2015). Indeed, proteins, that have a stoke radius smaller than the observed PD SEL, can still be retained in a cell if they possess a strong signal or transit peptide. In plant cells, there is a dual competition between passive diffusion through PD and active targeting to subcellular compartments (covered in Chapter 4 of this thesis).

1.3. Specialised PD for long distance transport

As the size of land plants increased over time, specialised tissues evolved to facilitate the transport of nutrients, solutes and macromolecules between otherwise separated symplasmic domains. The xylem vessels, as part of the apoplast, form hollow tubes that mediate the transport of water and some nutrients along the transpiration stream, effectively connecting the root to the shoot. It does not however support movement of organic nutrients as some originally believed (reviewed in Crafts, 1931). The transport of organic material did indeed puzzle scientists for a long time. Phloem tissue was first described by Hartig (1854) who also recognised its primordial role in food transport. He proposed that organic material could symplasmically diffuse in the phloem and could be rapidly conducted by cytoplasmic streaming. This was long thought to provide the sufficient acceleration to account for fast rates of growth and food storage in the plant. This idea prevailed until Münch revolutionised the field in 1930 with his dual osmotic system. In his artificial set up, Münch showed that mass flow occurred along a tube connecting two osmometer cells, which had different concentration of solutes, after submersion in pure water. He extended his observations to plants describing how translocation of sugars could be maintained over long distances from photosynthesising tissue (i.e. source tissue with high sugar concentration) to consuming or storing tissues (sink tissue with low sugar concentration). Although debates still persist as to how a gradient pressure could be maintain over distances as large as the one found in trees (i.e. over 87 m for some giant sequoia), it is now a well-accepted model whereby solutes and other macromolecules translocate by mass flow in the sieve tube in a source to sink fashion (Knoblauch and Peters, 2010; Ross-Elliot *et al.*, 2017).

To accommodate mass flow, phloem-specific PD had to evolve in land plants. The highest degree of specialization is found in Angiosperms with the presence of sieve plates at the interface of sieve-tube members, and pore-PD units (PPUs) that connect companion cells (CC) to sieve elements (SE) (van Bel and Knoblauch, 2000).

1.3.a. Sieve pores

During SE maturation, protophloem cells join the sieve tube system after undergoing a so-called 'programmed cell semi-death' (van Bel, 2003). Their nucleus is degraded, their vacuolar membrane is lost as well as cytoskeletal elements, ribosomes, Golgi bodies and most of their plastids. What remains is a parietal layer of stacked or fenestrated sieve element reticulum (SER), shielding a residue of cytoplasm from the flowing phloem sap, a few dilated mitochondria and phloem-specific plastids. A drastic transformation of PD at the SE/SE interface also occurs during the latest stage of sieve tube development. Initially, callose is deposited at their neck occluding the main channel. It is then followed by the decomposition of their internal structure and, finally callose degradation, turning these simple PD into empty pores, with the presence of SER strands in some (Esau and Torsch, 1985; Fitzgibbon *et al*., 2010) (see Figure 1.6). These pores, together forming a perforated sieve plate, vary greatly in size and number depending on the plant species. They typically range between ~200-400 nm, but can go up to 1 µm in some cucurbits (Sjölund, 1997). While this facilitates mass flow of macromolecules between sieve element members, it limits the control on macromolecular transport usually displayed by PD (Ross-Elliott *et al*., 2017).

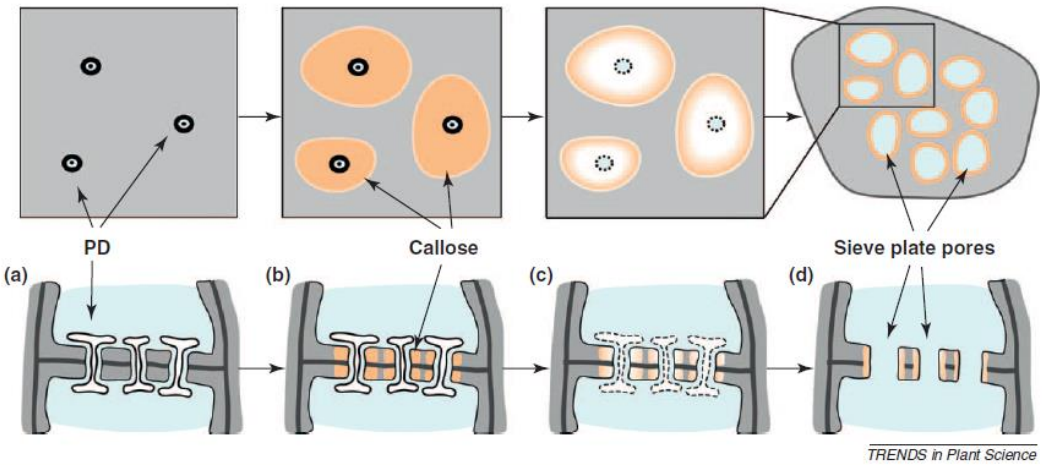

Figure 1.6: Transient callose accumulation during sieve plate pore formation. A simplified model depicting development of sieve plates. (a) Plasmodesmata (PD) at the future pore sites. (b) A massive callose deposition occurs at the plasmodesmata, which is followed by (c) degeneration of appressed ER and widening of the plasmodesmal cytoplasmic space. Callose plugs are degraded, and open pores with residual callose are formed in the mature sieve plate (d). Source: Lee and Lu, 2011.

The sealing of sieve pores is thought to be essential to prevent extensive sap loss after damage to sieve tubes. Initially, the first TEM images of sieve element consistently reported what looked like occluded sieve plates (Esau and Thorsch, 1985). Callose deposition at the neck region, as well as structural phloem-specific proteins (P-proteins), were apparent and thought to cause pore obstruction. It was argued that this reflected a wound response, probably induced by the invasive methods of EM processing. Careful preparations of plant tissue led indeed to the observation of un-occluded pores (Esau and Thorsch, 1985).

P-proteins were first designated as slime plugs (Hartig, 1854). They have since been described as amorphous, crystalline, filamentous, tubular and fibrillary proteins. Some form P-proteins bodies located on the parietal layer of the sieve element. They

are thought to be released in the main streamflow after a loss of pressure during damage. The most studied P-proteins are found in papilionoid legumes and in cucurbits. In Papilionoid legumes, sieve tubes contain non-dispersive proteins called forisomes which are encoded by the Sieve Element Occlusion (SEO) gene family (Knoblauch and Peters, 2010). Although still a matter of debate, forisomes are believed to occlude sieve pores due to their ability to change from a low volume state to a higher one upon Ca^{2+} exposure (Froelich *et al*., 2011; Knoblauch *et al*., 2014). Homologs of the forisomes have been found in non-papilinoids and are regrouped in the sieve element occlusion related (SEOR) gene family. In Arabidopsis, AtSEOR1 and AtSEOR2 are expressed in nucleated maturing protophloem. They are both necessary to the formation of filaments and agglomerations in SEs (Jekat *et al*., 2013). In cucurbits, Phloem Protein 1 (PP1), a 96-kD filamentous proteins, and PP2, a 48-kD dimeric lectin covalently bind to form filaments. These were initially thought to static in SE. However, their mobility was clearly demonstrated by heterografting (Golecki *et al*., 1998; Golecki *et al*., 1999). They are originally made in CC and translocated in SE through PPUs to distal tissue (Golecki *et al.*, 1999).

1.3.b. Pore-Plasmodesma Units (PPUs)

The functional core unit of the phloem in angiosperms is the contact made between SEs and their adjacent CCs (Oparka and Turgeon, 1999; van Bel and Knoblauch, 2000). Resulting from the longitudinal division of the same procambial cell, CC and SE maintain an intimate connection throughout development (Esau and Thorsch, 1985). While CC are not necessary for the proper differentiation of SE, they act as nurturing cells, helping enucleate SE to reach a longer lifespan. CC provide

replacement proteins and other metabolites to mature SE which have lost their own production capacity. Thus, as opposed to SE, CC tend to display a dense protoplasm rich in mitochondria, an indication of their high metabolic rate (see Figure 1.7.A). The exchange of material between these two cell types occurs through PPUs. These develop at the CC/SE interface from simple PD. They take the shape of a single pore, emerging from the SE, and branching passed the middle lamella into the thickened wall of the CC. All branches have a DT which coalesce in the central cavity emerging as a single ER strand in the main pore (see Figure 1.7.27 and 28) (Oparka and Turgeon, 1999).

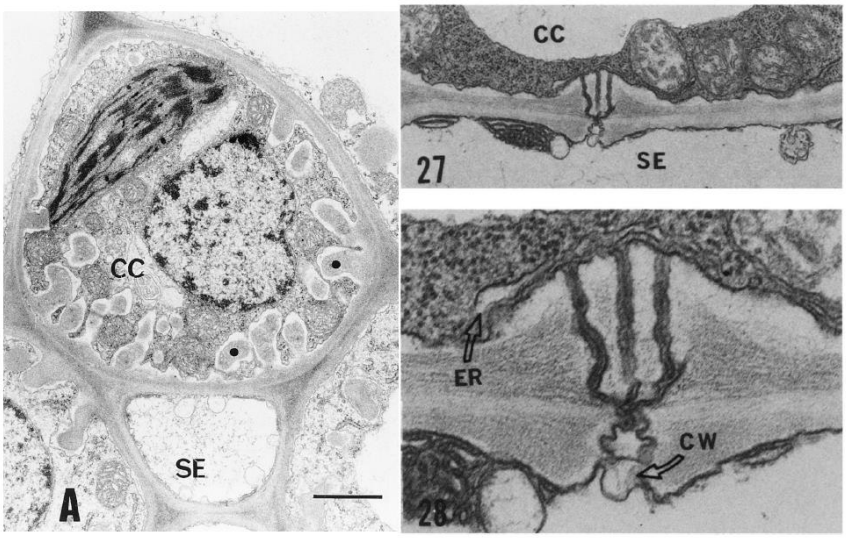

Figure 1.7: A. CC-SE complex displaying a dense cytoplasm in CC as opposed to an apparently empty lumen in SE. 27. PPU across the cell wall between CC and SE showing a branched structure joining to a single pore. 28. close up to 27. CC: companion cell, SE: sieve element, CW: cell wall. Source: A. Oparka and Turgeon, 1999; 27.28. Esau and Thorsch, 1985.

The functional continuity of the ER between CC and SE was established by Martens *et al.* (2006) using an intercellular Fluorescence Recovery After Photobleaching (FRAP) experiment. After photobleaching SEs, they showed the rapid redistribution of the lipophilic dye, $DIOC_6$, from CC on the SER, indicating a high degree of ER coupling between these cells. They suggested that the ER could therefore be a path of transport for proteins destined for the SE organelles and PM. Moreover, ions might freely diffuse through the continuous ER lumen. In which case, CC might act as reservoir for ions such as Ca^{2+}, known to be present in SER. This might enable the propagation and maintenance of calcium waves necessary for long-distance signalling, wound and pathogen responses along the sieve tube (Furch *et al*., 2009).

Macromolecules and solutes such as sugars, which fall below the PPUs SEL, can also diffuse freely through the cytoplasmic sleeve. This path is involved in the loading of sucrose in SE which is essential to maintain a pressurised system. Sucrose can reach the SE-CC complex from either the extracellular space or the symplasm with the CC acting as the point of entry (van Bel, 2003). In apoplasmic loading, sucrose is actively taken up by proton symporters of the SUT gene family which are mainly embedded in the plasma membrane of the CC (Lalonde *et al*., 2004). In symplasmic loading, sucrose diffuses from the mesophyll via bundle sheath and phloem parenchyma into CC, which contain most of the PD connections of the SE/CC complex to neighbouring tissue. Soluble GFP-fusion proteins as large as 67 kDa were found to cross PPUs (Stadler *et al*., 2005b), suggesting that PPUs have an abnormally large SEL when compared to other PD. A large variety of macromolecules have been found in SE ranging from RNA molecules to proteins. It is not clear however if these are actively targeted and translocated at PPU for specific long-distance signalling

functions (covered in Chapter 4 of this thesis) or whether they enter the SE by default (Stadler *et al*., 2005b). Moreover, the final destination of these macromolecules in sink tissue has not yet been elucidated (covered in Chapter 5 of this thesis).

This thesis aims at addressing these issues by using grafting, firstly as a case study to examine the formation of symplasmic continuity between stock and scion, and secondly as a tool to unravel some of the rules that apply to long distance transport. I will explore the nature of the materials exchanged at the graft interface during symplasm recovery. Techniques such as correlative imaging and microfluidics will be presented as new tools to investigate the movement of macromolecules across secondary PD, as well as the factors that influence the formation of secondary PD. This will lead onto the description of a novel specific domain in plant roots that has previously not been described.

CHAPTER 2: Materials and Methods

2.1. Plant material and growth conditions

The transgenic lines of *Arabidopsis thaliana* and *Nicotiana tabacum* that have been used during this project are listed in Table 1.

Table 2.1: List of lines used in this study

Arabidopsis thaliana					
Transgene	**Reference**	**Transgene**	**Reference**	**Transgene**	**Reference**
35S:H2B-RFP	Federici et al., 2012	*35S*:CT-GFP	Köhler et al, 1997	*35S*:STmd-GFP	Boevink et al., 1998
35S:mCherry-LTi6b	Federici et al., 2012	*35S*:CP-eGFP	Unpublished	*AtSUC2*:FT-GFP *ft-7*	Corbesier et al., 2007
35S:eGFP-LTi6b	Kurup et al., 2005	*35S*:tpPC-eGFP	Marques et al, 2003	*AtSUC2*:FT-GFP *ftip1-1*	Liu *et al*., 2012
35S:MP17-GFP	Hofius et al., 2011	*35S*:A5-eGFP	Cutler et al, 2000	*AtSUC2*:Ubiquitin-GFP	Stadler et al., 2005
35S:tpFNR-GFP	Marques et al, 2003	*35S*:FABD2-GFP	Ketelaar et al, 2004	*pcals8*:icals3m	Ross-Elliott et al. 2016
AtSUC2:GFP	Imlau et al., 1999	*35S*:H2B-YFP	Federici et al., 2012	*35S*:spRFP-AVY	Hunter *et al*., 2007
AtSEOR:SEOR-YFP	Froelich et al., 2011	*35S*:HDEL-GFP	Haseloff et al., 1997	*35S*:RTNLB6-GFP	Knox et al., 2015
pDR5:ER-GFP	Friml et al., 2003				

Nicotiana tabacum	
Transgene	**Reference**
35S: TMV-30K-GFP	Reichel and Beachy, 2000
Pt-spec:GFP	Stegemann and Bock, 2009

The *Arabidopsis* mutants *cals6, cals7, cals8, cals7/8* (provided by Prof. Helariutta) and *nakr1-1* (Tian *et al*., 2010) were also used.

The seeds were surface sterilized in an 8% bleach and 1% TWEEN solution for 10 min. After 5 washes in distilled water, the seeds were plated on Petri dishes containing Murashige and Skoog (MS) basal salts, 0.3% sucrose (except where stated otherwise), 1.2% agar, pH 5.8 and stratified in darkness for 2-3 days at 4°C. Seedlings were then grown with plates oriented vertically at 23°C under Long Days (LD) length light (18h light-6h dark cycle).

Seeds sown directly on soil were kept in controlled climate chambers (21°C, 9h/day light, 50% humidity) and bottom watered twice a week.

2.2. Cross

Flowering 6-weeks old plants of MP17-GFP and LTi6b-mCherry were crossed. The flowers of LTi6B-mCherry were emasculated and their stigma rubbed with ripe stamen of MP17-GFP. The procedure was repeated 24h later. The resulting seeds were sterilized and sown on Petri Dishes as described previously. The plants with double fluorescence were selected.

2.3. Cloning

For the construction of the *AtSUC2* promoter - tpFNR-eGFP, 938 bp of *AtSUC2* promoter was PCR-amplified from the pES1 cloning vector (Stadler et al., 2005) using the primers 5'- AACAGCTATGACCATGATTACGC-3' and 5'-

ATATCTCGAGTTGACAAACCAAGAAAGTAAG-3' while the tp-FNR-eGFP insert was PCR-amplified from the pGreenII109 plasmid (courtesy of Dr. Martin Schattat) with the primers 5'- ATATCTCGAGATTCTTCCAATCATCGTACTC-3' and 5'-ATATGAGCTCGCCGCTTTACTTGTACAG-3'. The resulting *Hind*III-*Xho*I and *Xho*I-*Sac*I fragments, respectively, were then ligated into pES1 pre-treated with *HinD*III and *Sac*I to remove the AtSuc2/GFP construct. Successful clones were selected on Kanamycin LB plates, yielding pES1-tpFNR. The insert was sequenced using the primers: 5'-AGCTATGACCATGATTACGC-3', 5'-ACCCTACGCTATAGACACAGC-3' and 5'- AAGCTCCTCCGTCATTTC3'. The plasmid was then used to transform electro-competent *Agrobacteria tumefaciens* (strain Agl1).

2.4. Stable transformation

A floral dip procedure was carried out following the protocol of Clough and Bent (1998). Wild type *A. thaliana* (~3 weeks old) were floral dipped for 2-3 seconds in a 5% sucrose and 0.005% Silwet L-77 solution containing *A. tumefaciens* strain AGL1 with pES1-tpFNR (OD_{600}=0.8). The dipped plants were placed under a plastic dome for 24 hours on a lab bench and then left to grow in a controlled growth chamber. The harvested seeds were sterilized as described previously and plated on MS agar plate with 50 µg/ml kanamycin. Resistant plants were transferred onto soil after a week and checked for expression.

2.5. Biolistic bombardment

Up to 5 µg of the pGreenII109 plasmid containing the tp-FNR-eGFP insert was $CaCl_2$ precipitated onto 1.25 mg of 1-µm gold particles (Bio-Rad Laboratories) and re-suspended in 100 µl ethanol. 5-µl aliquots were bombarded onto leaves of 2 week-old *A. thaliana* plantlets using a biolistic particle delivery system (PDS-1000/He; Bio-Rad Laboratories) at 1,100 psi. The plants were returned to their growth conditions and monitored at 5 and 10 days post-bombardment by confocal laser scanning microscopy (see below).

2.6. Arabidopsis Callus Culture

After seed sterilization as described previously, seeds of MP17-GFP×LTi6b-mcherry were germinated on Callus Inducing Media (CIM) made of MS basal salts, vitamin mix, 0.5 g/L 2-(*N*-morpholino)ethanesulfonic acid (MES), 2% glucose, 0.25 mg/L kinetin, 0.5 mg/L 2,4-Dichlorophenoxyacetic acid and 1.2% agar. Calli were sub-cultured once a month on fresh CIM and left to grow in the dark at 25°C.

2.7. Tobacco Callus culture

Stem sections of 3 weeks old tobacco plantlets, expressing *35S*:TMV-30k-GFP and *Pt-spec*:GFP, were placed on callus inducing media (CIM: MS, Thiamin 1mg/L, inositol 100mg/L, sucrose 30g/L, phytoagar 6g/L, 2mg/L NAA, 0.2mg/L BAP, pH 5.6) and left to grow in the dark at 25°C. These were sub-cultured every two weeks for two months until calli were well established. Calli of 35S:TMV-30K-GFP and Pt-

spec:GFP were either placed next to each other or next to a callus from the same germline on CIM and left to grow into each other , in the dark at 25°C, for 2 weeks to ensure the formation of secondary PD. The same procedure was carried out for a culture of BY2 cells, expressing *35S*:HDEL-RFP and *35S*:TMV-30K-GFP. After 2 weeks, the 'fusion' area of *35S*:TMV-30K-GFP x *35S*:HDEL-RFP calli was observed for double fluorescence under a confocal microscope. The other set of fusion calli were placed on CIM or Regenerative Media (RM: same as CIM except for 1 mg/L BAP and 0.1 mg/L NAA) containing either 250 mg/L kanamycin, 500 mg/L spectinomycin or both in low light condition, at room temperature (bench conditions).

2.8. Protoplast isolation

Protoplasts were isolated from cultured calli following the method described by Chupeau *et al.* (2013). Approximately 0.5 g of callus cells were soaked in 5 ml of maceration-glycine-glucose media (MGG) (Chupeau *et al.,* 2013) and chopped in a Petri Dish. The volume was then brought up to 20 ml and left to incubate overnight at 25°C in the dark. The solution was filtered through a sterile 80-µm nylon mesh into 10 ml of washing solution (2.5% KCl and 0.2% CaCl2). After centrifugation (70g, 10 min), the protoplast pellet was gently resuspended in 20 ml of washing solution. This was filtered through a sterile 40-µm nylon mesh into 5 ml of washing solution and centrifuged again (70g, 10min). After on more wash, the protoplast pellet was resuspended in 1 ml of protoplast-induction media (PIM) as described by Chupeau *et al.* (2013), except for the lack of growth hormones. This was slowly pump-injected in a microfluidic device at a rate of 0.1 µl/min from a 1ml syringe. Once loaded, the

protoplast-pump was switched to one connected to a 20ml syringe containing clean PIM. The system was left to settle for 24h and observed under an inverted biorad confocal microscope.

2.9. Microfluidic device fabrication

The devices were made as described in Crane *et al.* (2014). The devices were fabricated using conventional soft-lithography techniques. The design of the devices was created using AutoCad software (Autodesk) by Dr. Ivan Clark and printed (Compugraphics) to a chrome-onglass mask. A 30 µm tall mold was fabricated at the Scottish Microelectronics Centre using SU8 3005 photoresist. Devices were made using a 10:1 mixture of Sylgard 184 (Dow Corning) and curing agent which was cured at 70°C. Holes were then punched to allow fluid access and the devices were bonded to coverslips following oxygen plasma treatment.

2.10. Micrografting

Unless stated otherwise, 3-4 days old seedlings were grafted following the hypocotyl-grafting procedure of Turnbull *et al.* (2002) consisting in a transverse cut and butt alignment with silicon collars. The seedlings were transversely cut in the upper region of the hypocotyl with ultrafine microknives (Interfocus, n°10315-12). Scions were grafted onto stocks using a short silicon collar for support on MS agar plates. For *nakr1-1* grafts, no sucrose was added to the media. The grafts were left to grow under LD with the plates still oriented vertically. The grafts were then processed for resin embedding after new lateral roots of the stocks were fully established (~10

days) or imaged between 5-dag and 5 weeks after grafting, at which point some tissue was collected for total nucleic acid (TNA) extraction.

2.11. *in vitro* Grafting of Arabidopsis

Calli expressing MP17-GFP were placed in close proximity to calli expressing H2B-mRFP on CIM and left to grow into each other. The interface was observed under the confocal microscope after a couple of weeks once the calli appeared to touch each other.

2.12. Transmission electron microscopy (TEM)

For TEM, samples were fixed in 3% glutaraldehyde in 0.1M Sodium Cacodylate buffer, pH 7.3, for 2 hours then washed in three 10 minute changes of 0.1M Sodium Cacodylate. Specimens were then post-fixed in 1% Osmium Tetroxide in 0.1M sodium cacodylate for 45 minutes, then washed in three 10 minute changes of 0.1M Sodium Cacodylate buffer. These sections were then dehydrated in 50%, 70% and 2x90% normal grade ethanol for 15 minutes each. Samples were then embedded in LR white resin. Ultrathin sections, 60nm thick, were cut, stained in Uranyl Acetate and Lead Citrate then viewed in a Phillips CM120 Transmission electron microscope.

2.13. Correlative microscopy

2.13.a. Method of fixation and dehydration

Tissue samples were fixed for 2h or overnight at 4°C in a solution of 4% formaldehyde, 0.5, 1 or 2% glutaraldehyde, 50mM 1,4-piperazinediethanesulofonic acid (PIPES) and 1mM $CaCl_2$. Unless stated otherwise, all the following steps were carried out in an ice bucket on a rocker. The samples were then washed in buffer (50mM PIPES, 1mM $CaCl_2$) three times for 10 minutes before dehydration in a graded ethanol series (50%, 70% 2x 90%). The ethanol solutions also contained 1mM dithiothreitol (DTT) to reduce tissue autofluorescence (Brown *et al.*, 1989). Grafts had their collar removed and infiltrated in resin.

2.13.b. Infiltration and polymerisation in London Resin (LR) White

Oven polymerisation

The tissue samples were then infiltrated in medium grade LR White at 1:1, 1:2, 1:3, 1:9 ratios of 90% ethanol:resin for 45 minutes each before two 60 minute changes in 100% LR White. The final embedding step was done at ambient temperature. The samples were then polymerised in gelatin capsules (TAAB) at 50°C for 24 hours.

-20 °C cold polymerization

The infiltration steps described above were carried out at -20°C. The pH of the LR White resin was also adjusted to 6.8-7 with a weak base, ethanolamine, as described by Brown *et al.* (2010). After the overnight infiltration in pure resin, the samples were infiltrated for 3 hours in 100% LR White (pH 6.85-6.95) with 2µl/ml of

LR White accelerator (Ted Pella), a further 3 hours in 100% LR White with 4 µl/ml of LR White accelerator and 30-40 min in 100% LR White with 8µl/ml of LR White accelerator. The samples were then polymerised in gelatin capsules containing 100 % LR White with 8µl/ml of LR White accelerator at -20°C for 24 hours. This procedure was also tried with different concentrations of ethanol, 70% and 95%.

2.13.c. Infiltration and polymerisation in methyl methacrylate/n-butylmethacrylate (MBM)

The dehydration and infiltration step were carried out at -20°C. The resin was made of 20 % methyl methacrylate and 80% n-butyl methacrylate. Prior infiltration, the MBM resin was degassed for 20 min using Helium gas. The tissue samples were infiltrated at 3:1, 1:1, 1:3 ratios of 90% ethanol:resin for 30 minutes each before two 60 minute changes in pure resin. The samples were then left overnight in MBM resin. They were polymerized in gelatin capsules for 5 hours using a 10W long-wavelenght UV light source at 4°C with fresh MBM resin. The infiltration and polymerization steps were also tried at 4°C with MBM resin that had pre-polymerized for 4h using a 10W long-wavelenght UV light source at 4°C.

2.13.d. Dehydration, infiltration and polymerization in Fluka Durcupan

After being washed in buffer as described previously, the samples were dehydrated at 1:1, 1:2, 1:9 ratios of dH_2O:Component A for 45 min each before two 90 minute changes in 100% Component A. The samples were then left to infiltrate overnight at 4°C in a polymerization mixture made of Components A, B, C and D with

the following proportions: 1ml, 2.34 ml, 0.2 ml and 0.04 ml. The samples were polymerized in gelatin capsules for 4 days at 40°C.

2.14. Imaging

2.14.a. Confocal microscopy

For resin-embedded samples, semi-thin sections (1-2 µm) were cut using a glass knife on a Leica Ultracut UCT ultramicrotome (Leica Microsystems UK Ltd, Milton Keynes). Before imaging, some of these sections were stained with 10 µg/ml calcofluor white. Grafts without collars were imaged without further preparations.

Images were taken using a Leica SP2 and SP8 confocal laser scanning microscope (Leica Microsystems) with either a ×5 (HC PL FLUOTAR; Leica Microsystems), or a ×20 and a ×63 water-immersion lenses (HCX PLAPO CS; Leica Microsystems). Calcofluor was excited at 405-nm, GFP at 488-nm, YFP at 514-nm, RFP at 561-nm and mCherry at 594-nm.

2.14.b. Light microscopy

Grafts were photographed using a Nikon digital camera (D40×) mounted on a phototube which was itself attached to a Leica Wild M3C stereozoom microscope (Leica Microsystems) at ×40.

2.15. Total nucleic acid extraction and cDNA synthesis

The rootstocks of 18-24 grafts were pooled into three biological replicates for each transgenic line. The roots were harvested immediately below the root collar of 5 week-

old grafts. This was carried out under a stereomicroscope (Leica, wild m3c) to prevent tissue contamination from the scion. Grafts showing the formation of adventitious roots above the graft junction were disregarded. TNA (DNA and RNA) was extracted using the modified protocol of White and Kaper (1989). Briefly,

TNA samples were used for cDNA synthesis. 3 µg of TNA was treated using a TURBO DNA-free kit (Ambion). 1 µg of DNA-free TNA was then reverse transcribed using a RevertAid first strand cDNA synthesis Kit (Thermo Scientific). The presence of the eGFP coding sequence was analysed by PCR using primers: 5'-ACGGCGTGCAGTGCTTC-3' and 5'-CCATGTGATCGCGCTTC-3'. F-box gene (At5g15710) specific primers were used as cDNA quality and loading controls from Lilly *et al.* (2011).

2.16. Bioinformatic and statistical analysis

This work was done in collaboration with Dr. Marie-Paule Gustin (Université Claude Bernard, Lyon). Gene expressions of *Arabidopsis* phloem tissue were found in the GSE10247 Gene Expression Omnibus (GEO; http://www.ncbi.nlm.nih.gov/geo/) dataset for 22,746 proteins (Deeken et al., 2008). Their corresponding molecular weights and subcellular location were obtained from Uniprot (http://www.uniprot.org) using the retrieve/ID mapping tool. This led to identification of 21,072 proteins with a unique transcript-ID. Mean expression level was computed for each protein. The two files were merged to obtain both mean expression and molecular weight for 21,072 phloem proteins. In this set of proteins, we retrieved 264 phloem exudate proteins from among the 287 identified by Batailler *et al.* (2012).

A logistic regression in a Bayesian framework with a non-informative prior distribution was used to determine whether the probability of a protein to be found in a given location was significantly different between exudate proteins (n=287) and other proteins of the Arabidopsis proteome (n=27,056). The Arabidopsis proteome was downloaded from Uniprot (http://www.uniprot.org). The analysis was performed in turn for each of the 15 possible subcellular locations. For each model, the response binary variable was the location (yes/no) and the explicative variable, the group (proteins from the phloem exudate/proteome without proteins from the phloem exudate). If 1 belonged to the 95% credible interval of the Odd Ratio, the probabilities to be in a subcellular location for proteins in the phloem exudate and for the other proteins were not significantly different. In the inverse case, the difference was significant at the 5% level. The Bayesian analysis was performed using the rjags R package available at https://sourceforge.net/projects/mcmc-jags/.

Gene expression distributions of proteins with and without targeting sequences were compared using 'Wilcoxon test' also known as 'Mann-Whitney' test (R command wilcox.test). The impact of molecular weight and gene expression on the probability of a protein to be found in the phloem was studied using a logistic second degree polynomial regression model taking into account the interaction between both variables, after base-10 logarithm transformation, to obtain normal distributions. Statistical analysis was performed using R language accessible at https://cran.r-project.org (version 3.2.2).

To compare the root growth of seedling kept in different treatments (see 2.18), a t-test between two-samples was performed assuming equal variances using the data analysis tool in Excel (Microsoft Excel 2016). The t-test was set with a 95 % level of confidence (α=0.05). For each type of phloem probes tested (see 2.19), the percentages of success between the two groups WT and *nakr1-1* were compared using a Fisher test (R command Fisher test).

2.17. Clearsee

6-days old grafts made of WT scions and *AtSEOR*:SEOR-YFP stocks were processed using the method by Kurihara *et al.* (2015). The grafts were fixed as described previously. They were then immersed in a clearsee solution (xylitol, 10% (w/v), sodium deoxycholate, 15% (w/v), and urea, 25% (w/v)) for 1 week. The cleared grafts were stained with calcofluor white (1 µg/ml) in ClearSee solution for 1 h. After staining, stained grafts were washed in ClearSee for 1 h.

2.18. Growth assays and phloem unloading analyses

pCALS8:icals3m seeds were stratified for 2 days at 4ºC in the dark and were sown on media containing 0.5 MS and 1.2% plant agar, pH 5.8. At 4 days post sowing, seedlings were induced in plates containing the same media with added Beta estradiol (5µM) or with an equal amount of DMSO (mock). Plates were scanned at times 0, 4, 8, 24 and 48 hours after the induction. Roots from 40 seedlings per time-point were measured with an eyepiece reticle under a Leica Wild M3C stereo-zoom microscope. Some seedlings were subsequently used for CTER loading. 0.2 µL of 0.8 mM CTER

in a 20% acetonitrile solution was applied to the adaxial side of leaves which had been treated with a 2.5% Adigor solution (Syngenta) for 1h. The roots were observed 1h to 1h30 after loading and imaged by confocal laser scanning microscopy.

2.19. Translocation of phloem probes

A 0.2 µl drop of a 2.5% Adigor solution (Syngenta) was applied on one cotyledon of 10-day old *Arabidopsis* seedlings either WT or *nak1-1* for 1h. The phloem probes carboxytetraethylrhodamine (CTER) (0.8 mM), esculin (9 mg/ml) and 8-acetoxypyrene-l,3,6, trisulphonic acid, trisodium salt (HPTS) (8.8 mM) dissolved in a 20% acetonitrile solution were then loaded as a 0.5 µl drop. The time of observation stopped after all WT seedlings showed translocation in the root phloem. It took 1h for CTER (n=7) and overnight for esculin (n=5) and HPTS (n=7).

CHAPTER 3: Symplasm recovery during graft development using *Arabidopsis thaliana* micrograft as model

3.1. Introduction

Grafting is an old horticultural technique that involves the fusion of the aerial parts of a plant (the scion) to the root system of another plant (the stock or rootstock) until new vascular connections form. While references to grafting are found in biblical sources, suggesting it was already a common practice at the time (ca. 1400-400 BCE), dating its origin is still difficult. It is thought that grafting was first inspired by observations of natural grafts that occurred readily between certain plant species, such as vines and strangler figs, when growing on their substrate. Grafting was later developed during the development of agriculture to propagate cultivated plants such as fruit trees that are not as genetically malleable as other annuals (Mudge *et al.*, 2009).

Grafting now has many horticultural and biological uses, such as the creation of biotic and abiotic resistance, tissue repair and plant size control. In plant physiology studies, grafts have also enabled the discovery of long-distance signalling molecules such as microRNAs (reviewed in Harada, 2010) or the elusive Florigen, responsible for flowering (reviewed in Zeervaart, 2006).

Despite its importance, graft development is still poorly understood. Studies on horticulturally relevant species including Solanaceae and fruit trees have shown that during grafting, a necrotic layer, which results from the cellular debris caused by cutting through tissue, is first formed and separates the scion from the stock. Parenchymatous cells from both graft partners then start to divide, filling up the empty spaces at the graft interface. They eventually push through the necrotic layer and form

new contacts with the abutting cells, producing the callus bridge. Cell division may carry on to the point where structurally identical cells (but of different origins) interdigitate. Compatible grafts eventually restore the integrity of their symplasm with the *de novo* formation of secondary plasmodesmata and redifferentiation of vascular tissue (Pina and Errea, 2005).

The idea that secondary PD could form entirely *de novo* between grafted cells was long doubted because traditional EM imaging could not guarantee cell origin. The study by Jeffree and Yeoman (1983) on homografts of tomato (*Lycopersicon esculentum*) gave the first clue as to how secondary PD could form entirely *de novo*. They showed that newly inserted PD between abutting and unrelated callus cells co-localised with regions of the wall that appeared to have thinned. They suggested that the local enzymatic digestion of the wall was the first step in a recognition system necessary to restore symplasmic continuity, and this probably contributed to graft compatibility. Their results did not indicate whether PD were inserted from one side of the cell or whether they ensued from the fusion of two half PD. However, a one-sided penetration of PD is thought to be unlikely because no discontinuous PD, spanning more than half the wall, had yet been recorded in a graft union (Kollmann *et al*., 1985).

Kollmann and Glockmann (1991) gave a more extensive description of secondary PD formation from their observation on heterografts displaying species-specific cell markers, avoiding any possible criticism of cell origin. Based on their heterograft system, they proposed that secondary PD were the result of half-PD fusions, and that branched secondary PD occurred when the ER was entrapped beforehand by Golgi-derived vesicles containing wall material. They also observed

that successful fusions of PD were achieved only at the site of cell wall thinning, and when the wall was reduced from both sides of the middle lamella. This suggests that both graft partners have to co-operatively orchestrate half-PD fusion. If they do not, this can lead to graft failure, as observed in grafts of incompatible species, which show a preponderance of mismatched half-PD at their graft interface (Kollmann and Glockmann, 1991). Coordination is therefore a prerequisite to restore the symplasm in the first stages of grafting and must be attained with proper cellular communication. This raises the question as to how secondary PD formation is initiated and signalled between graft partners? What signalling molecule(s) are responsible for secondary PD formation? Jeffree and Yeoman (1983) proposed that lectins, apoplastic proteins with a sugar residue, found in the cell wall might play a role in secondary PD formation. However, no evidence has been put forward that could support such a claim and alternative molecules have not been identified. This is due to the impracticability of forward genetic when studying grafting. A mutant might be lost during the procedure and structural defect in their secondary PD would only be observed under EM which requires dead tissue. The possibility to use an *in vitro* system however, offers promises of new progress. It was shown in 2001 that under certain criteria, such as cell arrangement and the presence of phenolic compounds, grafted callus grown *in vitro* would behave similarly to grafted plants (Errea *et al*., 2001). Further work using this technique has shown that, for calli of fruit trees, *in vitro* heterografts could change the symplasmic conductivity of one of the grafted callus partners. By fusing one callus to another, a signalling molecule could diffuse either from the apoplasm or the symplasm and change either the size and/or the number of PD of one of the grafted partner (Pina *et al*., 2009).

Although a signal has yet to be identified for secondary PD formation, vasculature dedifferentiation of the grafted calli is thought to occur by the diffusion of auxin (Moore, 1984). Moore (194) showed that vasculature could dedifferentiate across a graft, initially from the scion, after a thin membrane had been inserted between the scion and the stock. This suggested that the apoplastic diffusion of a signalling molecule from the scion was sufficient and necessary for successful vascular reconnection. This signal was hypothesised to be auxin because of previous work on callus that showed vascular differentiation after local application of the hormone (Wetmore and Rier, 1963). The introduction of micrografting of the model plant *Arabidopsis thaliana* by Turnbull *et al.* (2002) enabled more understanding of the molecular events that lead to vascular connection in compatible grafts, and confirmed the importance of auxin. Yin *et al.* (2012) were the first to demonstrate that auxin accumulated on either side of the graft interface by using GUS-stained micrografts which either had a scion expressing the GUS protein under the auxin-sensitive promoter DR5 and a WT stock, or vice versa. At the molecular level, auxin responsive genes such as ABERRANT LATERAL ROOT FORMATION 4 (ALF4) enable cell-cell communication and tissue specific responses to auxin for vascular differentiation (Melnyk *et al.*, 2015). These studies have also shown that phloem can reconnect as early as 3 dag before the xylem. Secondary PD are thought to form before or during vascular connection as phloem development would inevitably require PD formation.

Interestingly, reports on macromolecular transport at the graft junction have shown that organelles such as chloroplasts, mitochondria and nuclei can be transferred between the scion and the stock (Stegemann and Bock, 2009; Fuentes *et al.*, 2014; Gurdon *et al.*, 2016). These cases of 'graft hybridisation' are a fascinating occurrence

of symplasmic transfer of large subcellular structures that are up to 1000 times bigger than PD. Whether the transfer is performed during secondary PD formation or at another stage during symplasmic recovery is an issue that needs to be addressed.

3.2. Aims

For this chapter, the aim was to develop new imaging techniques to visualise and assess molecular movement over short distances across the graft junction. The use of LR white enabled the preservation of fluorescence in semi-thin sections, providing a unique view of the grafted tissue. The graft junction is shown here to become a sink tissue with a high SEL. The possibility that organelles are transferred during vascular remodelling is also investigated. Finally, I offer preliminary data advocating the use of microfluidics to investigate secondary PD formation in callus cells.

3.3. Results

3.3.1. London Resin (LR) White embedding technique to study micrograft formation

Semi-thin sections which retained fluorescence were successfully obtained with the epoxy resin MBM (methyl methacrylate/n-butylmethacrylate) and LR-white. Samples embedded in Durcupan retained their fluorescence but the resin did not polymerize enough to cut the tissue. Samples embedded in MBM also showed a partial collapse of cell structure (see Figure 3.1.A). This is thought to be due to shrinkage of the resin during polymerization. I therefore tried embedding in pre-polymerized resin as advised in the technical data sheet of Electron Microscopy Sciences (EMS) but this did not yield satisfactory results (see Figure 3.1.B). The results in LR-white varied depending on the batch used, a limitation that has already been assessed by Watanabe *et al.* (2011). Fluorophores such as GFP and other fluorescent proteins are sensitive to pH and temperature. LR-white has generally a low pH that can vary from one batch to the next (it was found to range between 4.6 and 6.5). This is possibly due to its hydrophilic nature that leads to water absorption from the environment. Low pH of the resin associated with heat cure (i.e. 50°C) can cause a complete loss of fluorescence. I therefore tried pH adjustment with a weak base, ethanolamine, as suggested by Brown *et al.* (2010), and cold polymerisation (-20°C). In this case, GFP fluorescence was preserved throughout the curing process (see Figure 3.1.C), however, the resin showed poor cutting qualities. This was due to the added ethanolamine that prevented full polymerisation of the resin and an only partial infiltration of the tissue, the resin being more viscous when kept at –20°C.

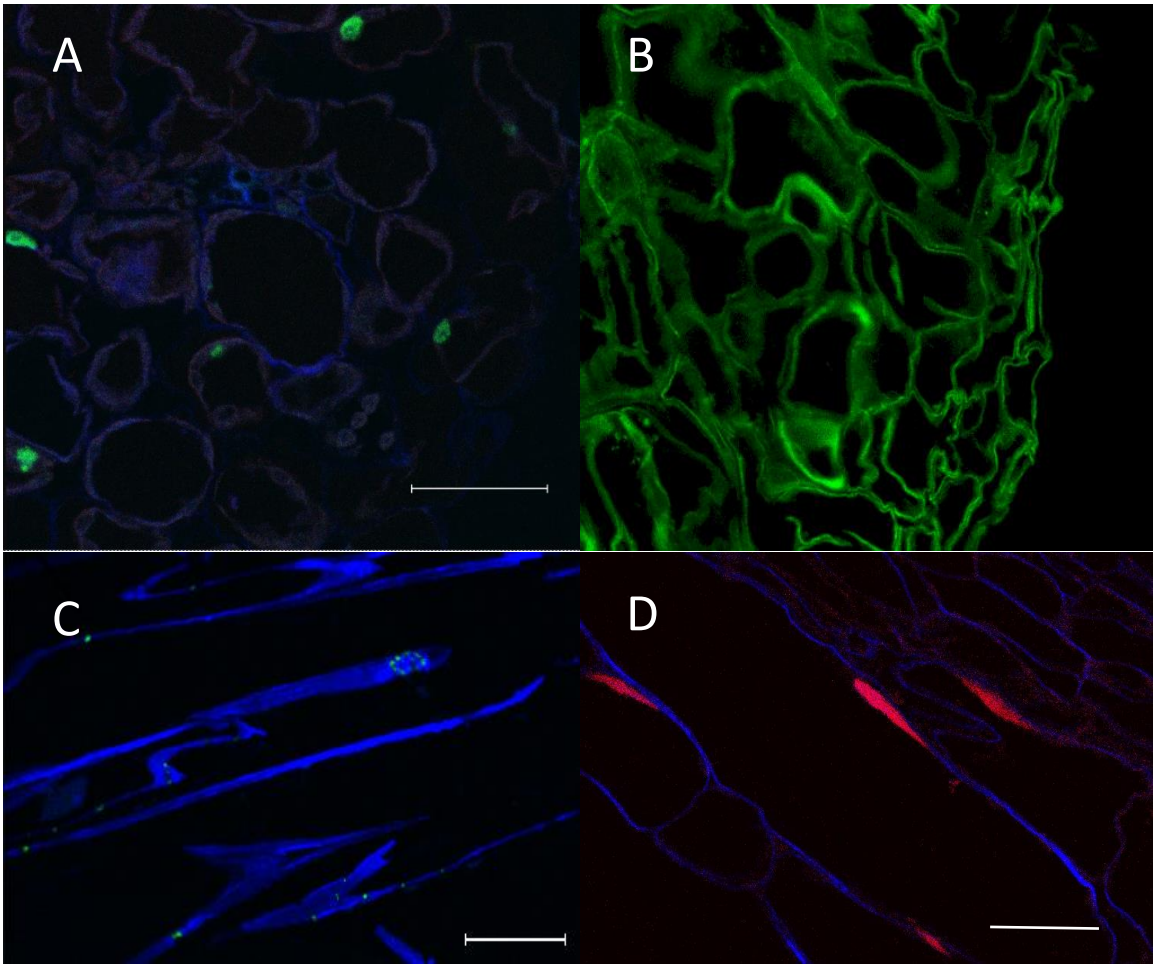

Figure 3.1: A. Semi-thin section of cotyledon tissue expressing *35S*:LTi6b-mCherry and *35S*:H2B-YFP showing a partial collapse of cell structure after processing in MBM resin. Scale: 100 µm.

B. Semi-thin section of cotyledon tissue, expressing *35S*:LTi6b-GFP showing a partial collapse of cell structure after processing in pre-polymerized MBM resin. Scale: 30 µm.

C. Semi-thin section of a petiole of *N. tabacum* expressing TMV-30k-GFP and stained in calcofluor. The tissue was embedded in pH adjusted LR-white that was polymerised at -20°C. Scale: 40 µm.

D. Semi-thin section through the hypocotyl of a 10 days old seedling expressing *35S*:H2B-mRFP. Scale: 50 µm

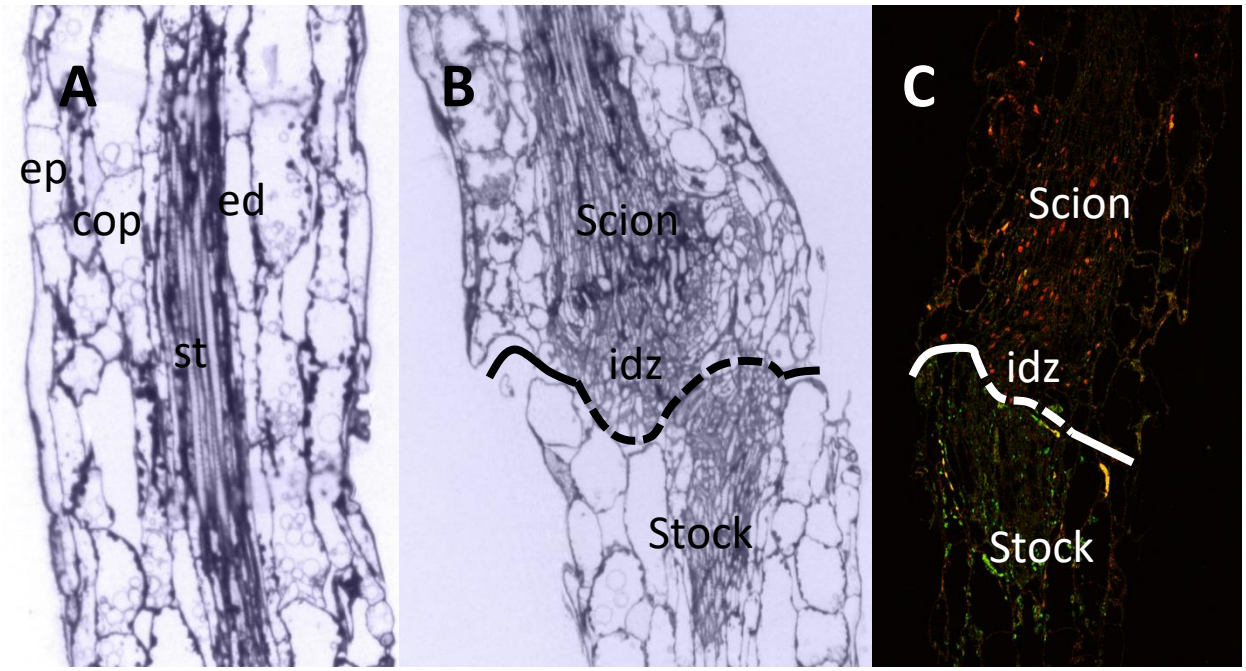

Figure 3.2: A. Semi-thin section of a hypocotyl from a 10 days old *Arabidopsis* seedling as seen under bright-field. ep: epidermis; ed: endodermis; cop: cortex parenchyma; st: stele.

Standard bright field picture of homografts 5 dag **B.** contains little information on cellular identity where callus cells interdigitate (idz: interdigitated zone) compare to confocal images of semi-thin sections where fluorescence is preserved **C**. homografts,5 dag, expressing *35S*:H2B-mRFP in the scion and *35S*:tpFNR-GFP in the stock.

‘Good’ batches of LR-white could preserve the fluorescence of mRFP, YFP and GFP throughout the polymerisation process at 50°C (see Figure 3.1.D). mCherry was also tested however fixation in glutaraldehyde followed by embedding in resin caused a partial loss of fluorescence with the appearance of artefacts. Concentrations of glutaraldehyde as low as 0.1% was successfully used to embed zebra fish tissue in LR-white and preserve GFP fluorescence (Luby-Phelps *et al*., 2003). However, I found that during fixation, glutaraldehyde had to be between 1% and 2% to prevent plasmolysis of plant tissue during dehydration and infiltration. Glutaraldehyde is known to quench fluorescence at high concentration and increase background autofluorescence (Lee *et al*., 2013). At concentrations as high as 1-2%, the loss of fluorescence was prevented by keeping the samples below 8°C, while autofluorescence was reduced by adding dithiothreitol (DTT) during dehydration and infiltration (Brown *et al.*, 1989). A concentration of 2% glutaraldehyde was also the most adequate to cut ultrathin sections for further imaging with EM (data not shown). We therefore successfully developed a protocol that can be used for correlative imaging of plant tissue (Bell *et al*., 2013). It is, however, noteworthy that this protocol might be applicable only for strong fluorescence signal because low or diffuse fluorescence might not be distinguished from background fluorescence.

This method can also offer a unique insight in macromolecular/cellular behaviour at the graft interface. When appropriate cellular makers are used in each of the graft partners, cellular identity can be determined based on the displayed fluorescence. Figure 3.2 show semi-thin sections of a graft as seen either under a bright-field (see Figure 3.2.B) or a scanning confocal microscope (see Figure 3.2.C). The latter image contains more information at the interdigitated zone (idz) as seen in

a graft expressing a nuclear marker in the scion and a chloroplast marker in the stock. This could be used instead of heterografts to observe and identify 'true' secondary PD formation in homografts. In this study, observing fluorescently-labelled semi-thin sections of *Arabidopsis* grafts has enabled the identification of a symplasmic domain above and below the graft interface which might be delimited by PD closure and/or a necrotic layer.

3.3.2. A symplasmic domain develops that is isolated from the surrounding cortex

LR white embedded grafts expressing *35S*:H2B-GFP marker in the scion and *35S*:tpFNR-GFP in the stock were originally intended for observing the possible transfer of organelles across the grafts as reported by Stegemann and Bock (2012) and Fuentes *et al.* (2014). While looking for double-labelled cells at the graft interface, necrotic layers frequently appeared in all of the grafts observed (n=15). They seemed to delimitate the wound-induced callus in the stele from the cortex parenchyma, probably affecting the endodermis. In some instances, the necrotic layer would span from the cut site well into the hypocotyl (see Figure 3.3.A and B) or on either side of the developing callus cells (see Figure 3.3.C). These might be due to the mechanical stress imposed by the cut. However, the necrotic layer consistently affected the same tissue layer, isolating the cortex from the stele. Melnyk *et al.* (2015) pointed out the importance of auxin-induced expression of ALF4 in the pericycle for the growth of vascular bundle and phloem reconnection. Auxin is a small solute (~200 Da) that can freely diffuse across PD. However, at the interface of 6-day old grafts, expressing *pDR5*:GFP-ER in the scion and *35S*:H2B-RFP in the stock, auxin seems to be

contained in the epidermis and stele, not moving beyond the pericycle (see Figure 3.4.A and B). This has been observed in other studies (Melnyk *et al*., 2015; Jeffree and Yeoman, 1983). During grafting, auxin not only accumulates from the phloem but also by the concerted action of PIN proteins which become highly expressed in the vascular bundle (Wang *et al*., 2014). The restriction at the pericycle might be due to an auxin-induced closure of PD to establish an auxin gradient. In tissue already traumatised by injury, this might lead to cell death. The isolation of the symplasm to create an auxin gradient was reported necessary for lateral root growth and hypocotyl tropism (Han *et al.*, 2014; Benitez-Alfonso *et al.*, 2013) and, in the present case, might be essential for efficient cell division and vascular reconnection.

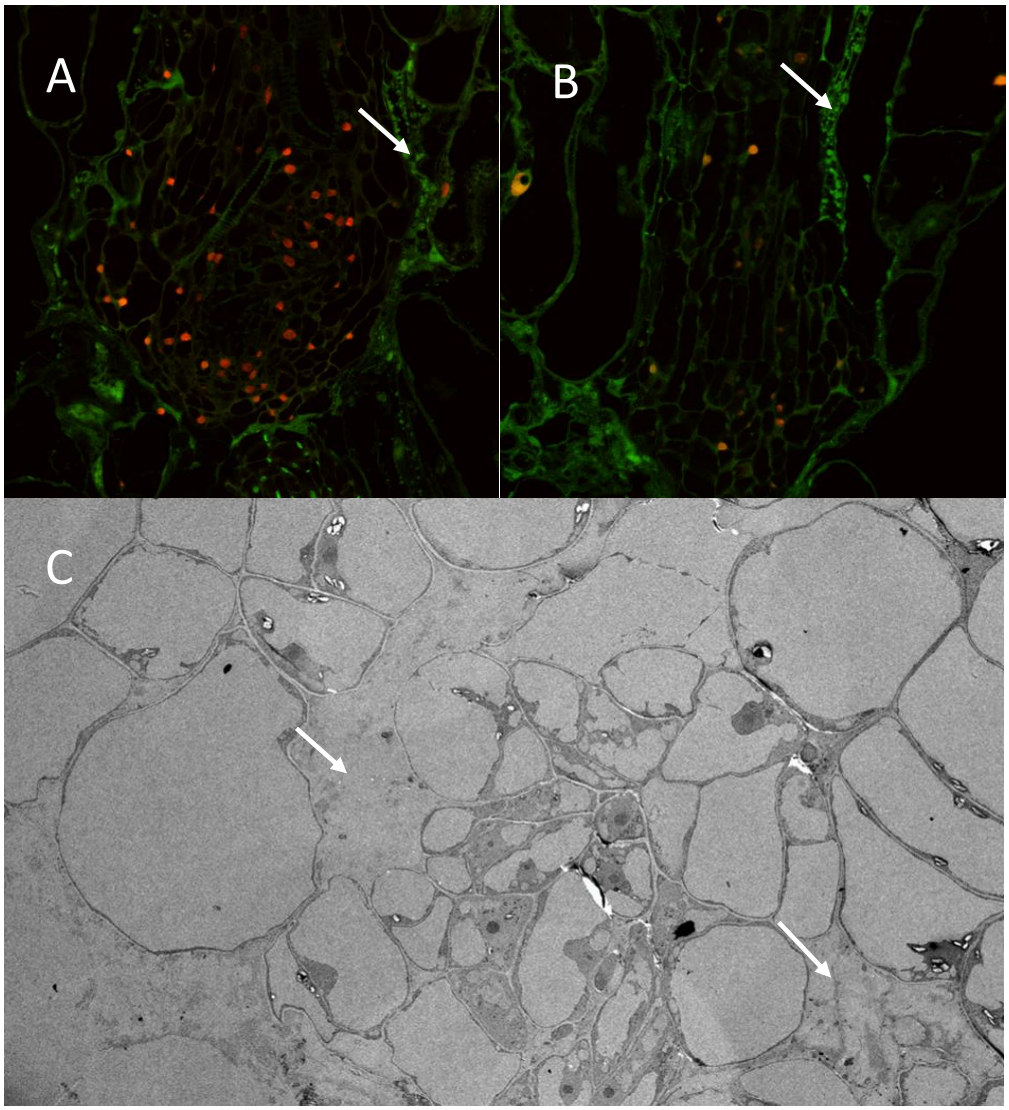

Figure 3.3. A. and **B.** Homograft 5 dag, expressing *35S*:H2B-mRFP in the scion and *35S*:tpFNR-GFP in the stock, which has developed a necrotic layer (see arrow). The necrotic layer is full of autofluorescent debris, starting at the graft junction and progressing into the scion.

C. TEM view of the scion of a homograft 4 dag showing a necrotic layer on either side of the growing callus (see arrows).

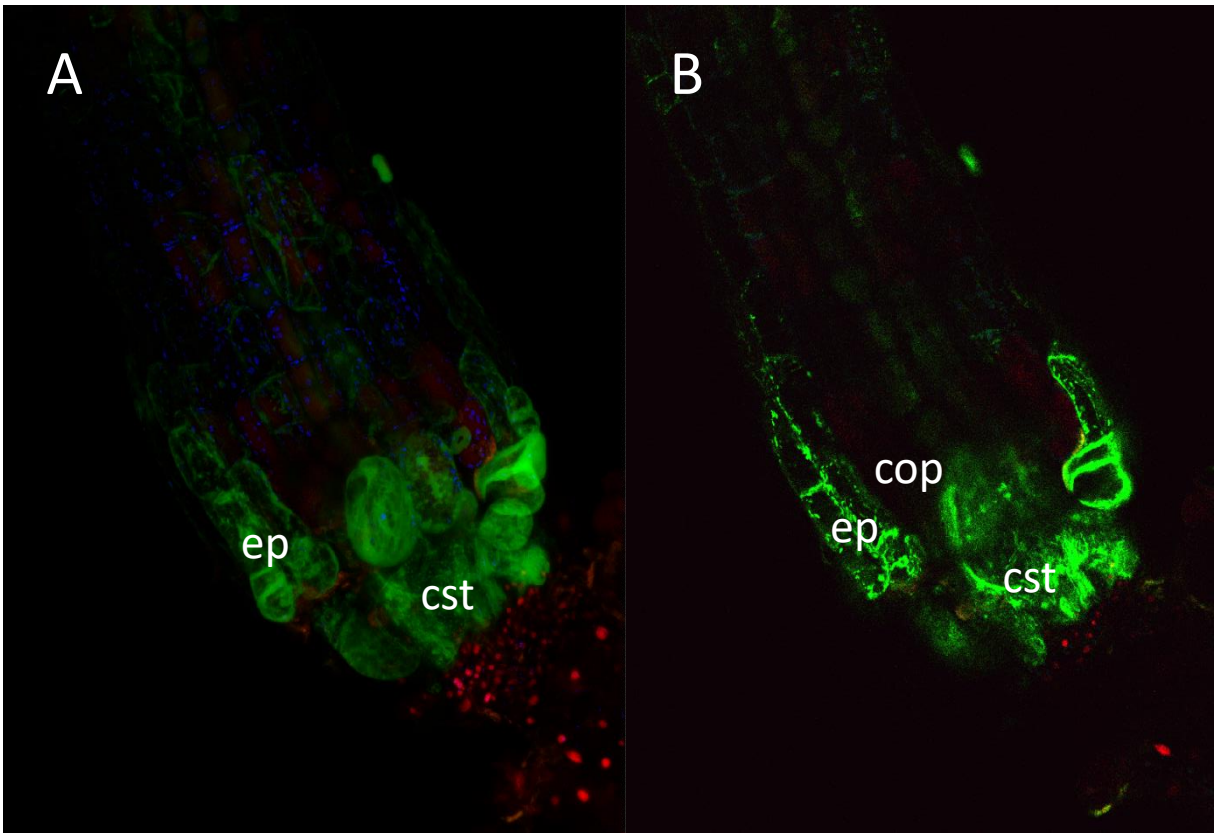

Figure 3.4. A. Projection of a serial confocal scan representing a *pDR5*:ER-GFP scion and a *35S*:H2B-mRFP stock, 5 dag **B.** scan section through **A.** The fluorescence is restricted to the callus of the stele as well as epidermal cells which appear enlarged without signs of division. The cortex parenchyma cells do not express GFP. ep: epidermis; cst: callus stele; cop: cortex parenchyma.

3.3.3. Tissue become sink below and above the graft junction during vascular reconnection

During translocation, solutes and macromolecules are contained in the phloem. *AtSUC2*:GFP seedlings were grafted onto wild type to observe the fate of macromolecules at the wound site. While the phloem is known to reconnect within 3 dag (Melnyk *et al*., 2015), it might be preceded by symplasmic recovery. GFP was indeed perceived 2 dag in cells of the rootstock presumably diffusing through secondary PD (see Figure 3.5). At 3 dag, the fluorescence intensified at the graft interface, in the developing callus cells. This suggests that the dividing and dedifferentiated cells generated in this area form an isolated symplasmic domain and might be a site for phloem unloading. This was confirmed by using semi-thin sections of *35S*:H2B-RFP scion grafted on a *35S*:tpFNR-GFP stocks, which showed doubly labelled cells in the stele of the scion (see Figure 3.6.A and B). Green fluorescence was also detected in the stele of reciprocal grafts (see Figure 3.6.D.). It is unclear whether tpFNR-GFP found its way in the scion or stock strictly through secondary PD or partially via differentiating SE and CC. However, this symplasmic domain is clearly isolated from the ground tissue for proteins as large as tpFNR-GFP i.e. 35 kDa. Interestingly, SEOR protein fused to YFP were also found to unload in WT scion. These fusion proteins are 112 kDa and form large aggregates (Knoblauch *et al*., 2014; Ross-Elliott *et al*., 2017). The movement of these proteins seemed more restricted to a single cell file, probably following the differentiation of new SEs. However, at a time when the phloem should have been fully functional across the graft (6 dag), these large aggregates did not translocate further than 150 µm from the graft junction (see Figure 3.6.C). In the last scion cell showing SEOR-YFP, the aggregates looked smaller

suggesting possible degradation (see Figure 3.6.C). Because SEs lack the necessary cellular machinery for proteolysis, these cells might either be partially differentiated or perhaps of another type of SE with PD that display a very large SEL.

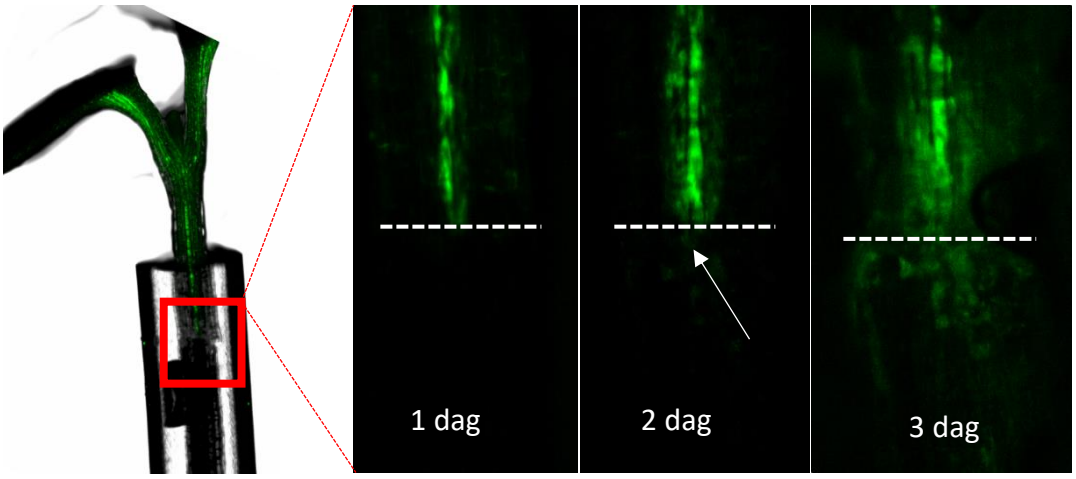

Figure 3.5: Development of a *AtSUC2*:GFP scion grafted on WT stock showing symplasmic recovery from 2 dag (see arrow).

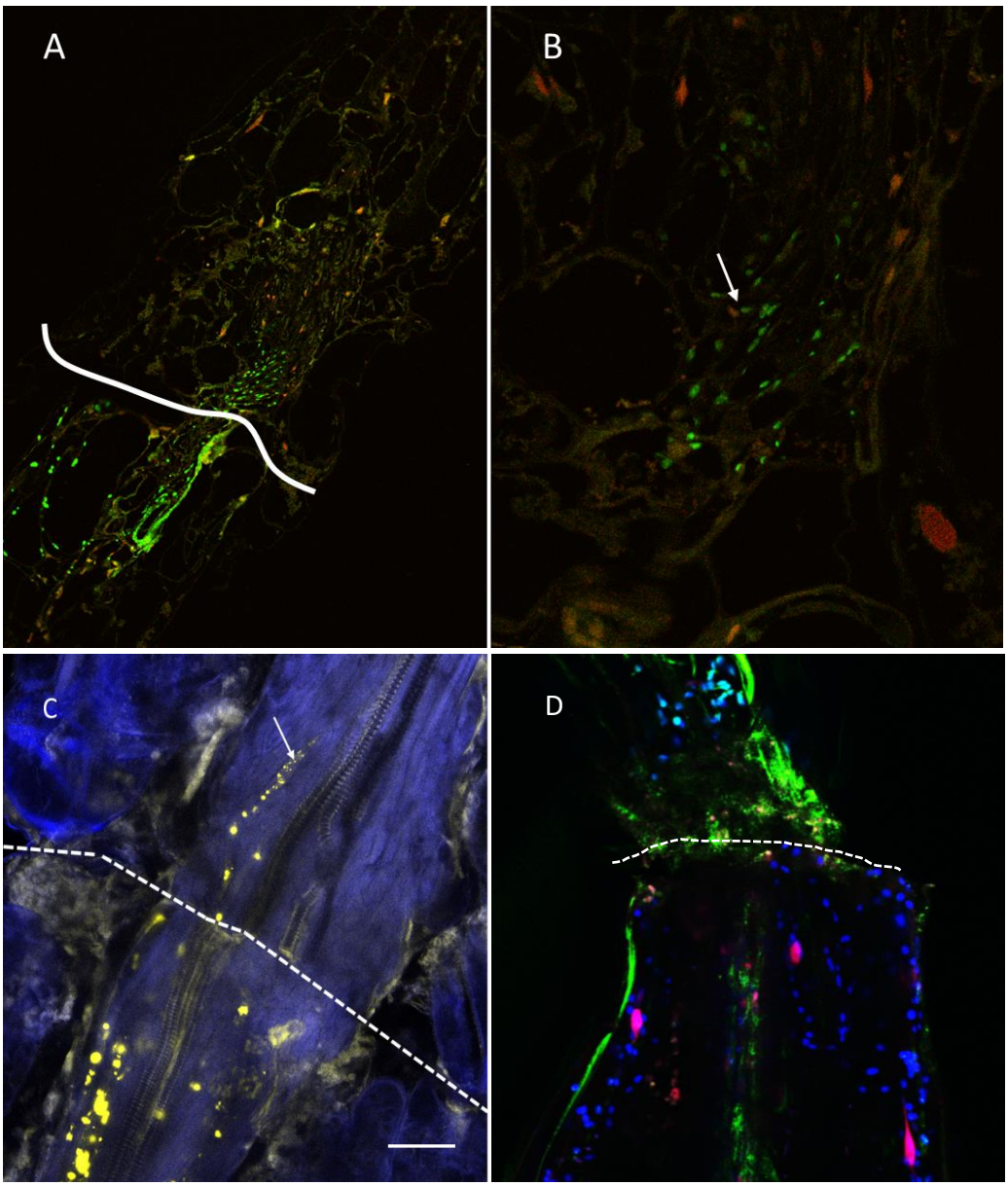

Figure 3.6 A. and **B.** semi-thin sections of an homograft, 10 dag, expressing *35S*:H2B-mRFP in the scion and *35S*:tpFNR-GFP in the stock. Some cells restricted to the stele show double labelling in the scion (see arrow). This might represent an unloading domain with a high SEL at the graft interface.

C. Cleared tissue of *AtSEOR*:SEOR-YFP stock grafted on WT scion, 6dag. The protein aggregates appear smaller as they go further into the scion (see arrow) Scale: 50 µm

D. 5 days-old graft expressing *35S*:tp-FNR-GFP in the scion and *35S*:H2B-mRFP in the stock and showing green fluorescence, below the graft junction, in the stele of the stock.

3.3.4. Formation of secondary PD during *in vivo* and *in vitro* grafting

To study the formation of secondary PD at the graft junction using the LR-white embedding method developed in our Lab, semi-thin sections of 10 day-old grafts, made of a scion expressing *35S*:H2B-mRFP and a stock expressing *35S*:MP17-GFP, were obtained (see Figure 3.7). The grafts give an appreciation of how many callus cells of different origins can interdigitate and show unambiguously that secondary PD do form *de novo* between non-division walls at the homograft interface. These are promising results for the use of correlative imaging at the graft junction. It could indicate whether the results and the conclusions drawn from the study of Kollmann and Glockmann (1991) are applicable to true homografts. In their heterografts system, *Vicia faba* was grafted onto *Helianthus annus*. These plants are not from the same family (subclasses Rosidae and Asteridae, respectively) which is generally seen as a prerequisite for successful grafting. This heterograft system indeed shows a certain degree of incompatibility; the grafts are short lived and the necrotic layer persists at the graft junction except for a few local disruptions in the pith and at regions of matching vascular bundles (Kollmann and Glockmann, 1991). Although the causes of graft incompatibility are still unknown, it is thought that the mismatching half-PD observed by Kollmann *et al.* (1985) may contribute to graft failure (Pina and Errea, 2005). These might therefore not be observed in this present homograft system, as well as the asymmetrical branched PD that were reported by Kollmann and Glockmann (1991).

The transfer to an *in vitro* system could be used to study secondary PD formation between callus cells. When *Arabidopsis* calli expressing the PD marker MP17-GFP (Hofius *et al*., 2001) were allowed to grow next to calli expressing H2B-

mRFP, the movement of MP17-GFP was observed. This is shown by the appearance of a GFP signal in some area of the H2B-mRFP callus and confirmed by the presence of cells showing double labelling (see Figure 3.8.B and D). This is possible if these cells have formed new secondary PD because MP17 does not travel apoplastically. The same behaviour was observed between tobacco calli (see Figure 3.8 A. and C). Grafted calli are usually pre-cut prior to contact. In my set up, it appears that cells do not need a 'wounding' signal to initiate PD formation. They only require contact. This could indicate that exposed surfaces of callus cells continuously release a signal that is activated when in presence of a compatible partner.

Because callus cells can graft *in vitro* without external interventions, solely by forming secondary PD, the *in vitro* system could be used to test the ability of organelles to be transferred during secondary PD formation alone, and to test for external molecules that might affect the occurrence of secondary PD.

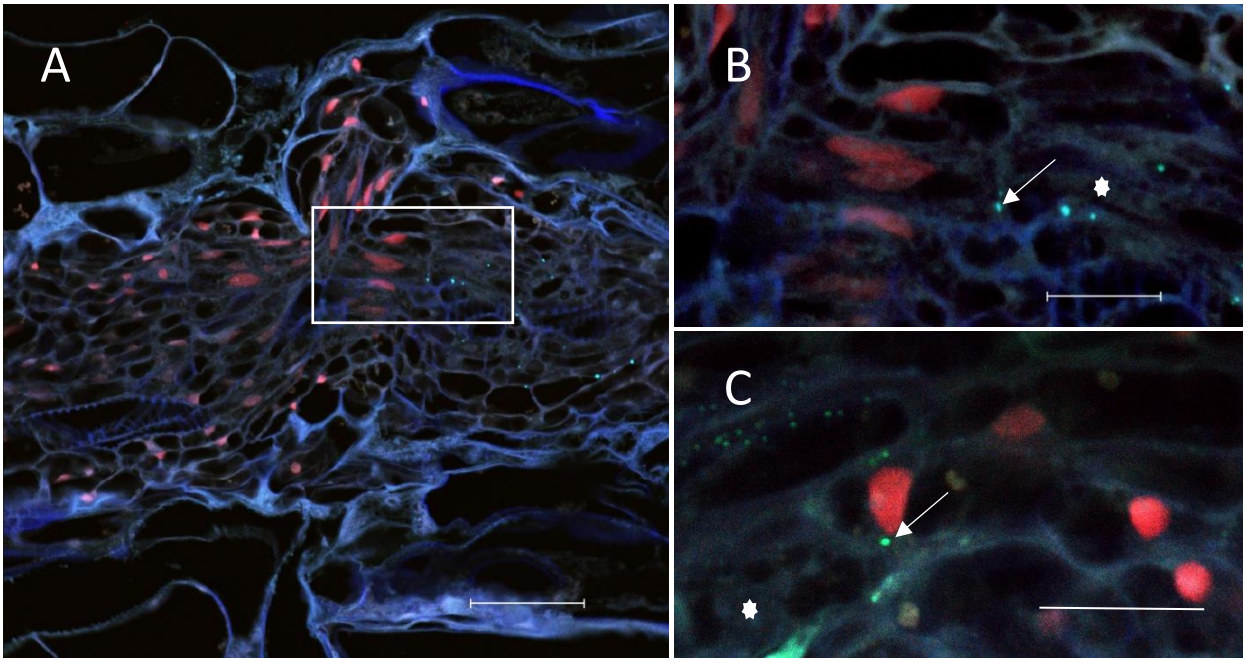

Figure 3.7. Grafts expressing *35S*:H2B-mRFP in the scion and *35S*:MP17-GFP in the stock **A.** molecular markers can give a clear distinction between scion and stock cells. Scale: 40 µm. **B.** Close view of the region highlighted in **(A)**. **B.** and **C.** have a GFP signal in the PD of cells expressing H2B-mRFP abutting a cell which has a non-fluorescent nucleus (stars). This enables the identification of 'true' secondary PD (arrows) between a non-division wall separating scion and stock cells. Scale: 15 µm

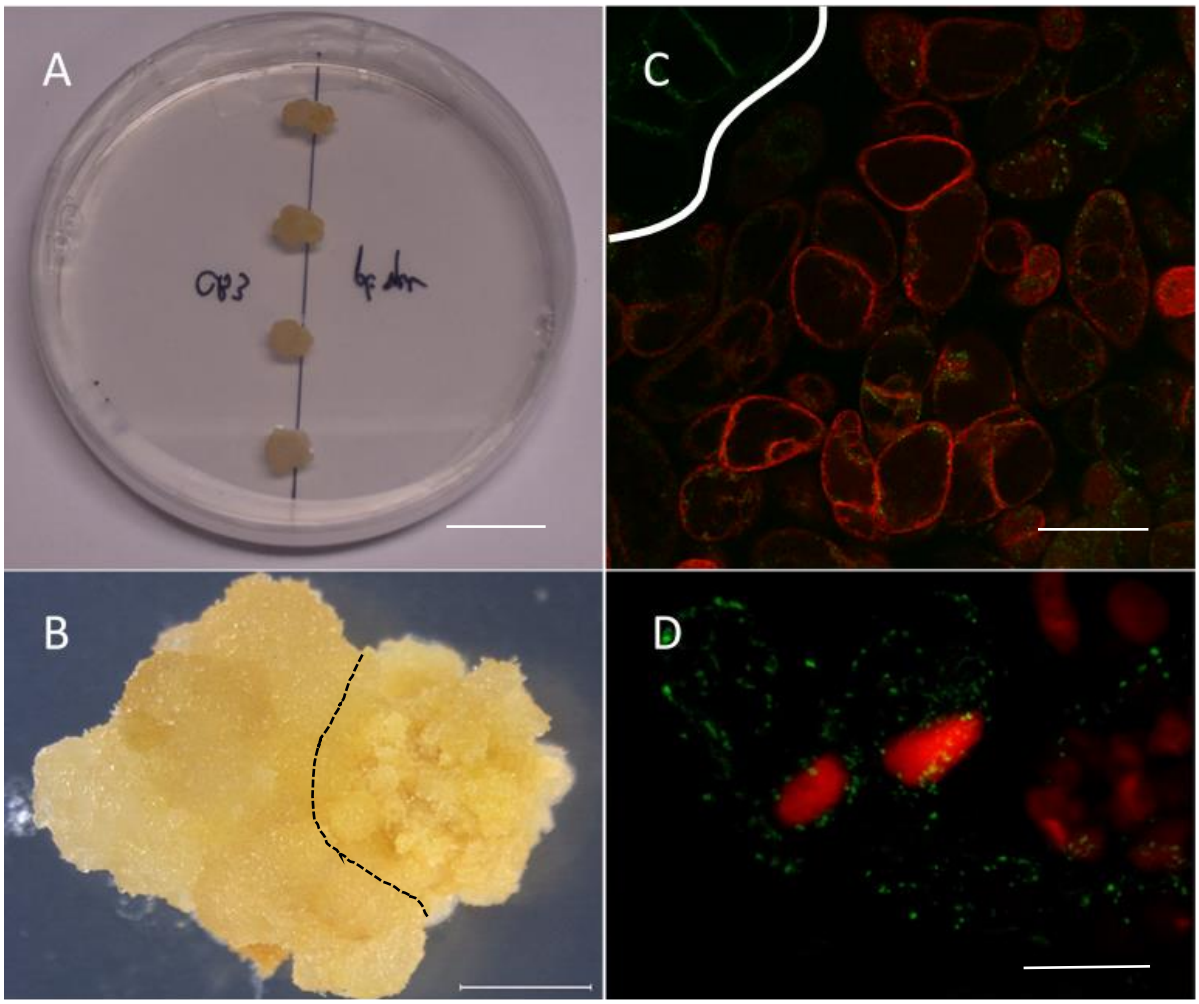

Figure 3.8. A. Tobacco calli of *35S*:TMV-30K-GFP and *Pt-spec*:GFP, containing a chloroplast marker (Stegemann and Bock, 2009), left to grow into each other on callus inducing media (CIM). Scale: 2 cm **C.** After two weeks, the fusion area of *35S*:HDEL-tagRFP and *35S*:TMV-30K-GFP (the two cell populations are delimited by the white line) shows cells which are doubly labelled indicating symplast recovery. Scale: 50 µm

B. Callus resulting from the fusion of a callus expressing *35S*:H2B-mRFP (left side) and another expressing *35S*:MP17-GFP (right side) as seen under the dissecting microscope. Dashed line: graft junction. Scale: 2 mm. **B.** Individual cells of the callus showing double labelling. Scale: 35 µm

3.3.5. Organelles may transfer during vascular remodelling

The transfer of organelles at the graft interface has been reported in tobacco for chloroplasts, nucleus and mitochondria (Stegemann and Bock, 2009; Fuentes *et al*., 2014; Gurdon *et al.*, 2016). The molecular events, leading to this mixing of organelles, are still unknown. It was suggested that organelles could move either through secondary PD or by intercellular transfer of small amounts of cytoplasm following local enzymatic removal of the cell wall separating the opposing stock and scion cells. To test this hypothesis, *in vitro* homografts and heterografts calli of *Pt-spec*:GFP, which were originally used in Stegemann and Bock (2009) to demonstrate chloroplast transfer, and *35S*:TMV-30K-GFP, were made. The former is a nuclear-transgenic line resistant to kanamycin, while *Pt-spec*:GFP is a plastid-transformed line resistant to spectinomycin. These calli were left to grow into each other for 2 weeks in the dark on callus inducing media (CIM) which is sufficient to obtain secondary PD in tobacco callus culture (see Figure 3.9). After this period, the fused calli were moved to CIM and regenerative media (RM) with antibiotics. The homografts were place on single antibiotic selection as a control, while heterografts were submitted to double selection. The calli were observed daily for 4 weeks to observe signs of regeneration on the selective media. In the positive control homografts, only greening of the tissue was detected as an indication of antibiotic resistance (see Figure 3.9). Kanamycin and spectinomycin both prevent plastid protein synthesis by interacting with the 30S subunit of the plastid ribosome which can cause chlorosis in susceptible plants (Pyke *et al*., 2000). In calli heterografts, antibiotic resistance would occur if a chloroplast or a nucleus was to be exchanged through secondary PD between the grafted partners. However, no heterografts displayed green tissue, showing a lack of resistance to the

double selection. There was therefore no exchange of plastids or nucleus between the grafted calli. Further work should include grafts *in planta* to confirm that doubly resistant callus cells can indeed be obtained. However, comparing these *in vitro* results to the published work of Stegemann and Bock (2009) indicates that PD alone cannot account for the exchange of large organelles. In that respect, it might be that vascular remodelling is necessary for organelle transfer. During vascular dedifferentiation, larger pores are created within cells sustaining high internal pressure. Both parameters might be a prerequisite for the transfer of large subcellular structure.

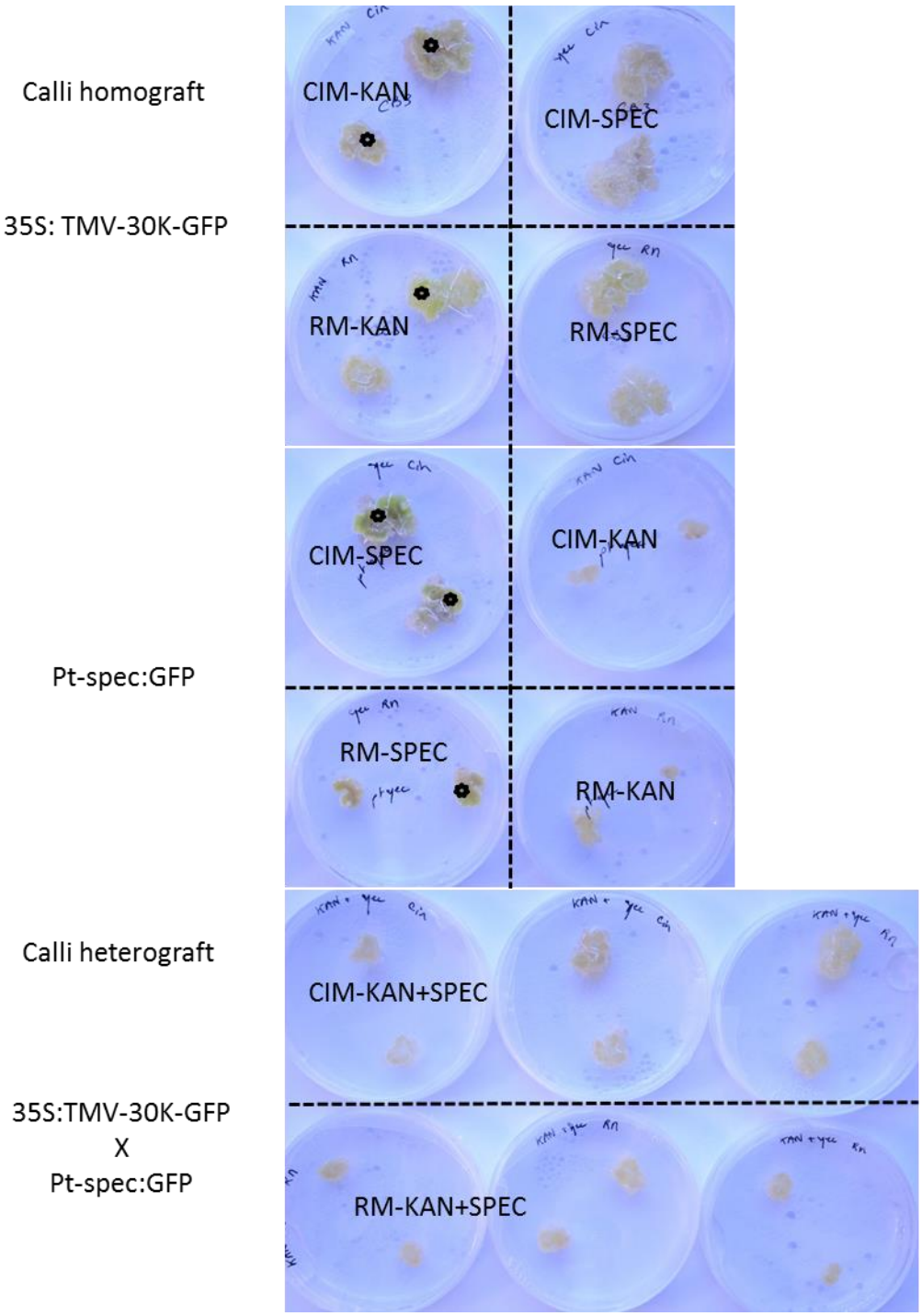

Figure 3.9: Grafted calli, 4 weeks after being placed on selective media. Heterografts on doubly selective media, whether CIM or RM, did not show greening tissue, indicating a lack of resistance to both antibiotics. The greening tissue in the homografts is highlighted by the stars. It only appeared on selective plates for which the calli had a known resistance. RM: regenerative media; CIM: callus inducing media; KAN: kanamycin; SPEC: spectinomycin

3.3.6. ALCATRAS (A Long-term Culturing And TRApping System) to study secondary PD formation *in vitro*

The ALCATRAS device was originally designed for the single cell analysis of yeast (Crane *et al*., 2014). It was adapted to *Arabidopsis* protoplasts by Dr. Ivan Clark. This microfluidic device consists of a PDMS block containing a chamber fed by two inlets (one to load the protoplasts and the other to give a constant flow of media), a filter and a waste outlet (see Figure 3.10). The optimal width of the filter was found from protoplasts measurements and experimental trials. Filters were tried with gaps ranging from 5 to 20 µm. 10µm gaps in the filter were found to best retain protoplasts while still maintaining flow. After trying a gravity feeding of protoplasts, pumps set at 0.1µl/min were found to be less disruptive when switching from the protoplasts to the media inlet.

Some protoplasts from a MP17-GFP x mCherry-LTi6b callus culture were successfully inserted and monitored for 12h with a continuous flow of PIM media (see Figure 3.11). It is unclear, however, from these primary results if the GFP signal picked up at 12h is labelling genuine secondary PD (see Figure 3.11.D). Cells could be monitored for longer period of time. Wu *et al.* (2011) reported the accumulation of cell mass from tobacco protoplasts cultured in a PDMS chamber for 12 days. Eventually, different media composition could be applied to assess their effect on the frequency of secondary PD formation.

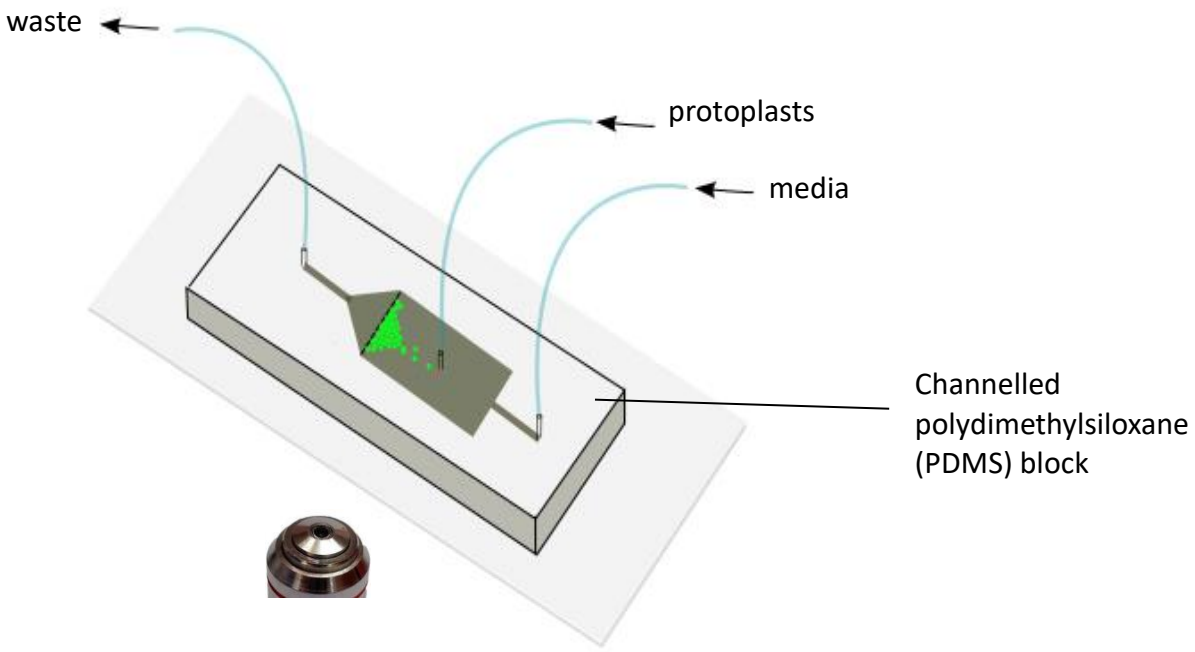

Figure 3.10: Experimental set up of the plant ALCATRAS. The device is fed protoplasts (green dots) through a tube attached to a pump set at 0.1µl/min. After loading, pumps are switched and media is passed through the device. Protoplasts can be observed through the coverslip with an inverted microscope.

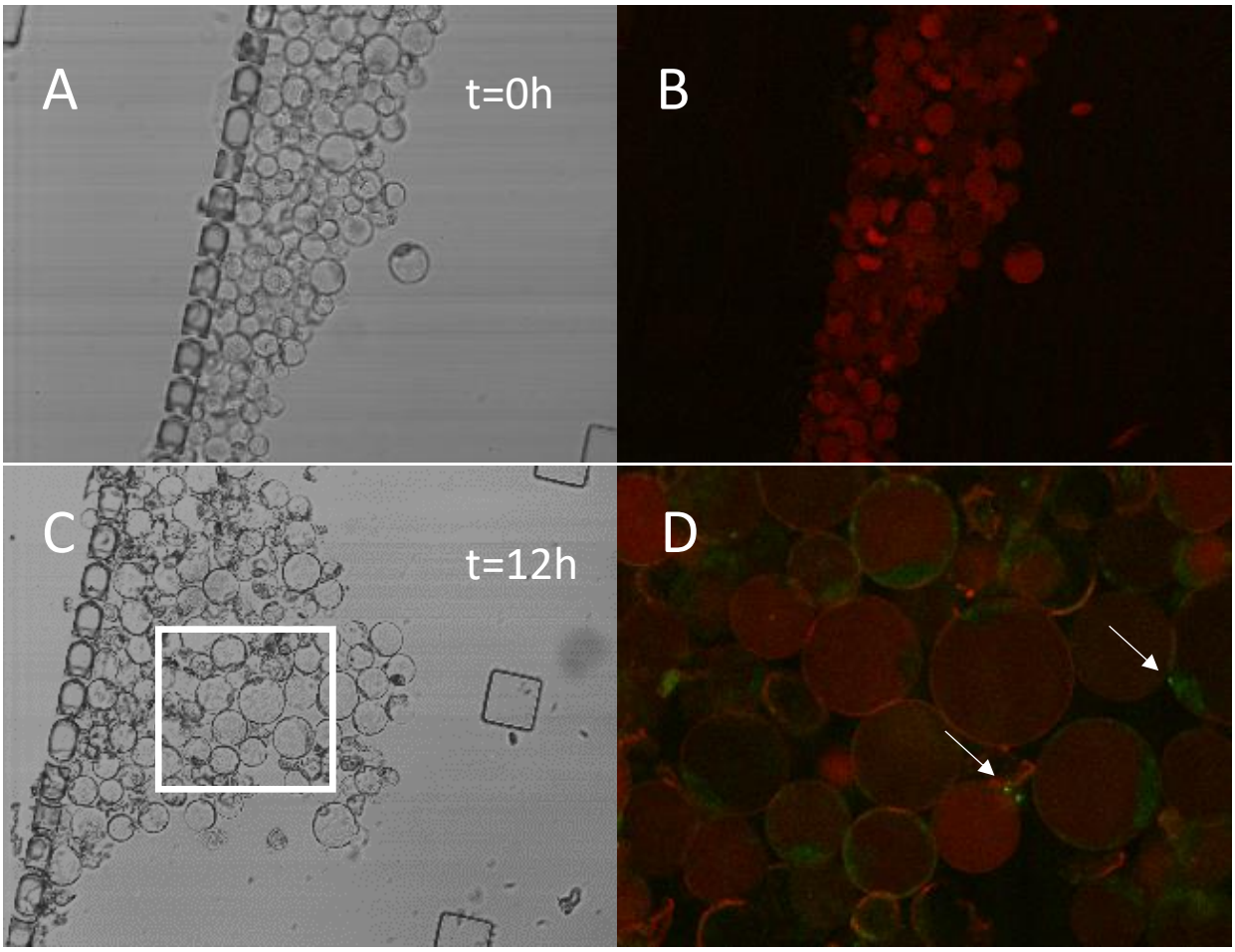

Figure 3.11: A. B. Device loaded with protoplasts of *35S*:LTi6b-mcherry x *35S*:MP17-GFP. No GFP was visualised before switching to the media pump (t=0h).

C. and **D.** (magnification of the boxed area in **(C)**) At t=12h, GFP accumulated in all cells. Some seemed to have a GFP signal on their outer wall (arrows) which could be either resulting from the formation of secondary PD or cell bursting.

3.4. Discussion

The use of LR white-embedded grafts offers a unique insight into cellular development during symplasmic recovery. The choice of appropriate markers can identify secondary PD. It can also be used to visualise organelles and might be relevant to observe a transfer *in planta* as suggested by Stegemann and Bock (2009), Fuentes *et al*. (2014) and Gurdon *et al.* (2016). However, this is only possible with reliable cell autonomous cellular markers. tpFNR-GFP was initially believed to be an adequate marker for monitoring chloroplasts transfer because of its subcellular compartmentalisation. This was thought to be sufficient to prevent passive diffusion through PD. However, cells expressing the *35S*:tpFNR-GFP construct extensively labelled cells in their grafted partner, suggesting that the protein escaped its origin of synthesis to unload/diffuse into a specific domain of the graft, the callus-derived stele. This domain might also contain small solutes such as auxin, which appears to concentrate in that region. Aniline blue labelling of the graft junction is required to confirm that PD are closed during callus formation. It is, however, tempting to assume that a graft would benefit from PD closure at the pericycle/endodermis boundary to establish an auxin gradient. This could enable rapid cellular division in the stele and the reconnection of the phloem (see Figure 3.12).

From this study, the *de novo* formation of secondary PD does not in itself facilitate organelle transfer. Attention should thus focus on the process of phloem remodelling across the graft union. In the WT scion grafted to *AtSEOR*:SEOR-YFP, large aggregates comparable in size to organelles were unloaded into 'living' cells in the graft partner. These cells might be connected to the differentiating vasculature by large pores which might eventually allow movement of organelles.

Interestingly, callus cells do not need a wounding signal to initiate the formation of secondary PD. A signal mechanism might be activated upon recognition of a peptide moiety and/or chemical after the first contact. However, protoplasts were observed to initiate secondary PD formation during the regeneration of their cell wall and in the absence of neighbouring cells (Ehlers and Kollmann, 1996). Unravelling the molecular events responsible for symplasmic fusion could help to understand the formation of secondary PD in other systems such the parasitic plant, *Cuscuta maxima*, and its hosts. A microfluidic devise such as the one developed in this study could allow different treatments (e.g. chemical/osmotic) to be applied on callus cells in order to observe their effect on the formation of secondary PD.

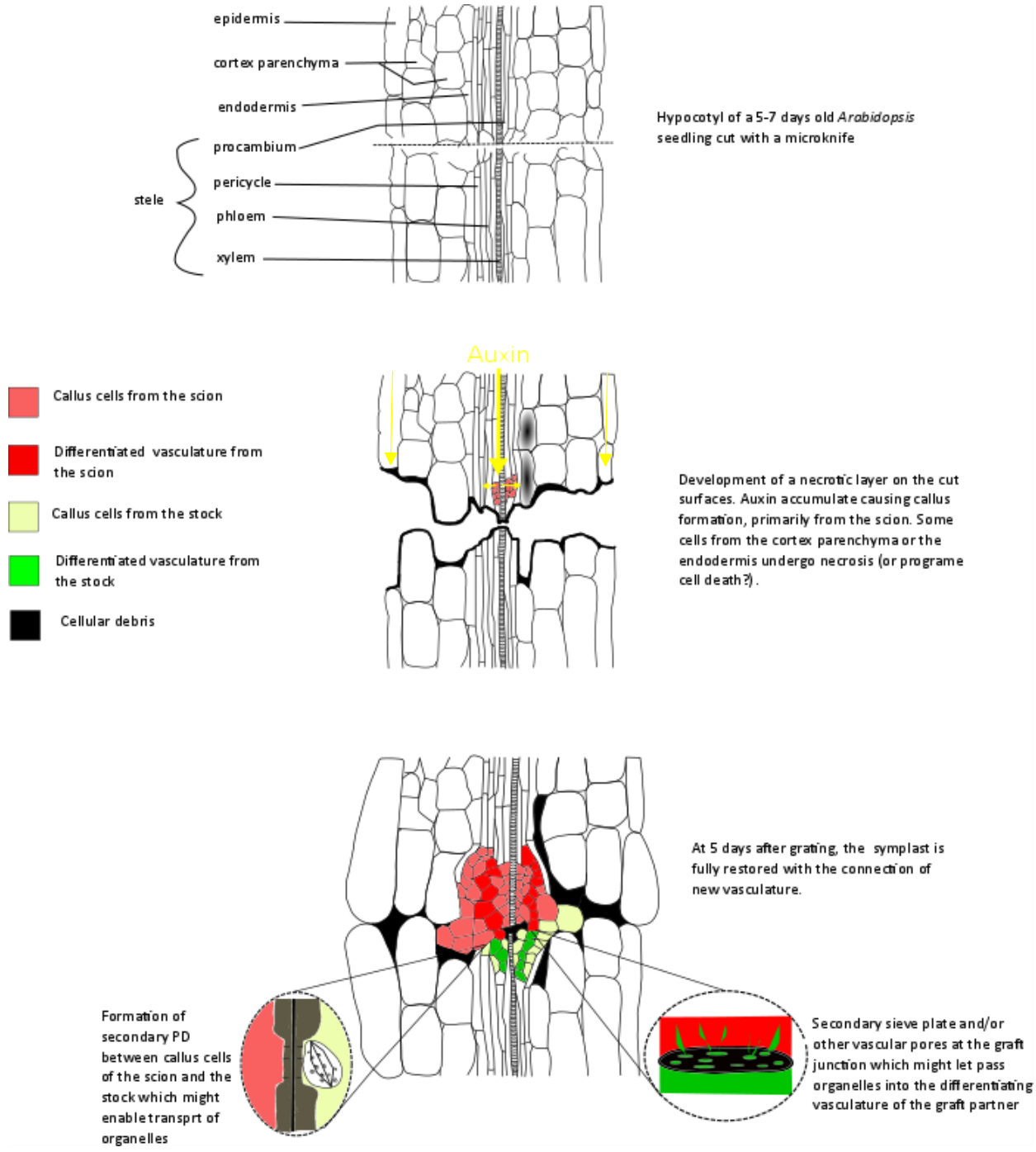

Figure 3.12: Shematic representation of the graft development including the possible events that lead to organelle transfer.

CHAPTER 4: Long-distance macromolecular transport across the graft junction

4.1. Introduction

The transport phloem is an elusive structure, difficult to access and observe. Studying any aspect of phloem-specific transport is therefore limited by technical restrictions. In particular, the nature and origin of the molecules translocated in sieve tubes cannot be established by microinjection or direct sampling of the sap. SEs are very thin (~3-4 µm wide in *Arabidopsis* (Froelich *et al.*, 2011)) which renders successful perforation with microneedles challenging. Moreover, the SE-CC complex is highly pressurised and often the target of pathogen to directly access food or the plant highway. It will therefore undergo drastic conformational changes upon mechanical stress. For instance, attempts at microinjecting high-molecular-weight fluorochromes in the SE/CC complex can lead to improper sealing of the plasma membrane, rapid gelation of the SE-contents and callose deposition (Kempers *et al*., 1993; Kempers and van Bel, 1997). This is reflected in an apparent under-estimation of the SEL of PPUs in reports using this method. In *Vicia faba*, the SEL of PPU was found to be around 10 kDa following the microinjection of fluorochrome-dextrans (Kempers and van Bel, 1997). In contrast, non-invasive methods such as the expression of fluorescently-tagged soluble proteins in CCs gave a much higher SEL (around 62 kDa for *Arabidospsis*; Stadler *et al*., 2005b).

Using aphids to feed on sieve tubes, sap leaking from cauterised stylets has been collected to determine compounds that are translocated in the phloem. Although sap collected from aphids is thought to be relatively pure, some contaminations can occur from the insect saliva. Nevertheless, stylectomy has enabled the detection of a broad range of proteins, mRNA and small RNAs present in SEs. However, constraints linked to this technique have led to the use of other extraction methods that might yield more sap than stylet exudate (Atkins *et al*., 2011).

Phloem exudate has also been collected from severed vasculature. To remove the obvious contamination from the surrounding tissue, the first exudation is disregarded. A chelating agent such as EDTA can be applied to prevent P-protein from coagulating and thus to maintain flow through the wounded surface (Tetyuk *et al*., 2013). Because of their inability to curb sap loss after incision, cucurbits have long been used as species of choice for this method (Atkins *et al.*, 2011). Zhang *et al.* (2010) showed, however, that the extrafascicular phloem (EFP) contributed most to the leaking exudate. This phloem is believed to be involved in defence and to exude a sap similar to latex. It forms a mesh of sieve tubes, outside the vascular bundle, that do not connect source to sink tissues (Gaupels and Ghirardo, 2013). This difference in function, when compared to the fascicular phloem (FP), is not only reflected in its metabolome but also in its proteome. When Zhang *et al.* (2010) compared the exudates of their sampled FP to published database, they found homology only for one protein (more than 1200 proteins were described in the phloem proteome of pumpkins, *Cucurbita maxima*; Lin *et al.*, 2009). In *Arabidopsis*, the analyse of phloem exudate from cut SEs has enabled the identification of more than 200 proteins with diverse metabolic functions (Batailler *et al*., 2012). Although, these proteins might be an over-

representation of phloem-mobile proteins. It has been shown that CCs undergo a drastic loss of pressure after the wounding of SE (Schulz, 2017) which might lead to intrinsic leaking into SE. It has also to be demonstrated whether their identified proteins are non-cell autonomous and translocated in sieve tubes to provide a long-range signalling function.

Grafting has proved valuable to assess the long-distance function of macromolecules in the phloem, avoiding the technical artefacts caused by sieve tube damage. Short-interfering RNAs were shown to be graft-transmittable and to successfully induce silencing in the recipient partner (Molnar *et al.*, 2010). The transmission of a floral stimulus was also initially observed in grafts which were made of a photo-induced plant part (donor) and a receptor bud. After the identification of FT in mutant screens looking at delayed flowering response, this protein was directly implicated as the flowering signal (Lifschitz *et al.*, 2006). In grafted tomatoes, the overexpression of the wild-type FT ortholog, SFT, in the donor was shown to rescue the *sft* phenotype in loss-of-function mutant. Using the same methods, the ability of FT to systemically induce flowering has since been confirmed in *Arabidopsis*, rice and cucurbits (Corbesier *et al*., 2007; Tamaki *et al*., 2007; Lin *et al*., 2007). One of the biggest questions arising when looking at macromolecules translocating in the phloem with a potential signalling function is whether these are selectively loaded into SEs or whether they reach the translocation stream by default. In this respect, the phloem has been alternatively compared to an 'information superhighway' (Jorgensen *et al*., 1998) and a 'sewage system' (Oparka and Santa Cruz, 2000).

So far, with the exception of viral components, no proteins or mRNA have been shown to reach SEs from other cells than CCs and immature SEs (Crawford and

Zambrisky, 1999). The high SEL of PPUs might suggest that most soluble macromolecules could diffuse freely from CC to SE. Could there be, however, a selective delivery of signals to and through PPUs? RNA binding proteins such as the 16-kD *Cucurbita maxima* phloem protein (CmPP16), have been found in SEs. CmPP16 is a paralog to viral movement protein (Xoconostle-Cázares *et al.*, 1998). After microinjection in mesophyll cells, it can interact with PD facilitating the cell-cell movement of dextrans and its own mRNA. Because this protein is present in SEs and is phloem mobile, it is thought to act as a mRNA chaperone at the CC/SE interface (Xoconostle-Cázares *et al.*, 1999). mRNA might indeed possess a sequence signal for phloem mobility. Zhang *et al.* (2016) recognized a tRNA motif that could enhance the movement of mRNA across the graft junction. Could this apply to most of the transcripts found in the phloem (more than 2000 transcripts were identified in an experiment by Thieme *et al.* (2015))? From a bioinformatic and statistical analysis carried out by Calderwood *et al.* (2016), the size and relative abundance of transcripts were found to be more relevant for transport in SEs. This suggests that passive diffusion of transcripts through PPU may prevail between CC and SE and that the SEL of PPU is therefore the delimiting factor to transport. Could this also apply to proteins?

4.2. Aim

In this chapter, the aim was to address the possible mechanism responsible for the movement of proteins from CC to SE. I show that not only soluble proteins but also reporter proteins carrying a subcellular localisation signal can be phloem mobile across graft union (Paultre *et al.*, 2016). It seems that the strength of the signal may

have an impact on transport, as well as the Stoke Radius of the fusion protein, which must fall below the predicted SEL of PPU. Most of the different signal proteins studied successfully reached their intended organelles in stellar cells of the rootstock after translocation. A statistical analysis of the phloem proteins in *Arabidopsis*, sorted by size and expression level, confirmed that macromolecules might be translocated more by default than design.

4.3. Results

4.3.1. Movement of chloroplast targeted proteins

The long-distance movement of chloroplast-targeted proteins was initially assessed in grafts made of a transgenic scion expressing the transit peptide of ferredoxin-$NADP^+$ oxidoreductase (tpFNR; Mulo, 2011) fused to GFP (tpFNR-GFP; Mr 35kDa), driven by the 35S promoter, and a WT rootstock (see Figure 4.1). The ability of the protein to cross the graft and reach the root tip was observed as early as 5 dag. In all homografts (n=50), a fluorescent signal was apparent in two cell files in proximity of the root meristem (see Figure 4.2.A). Under close examination, fluorescent plastids seemed to contained GFP in cells surrounding the protophloem (see Figure 4.2.B). Optical sections of the root revealed that labelled plastids were restricted to cells of the stele, including the pericycle, but not in the endodermis or cortex (Figure 4.2.C). As the roots continued to elongate, an increasing number of cells within the stele showed a GFP signal, resulting from the continued unloading of the protein near the root tip (Figure 4.2.D). Similarly, when lateral roots formed (~10 dag), the fluorescent plastid signal was associated with the terminal protophloem elements

of the emerging root (Figure 4.2.E). To test the capacity of tpFNR to gate PD, a binary vector carrying the transgene was bombarded onto leaves of *A. thaliana*. In all bombarded leaves, the expression of *35S*:tpFNR-GFP was contained within a single cell (Figure 4.2.F, n=100 cells). This indicates that, in epidermal tissue, tpFNR is cell-autonomous and does not increase the SEL of PD, confirming previous reports on the cellular compartmentalization of organelle proteins (Crawford and Zambryski, 2000). Transgenic lines expressing tpFNR-GFP driven by *SUC2*, a CC specific promoter, were made and grafted onto WT stock. The fusion protein was found to unload in an identical pattern to the one observed with a 35S promoter (see Figure 4.2.G). Because the *35S* promoter is expressed in CCs (Juchaux-Cashau *et al*., 2007; Corbesier *et al*., 2007; Mathieu *et al*., 2007), it is likely that tpFNR-GFP crosses the graft union by diffusing from CC into the adjacent SE and translocating in the phloem to the root tip.

Other chloroplast signals fused to GFP, expressed under the *35S* promoter, were tested for transport across the graft. Scions expressing the FP reporter fused to transit peptides for RecA homolog1 (CT-GFP; Mr 33 kDa), Rubisco subunit 1a (RBCS1a; CP-eGFP, Mr 37kDa) and plastocyanin (tpPC-eGFP, Mr 36k Da) were grafted onto WT rootstocks. At 10 dag, fluorescent plastids were observed adjacent to the terminal protophloem sieve elements in the root (movement of CP-eGFP shown in Figure 4.3.A; Table 4.1). The exception was the transit peptide for CT-GFP that, despite being smaller (Mr 33 kDa) than some of the other transit peptides, was not detected in any of the roots following grafting (Table 4.1).

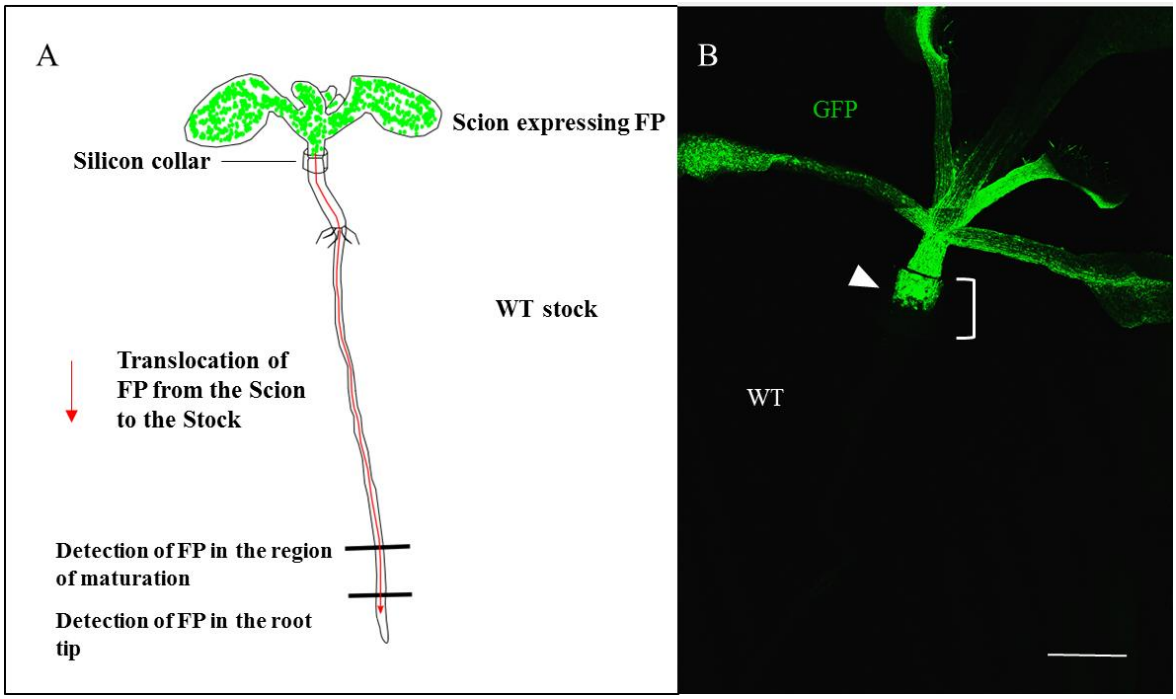

Figure 4.1. Experimental grafting system. (A) Transgenic scions expressing FP-fusions were grafted onto non-transgenic rootstocks using a plastic collar. 10 days after grafting (dag) the roots were examined for fluorescent protein (FP). (B) Fluorescence of the scion at the graft interface (the position of the collar is bracketed; the arrowhead indicates the graft junction). (Scale=1mm)

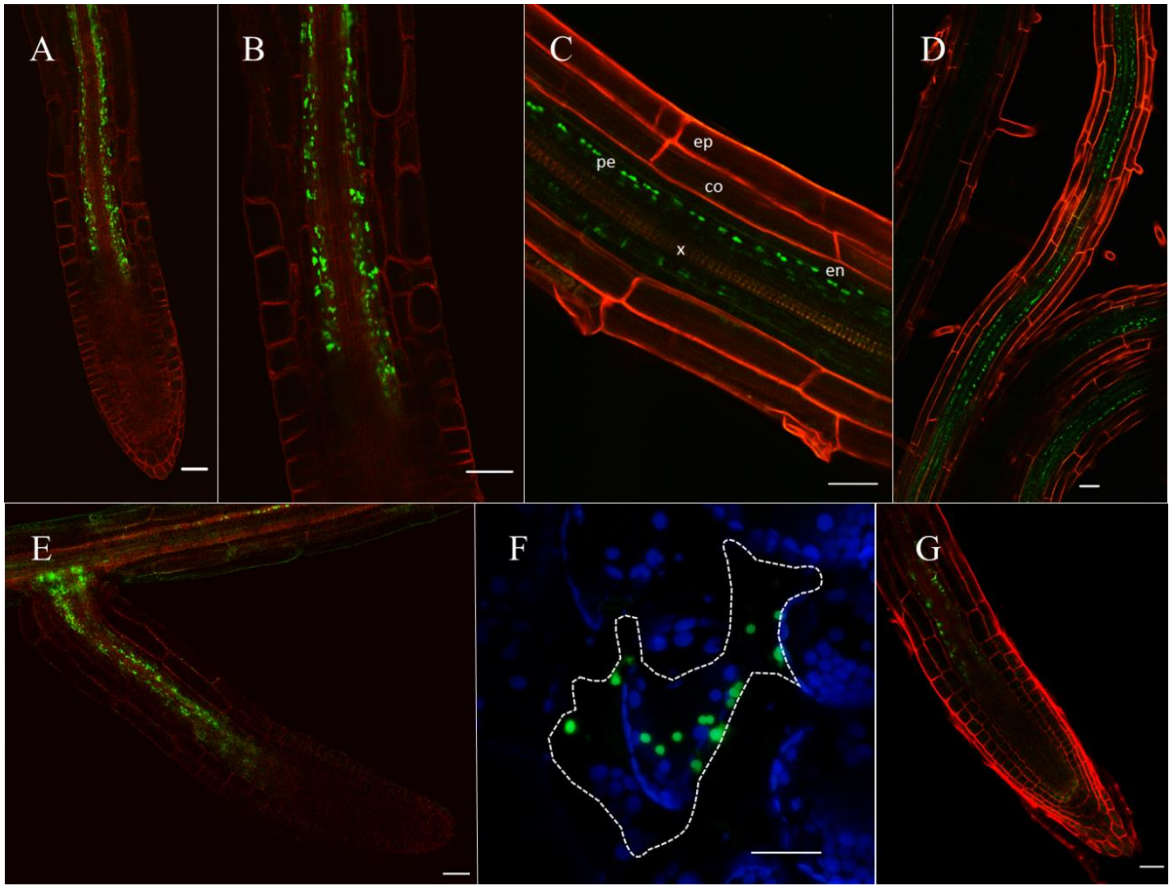

Figure 4.2. Translocation of tpFNR-GFP from scion to rootstock. At 10 dag a strong fluorescent signal was observed around the terminal protophloem sieve elements (A). (B) is an enlargement of A showing fluorescent plastids around the phloem poles. In the unloading zone of the root (C), fluorescent plastids are restricted to the stele (ep, epidermis; co, cortex; en, endodermis; pe, pericycle; x, xylem). (D), as roots continued to elongate the fluorescent signal remained confined to the stele. (E), emerging lateral root showing fluorescence around the phloem poles. (F), bombardment of tpFNR-GFP into single leaf epidermal cells (dotted lines) failed to show movement into surrounding cells. (G), expression of tpFNR-GFP from the *SUC2* promoter showed an identical pattern of fluorescence expression observed with the *35S* promoter. (Scale=30µm)

4.3.2. Movement of organelle-targeted proteins

The targeting of organelle proteins involves a variety of specialized mechanisms for protein transport. For chloroplast targeting, proteins are first recognised in the cytosol by a guidance complex made of the 14-3-3 protein and the heat shock protein, Hsp70. They are then directed to the translocon apparatus on the outer envelope of the chloroplasts (May and Soll, 2000; Lee et al., 2013). To test the retention ability of other transport pathways, scions expressing fluorescent reporters with targeting signals for peroxisomes (A5-eGFP), nucleus (H2B-YFP) and F-actin binding domain (FABD2-GFP) were grafted onto non-transgenic rootstocks. The fluorescent signal in the WT rootstock was compared to the transgenic scion to ensure an appropriate organelle targeting (see Figure 4.3 A-D and I-L). In all cases, unloading of the fluorescent fusion protein occurred in the equivalent subcellular structures of the stelar cells adjacent to the root protophloem (see Figure 4.3. E-H). Some of these fusion proteins contained a significant domain from the targeted protein (Table 4.1). The largest was FABD2-GFP with an estimated size of 67 kDa.

Table 4.1: Properties of protein fusions used in this study

Fusion Protein	FP	Size (kDa)	promoter	Targeted organelle(s)	In grafted root tip of Col	Frequency	Reference
Transit peptide (TP) of RecA homolog1: CT-GFP	S65T-mGFP4	~ 33	35S	chloroplast	no	100% N=20	Köhler et al, 1997
TP of RBCS1a: CP-eGFP	eGFP	~37	35S	chloroplast	yes	100% N=27	Unpublished
TP of FNR: tpFNR-eGFP	eGFP	~35	35S	chloroplast	yes	100% N=50	Marques et al, 2003
TP of Plastocianin: tpPC-eGFP	eGFP	~36	35S	chloroplast	yes	100% N=7	Marques et al, 2003
A5-eGFP	eGFP	-	35S	peroxisome	yes	100% N=32	Cutler et al, 2000
FABD2-GFP	S65T-GFP	~67	35S	actin	yes	67% N=29	Ketelaar et al, 2004
H2B-YFP	mYFP	~42	35S	Nucleus	yes	57% N=42	Federici et al, 2012
RTNLB6-GFP	sGFP	~57	35S	ER	no	100% N=5	Knox et al, 2015
sp-GFP-HDEL	mGFP4	~28	35S	ER lumen	no	100% N=15	Haseloff et al., 1997
STtmd-GFP	GFP	~33	35S	Golgi apparatus	no	100% N=14	Boevink et al., 1998
spRFP-AFVY	mRFP1	~33	35S	Vacuole	yes	100% N=5	Hunter et al., 2007

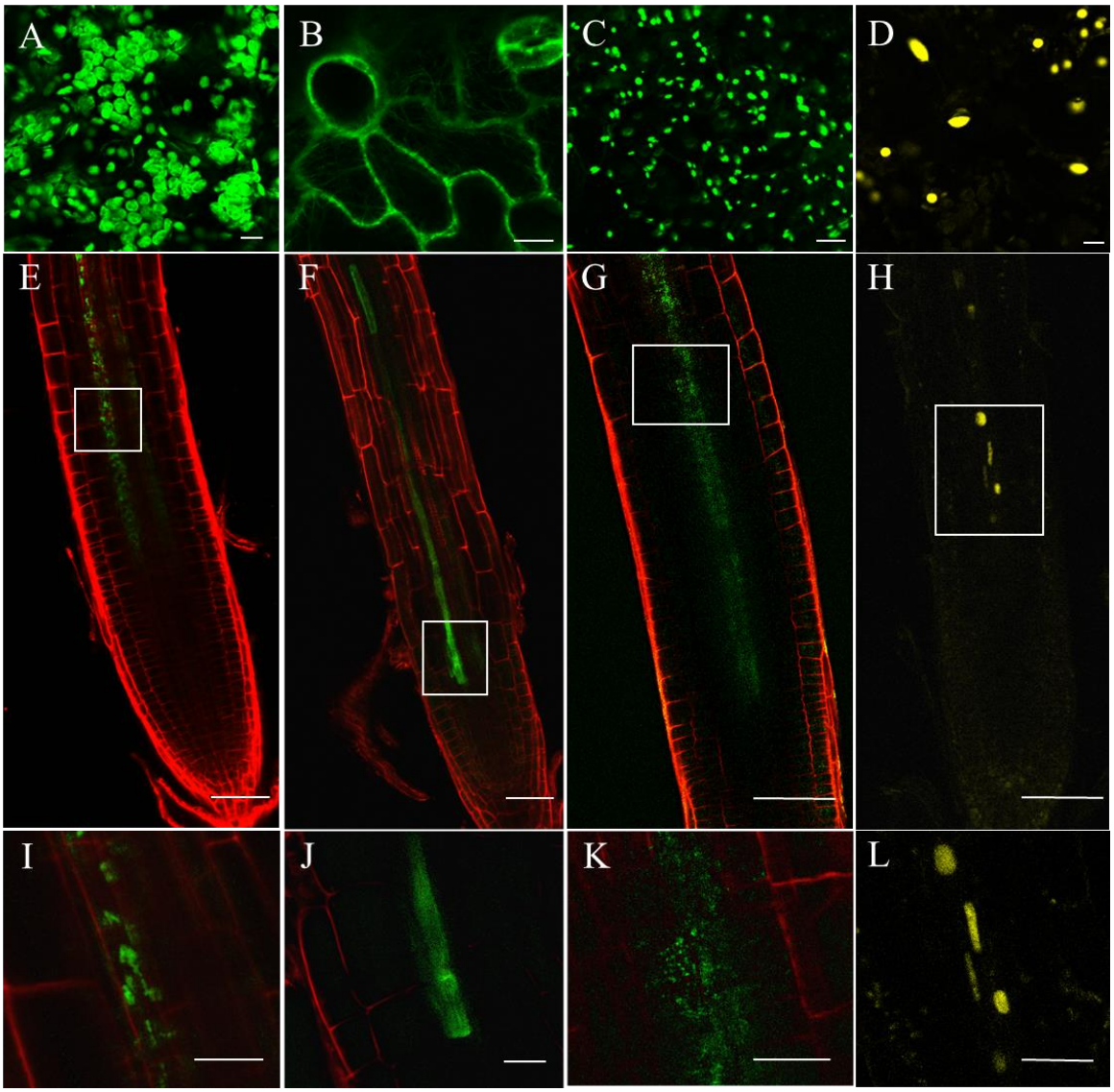

Figure 4.3. Phloem translocation across a graft union of (E), CP-GFP (chloroplast), (F), FABD-GFP (actin), (G), A5-GFP (peroxisome), and, (H), H2B-YFP (nucleus) markers (Scale = 50µm). The images compare the fluorescent signals from the transgenic scions (A-D; Scale = 10µm) with the non-transgenic rootstocks (I-L; Scale = 30µm). The boxed regions of the root are shown at higher magnification in the lowest panels.

4.3.3. Retention of Membrane bound proteins with the exception of vacuolar-RFP

Fusion proteins with a signal sequence for the secretory pathway were also tested for transport across the graft junction and unloading. These proteins use the co-translational translocation pathway. They are translated on ER-bound ribosomes, and destined for the endomembrane system. Lines expressing HDEL-GFP (ER lumen), reticulon 6 (RTNLB6)-GFP (ER membrane), sialyl transferase (ST) transmembrane domain-GFP (Golgi apparatus) and spRFP-AFVY were grafted onto WT rootstocks. With the exception of spRFP-AFVY, a fluorescent signal was not detected in the root for these fusion proteins at 10 dag (Table 1, see Figure 4.4). In the rootstock grafted to scions expressing spRFP-AFVY, the fluorescent signal was not localized in the vacuole but in the cytoplasm, indicating a mistargeting of the protein.

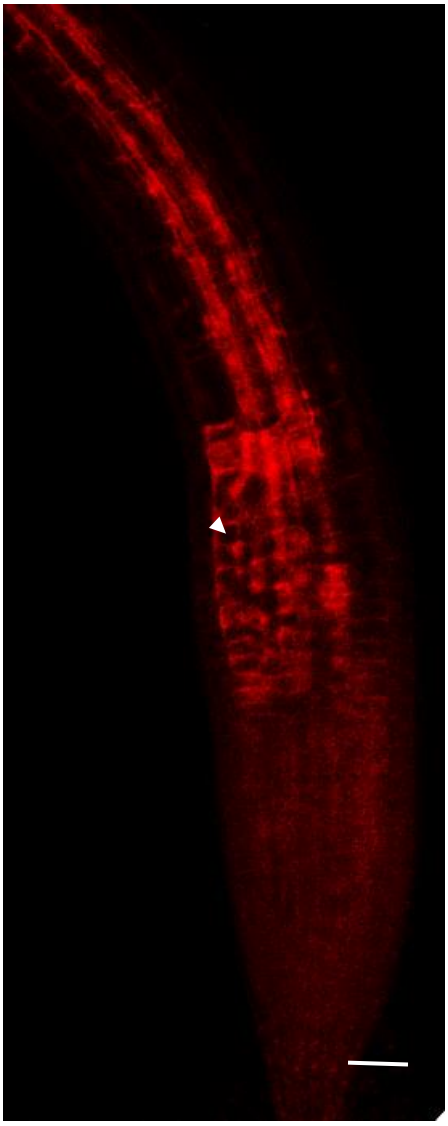

Figure 4.4: WT rootstock of a graft expressing 35S:sp.RFP-AFVY in the scion. A fluorescent signal is present in the unloading domain of the root at 10 dag. Although sp.RFP-AFVY is usually found in the vacuolar lumen, in the stock cells, the fluorescence was restricted to the cytoplasm. Arrowhead pointing at a non-fluorescent vacuole. Scale: 50 µm

4.3.4. mRNA analysis

Using RT-PCR, the non-transgenic rootstocks of between 18-24 graft partners were examined for evidence of mRNA trafficking. In this experiment, two chloroplast signal peptides (tpFNR-eGFP and CP-eGFP) and a peroxisomal signal sequence-fused GFP (A5-eGFP) were used. They all showed consistent movement across the graft union (Table 1). However, the mRNA of any of these fusion proteins were not detected in roots at 5 weeks after grafting (Figure 4.5) suggesting that mobile proteins are the likely source of fluorescent signals in the developing root tissues. To confirm that protein expression was visible at this time point the root tips were examined under the confocal microscope. For all three graft partners, a clear fluorescent signal was observed adjacent to the protophloem, although the signal was weaker than at 10 dag (see Figure 4.5).

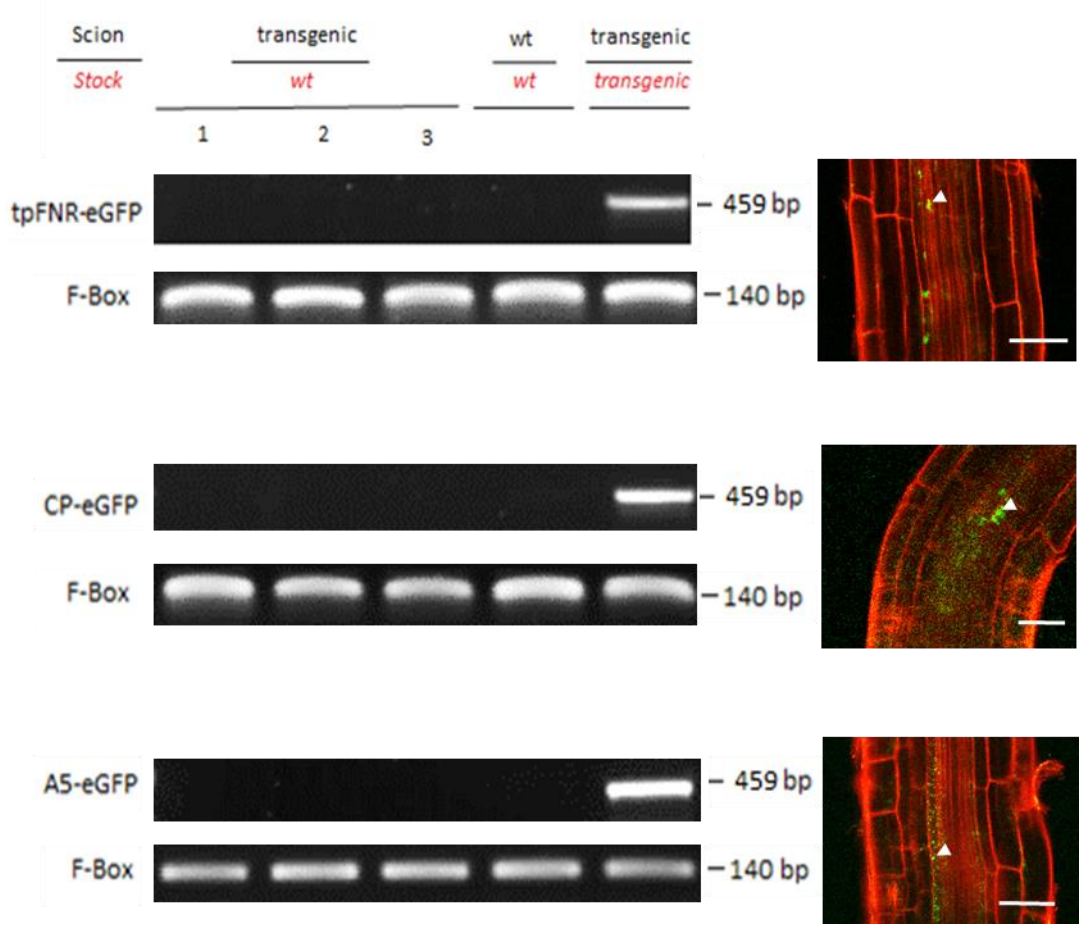

Figure 4.5. RT-PCR of different graft combinations at 5 weeks after grafting to detect the respective mRNAs present in the rootstocks when scions expressed tpFNR-eGFP, CP-eGFP (chloroplast) or A5-eGFP (peroxisome) protein signals (sampled tissue highlighted in red italics). Corresponding images of protein localization in the root at 5 weeks after grafting are shown to the right (Scale=50 µm).

4.3.5. Bioinformatic and biostatistic analysis

In these grafting experiments, GFP-fusions were expressed under the strong promoters *35S* and *SUC2*, raising the possibility that protein overexpression in CCs may have contributed to loss of fusion proteins to the SE. To address this issue, published data were examined relating to the profile of proteins found in the translocation stream, an approach independent of expression of GFP-fusions. A bioinformatic analysis was conducted on data concerning the occurrence of mRNAs in phloem tissue and proteins in the phloem exudate in relation to their corresponding molecular weight (data derived from Deeken *et al*., 2008; Batailler *et al*., 2012). Phloem-mobile proteins with known organelle-targeting sequences were separated from those without such sequences (Figure 4.6.A). In total, 149 proteins (52%) detected in phloem exudate were shown to have organelle-targeting sequences. The relative distribution of these proteins among different subcellular organelles is shown in Figure 4.6.B. Their corresponding gene expression levels in the phloem were not significantly different from other phloem-mobile proteins that lacked targeting sequences ($p=0.07$; non-parametrical statistical test), which rules out the possibility that mobile proteins with an organelle-targeting sequence are found in the phloem exudate only at high levels of gene expression. The data also reveal that the majority of proteins entering the translocation stream cluster in the size range 20-70 kDa, suggesting that molecular weight, or more specifically Stokes Radius (Dashevskaya *et al*., 2008), may govern the passage between CC and SE. This was confirmed using a logistic regression model that examined the impact of both protein size (kDa) and transcript abundance on the likelihood of a given protein to be found in phloem exudate

(Figure 4.6.C). The model shows that for proteins below 70 kDa there is an exponential-like relationship between gene expression level and protein size, i.e, the more abundantly a protein is expressed, the more likely it is to enter the translocation stream. Above 70 kDa the probability of a protein entering SEs declines dramatically, consistent with a simple diffusive model based on the size exclusion limit (SEL) of the pore-plasmodesmata that connect SEs and CCs (Stadler *et al*., 2005b). A small number of proteins detected in phloem exudate exceeded 70 kDa, one example being a chloroplast-targeted protein (AT5G04140; 179 kDa), arrowed in Figure 4.6.A.

A

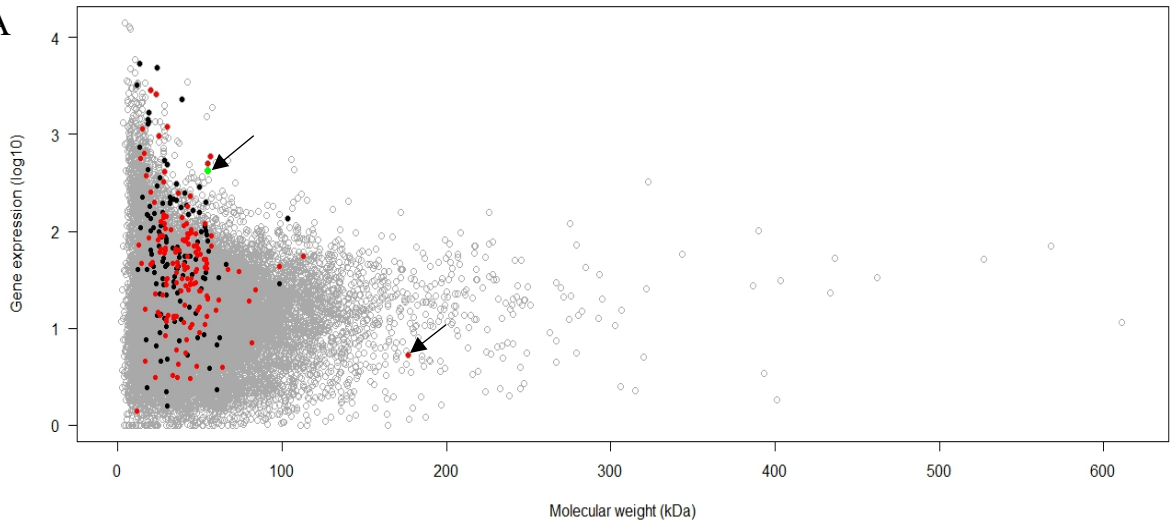

B

Subcellular location	Frequency	Percentage
Nucleus	20	7.0
Chloroplast	63	22.0
Mitochondrion	25	8.7
Peroxisome	7	2.4
Cytoskeleton	4	1.4
Cell membrane	3	1.0
Secreted	17	5.9
Vacuole	6	2.1
Glyoxysome	1	0.3
Endoplasmic reticulum	2	0.7
Total	**149**	**51.9**
Cytoplasm	59	20.6
Undetermined	79	27.5
Total	**138**	**48.1**
Total	**287**	**100**

C

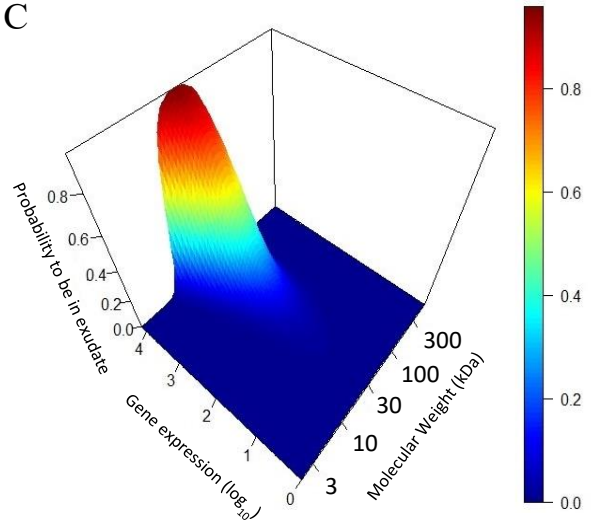

Figure 4.6. (A) Bioinformatic analysis showing relationship between proteins expressed in the phloem and those detected specifically in phloem exudate. The majority of phloem-mobile proteins cluster in the size range 20-70 kDa. The outlying arrows indicate a 179 kDa chloroplast-targeted protein and the green dot corresponding to *SUC2* expression. Data were derived from Deeken *et al.* (2008) and Batailler *et al.* (2012). Proteins with organelle-targeting sequences (red) are discriminated from those without such signals (black). (B) Table showing relative allocation of mobile proteins to different subcellular organelles and structures. (C) Figure showing the probability of proteins to be found in exudate according to gene expression and molecular weight. Gene expression and molecular weight are shown in base-10 logarithm.

4.3.6. Movement of FT-GFP in roots of *ftip1-1* mutants

The movement from CCs to SEs of FT-GFP, when expressed under the *SUC2* promoter, was shown to be hampered in the *ftip1-1* mutant (Liu *et al*., 2012). In these mutants, the protein failed to unload in the shoot apical region of 11 day-old seedlings. However, a GFP signal was perceived in these same mutants and in *SUC2*:FT-GFP *ft-7* in the root unloading domain 10 days-post germination (see Figure 4.7.A and B.). The signal was measured ~210 µm above the root tip. This falls within the unloading domain described by Stadler *et al*. (2005b) where *SUC2* was reported not to be expressed at this developmental stage.

Figure 4.7: movement of FT-GFP expressed under the SUC2 promoter in the root unloading domain of **A.** *ft-7* and **B**. *ftip1-1*, 10 days-post germination. Scale: 50 µm

4.4. Discussion

Soluble proteins as large as 67kDa were reported to escape CCs to reach the protophloem unloading domain when expressed under the strong CC-specific promoter, *SUC2* (Stadler *et al*., 2005b). This study shows that the same rule might apply to proteins that are usually targeted to specific cellular compartment. Proteins targeted to chloroplast, nucleus, peroxisomes, actin filaments and vacuoles were found to be phloem mobile and were unloaded in a sink domain adjacent to the protophloem. With the exception of the vacuolar lumen protein, these proteins all targeted their appropriate organelles in root stellar cells. This might reflect a lack of helper proteins necessary for certain posttranslational and co-translational transport pathway in CCs. Targeted proteins can form large complexes during their transport. The 14-3-3/Hsc70 complex was estimated to be 200 kDa when bound to a chloroplast protein (May and Soll, 2000) which is larger to the estimated SEL of PPUs. Because the *35S* promoter is highly expressed in CCs, flooding CCs with targeted proteins, that have a Stoke Radius falling under the SEL of PPUs, could saturate certain transport pathways and/or binding sites leading to their diffusion into SEs. The biostatistical analysis, based on previous published data, showed that the phloem mobility of a protein was more affected by its abundance and size rather than its subcellular location. These factors were also found to be a prerequisite for the transport of mRNAs (Calderwood *et al*., 2016).

The apparent diversity of proteins and mRNA translocating in SE has raised many questions on their role in long-range signalling. While some have been identified as key regulators for developmental and defence responses, most of them have no known systemic function. mRNAs are thought to be mainly involved in developmental

long-distance signalling. For example, BEL1-type homeodomain proteins, are thought to function as long-distance signals involved in tuberisation (Banerjee *et al*., 2006), while the Mouse Ears (*me)* mRNA affects leaf development in tomato (Kim *et al*., 2001). The extent to which these mRNAs are translated in sink tissues remains unknown (Spiegelman *et al*., 2013). Systemic-acquired resistance (SAR) is initiated by protein signals entering the translocation stream from tissue undergoing a pathogen attacked, priming distant tissue for defense (Fu and Dong, 2013). In most of these instances, the signals are produced in CC before reaching the SE. A common feature emerging from these long-distance signals is that they are produced temporally, i.e., within a discrete time window, in response to a developmental stage or sudden pathogen attack (Fu and Dong, 2013). Thus, one could envisage a scenario in which the movement of protein signals in the phloem is regulated by the timing of their translation in CCs.

The movement of FT-GFP in *ftip1-1* illustrates this scenario. In this mutant, FT-GFP does not reach the shoot sink tissue (Liu *et al*., 2012) but it is unloaded in the root tip. FT-GFP is a soluble protein with an estimated molecular weight of 47 kDa (below the SEL of PPUs). In the *ftip1-1* mutants, the expression of the protein is driven by *SUC2*, a promoter that is also active in root CCs. It can be argued that FT-GFP leaks from CCs that would not normally contain FT. In shoot CCs, there might be a retention mechanism for FT that is relieved by FTIP1-1. In the study of Stadler *et al*. (2005b), the fusion proteins were chosen as 'inert' soluble proteins which are not normally present in CCs of *Arabidopsis* (patatin is from potatoes and sporamin from sweet potatoes). These proteins could therefore easily reach the SEs because CCs have no means of retaining these foreign proteins. PPUs do indeed have a high 'native' SEL,

suggesting that gating of PPUs may be redundant for most proteins. It might be sufficient to either release small proteins from larger complexes or, for large macromolecules (> 70 kDa) modify their secondary structure with chaperones to form smaller heterooligomers. In this respect, the tRNA motif, described by Zhang *et al.* (2016), which conferred long-distance movement to otherwise inert mRNA, might have changed the Stoke Radius of these macromolecules once recognized by a RBP (RNA binding protein).

A plethora of macromolecules are transported in the translocation stream. For pressure flow to occur, these should eventually be removed from SEs to the risk of causing obstruction. These data indicate that macromolecules are removed from the protophloem at its terminus and 'sorted' within pericycle cells, preventing a potential hindrance to flow in SEs. Thus, a protein targeted to chloroplast in a leaf CC may eventually reach a plastid in a root pericycle cell. The fate of 'native' soluble proteins that leave the protophloem is still currently unknow. Similarly, it remains to be shown if all the mobile mRNA species detected in phloem exudate (Calderwood *et al*., 2016) enter this post-phloem domain. The challenge for future research will consist in identifying true signaling molecules which would cause a response beyond the pericycle boundary. Indeed, these cells might act as a 'recycling center', sorting constitutively leaking proteins from true signals, eventually relaying the information to the rest of the tissue.

CHAPTER 5: Phloem Pole-Pericycle cells are the recipients of translocated macromolecules in the root

5.1. Introduction

Since Münch first suggested an osmotically-driven mass flow in SEs (Münch, 1930), efforts have been made to unravel how accumulation and dispersal of photo-assimilates is achieved at the extremities of the phloem. The function of the phloem is linked to structural differences of the SE/CC complexes. While CCs are much larger than SEs in photosynthesizing tissue (source), they decrease in size along the pathway towards sugar-consuming tissues (van Bel, 1996). It appears that the phloem can therefore be divided into three zones; the collection phloem, in sources, the transport phloem that carries out most of the translocation, and the release phloem associated with sink tissues (van Bel, 2003).

In the collection phloem, CCs may take different forms depending on species and the mechanism by which sugar(s) are loaded into the SE/CC complex. In symplasmic loaders, sugars are transported against a sugar gradient in the symplasm to intermediary cells (ICs) which are highly connected to the surrounding leaf parenchyma (LP; with a density varying between 10 to 60 PD per μm^{-2}). In apoplasmic loaders, transfer cells (TCs) are relatively isolated from LP (with a density mostly lower than 0·01 PD μm^{-2}), and the TC/SE complex relies on the active transport of sugars across the PM from the apoplast (van Bel, 2003). In *Arabidopsis*, this is carried out by the H^+-sucrose symporter, SUC2 (Lalonde *et al.*, 2004). While SUC2 is essential to maintain sucrose uptake and turgor pressure in the collection phloem, it is

also required to prevent leaking of sucrose from SEs, and hence dissipation of pressure in the translocation phloem (van Bel, 2003).

The release phloem presents more diversity than the collection phloem because of the variation displayed in storage and utilization sinks. Photo-assimilates can be unloaded symplasmically, apoplastically or both, depending on the nature of the sink (Oparka, 1990; Stadler *et al*., 2005a). In developing apple fruit, the SE/CC complexes in the sepal phloem were found to be symplasmically isolated from the fruit, suggesting that sugars are unloaded from the apoplast (Zhang *et al*., 2014). Symplasmic markers, such as GFP and fusions of this protein, when expressed under the *AtSUC2* promoter, have enabled a more detailed description of symplasmic unloading domains. Stadler *et al*. (2005a) showed, using a transgenic line expressing *AtSUC2*:GFP, that the different layers of the seed coat can be represented as a mix of symplasmic and apoplastic unloading domains. The outer integument of *Arabidopsis* seeds was found to form a post-phloem unloading domain isolated from the endosperm, which effectively acquires sugars from the apoplast (Stadler *et al*., 2005a). In leaves, sink domains can quickly change to source. During this sink/source transition phase, minor veins receive photo-assimilates from the symplasm after the unloading of class III veins into mesophyll cells. Mature minor veins can then become symplasmically isolated due to the downregulation of PD and then start to load sugars apoplastically (Roberts *et al*., 1997).

The unloading domain of the root protophloem is easily accessible for imaging and has been described on multiple occasions (Oparka *et al*., 1994; Stadler *et al*., 2005b; Paultre *et al*., 2017). The soluble phloem probe, 5(6) carboxyfluorescein (CF), was first shown to symplasmically unload from the root protophloem radially towards

the epidermis (Oparka *et al*., 1994). Macromolecules were found to take the same path (Stadler *et al.*, 2005b). However, GFP-fusion proteins larger than 27 kDa were restricted to the perycicle/endodermis boundary (Stadler *et al*., 2005b; Paultre *et al*., 2016). Interestingly, targeted proteins unloaded into this domain became localised to their appropriate subcellular structures (Chapter 4; Paultre *et al*., 2016). Many macromolecules travel in the translocation phloem and presumably these reach this unloading domain. This domain might therefore act as a 'recycling' or 'sorting' centre, ensuring the non-obstruction of the protophloem terminus. This could be essential in a pressure driven system. Occlusion at the consuming end of the phloem might cause an increase in pressure and a subsequent dissipation of the turgor gradient between source and sink.

5.2. Aim

The aim of this Chapter was to identify the 'post-phloem domain' described in Chapter 4 using a combination of experimental approaches. This was achieved in collaboration with Prof. Yka Helariutta (Cambridge), Prof. Michael Knoblauch (Washington State University) and Prof. Kaare Jensen (Copenhagen). Here, I describe my contribution to this joint work. The full report is now published (Ross-Elliot *et al*., 2017). The fusion proteins used in Chapter 4 were all contained in pericycle cells. Possible candidates that might affect the SEL of PD in these cells were also investigated using different graft combinations with mutant rootstocks. Mutants in vascular callose synthases were first studied, as well as putative non-cell autonomous

proteins, NaKR1-1, a CC-specific metal transporter shown previously to escape the protophloem unloading domain as a 61-kDa fusion protein (Tian *et al*., 2010).

5.3. Results

5.3.1. Macromolecules unload into the PPP

The P-protein, SEOR, fused to YFP, expressed under its native *AtSEOR* promoter, was reported to unload as large aggregates into stelar cells adjacent to the root protophloem. These cells showed the same localisation, at the endodermis/pericycle boundary, as the one described in Paultre *et al.* (2016) and Ross-Elliott *et al*., (2017; Figure 5.1.C). However, while the fluorescence of organelles was conserved in the elongating zone of the root, aggregates of SEOR-YFP appeared to be quickly degraded (Ross-Elliott *et al*., 2017). Because SEOR-YFP aggregates are large and strongly fluorescent, the protophloem unloading domain, described in Chapter 4 of this thesis, and in Stadler *et al.* (2005b), was examined using *AtSEOR*:SEOR-YFP roots embedded in LR white (Chapter 3; see also Bell *et al*., 2013). Confocal scanning of semi-thin sections revealed that SEOR-YFP was unloaded into the phloem-pole pericycle cells (see Figure 5.1.A and B). In the eventuality that SEOR-YFP protein had diffused from immature sieve elements into the PPP, scions expressing *AtSEOR*:SEOR-YFP were grafted onto WT rootstocks. The unloading pattern of the fluorescent aggregates was identical to the one found in the *AtSEOR*:SEOR-YFP transgenic line (see Figure 5.1.C, D and E).

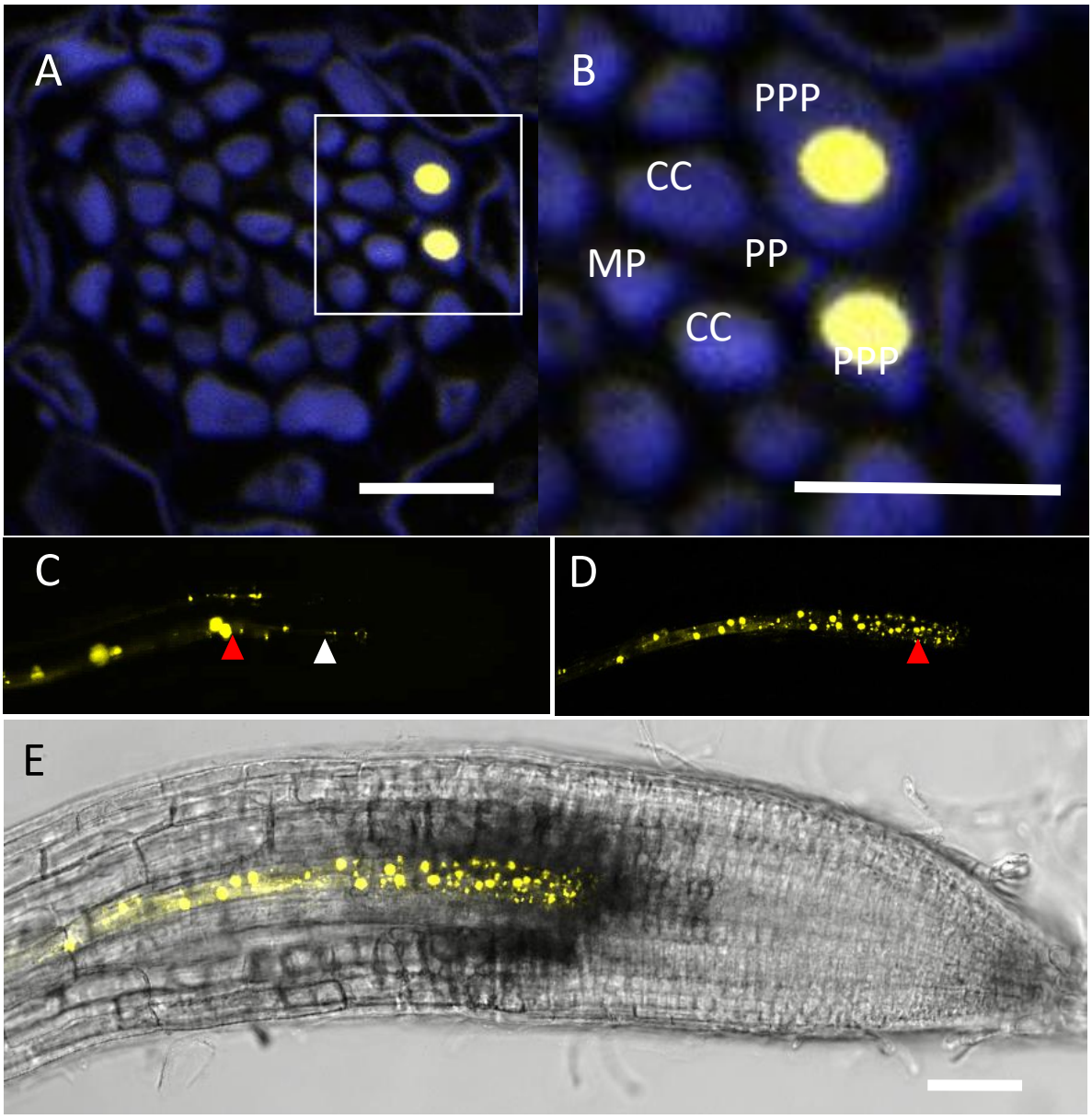

Figure 5.1: A. and B. Root cross section of a fixed and embedded transgenic Arabidopsis plant expressing SEOR-YFP protein. The micrograph identifies the two cell files into which SEOR-YFP escapes as the PPP. Scale: 10 µm **C.** Confocal imaging of the protophloem unloading zone in *AtSEOR*:SEOR-YFP roots showing the PPP (red arrowhead) and the developing protophloem (white arrowhead) compare to the one found in WT rootstock grafted on an *AtSEOR*:SEOR-YFP scion **D. E.** Scale: 50 µm.

5.3.2. Primary root growth is arrested after occlusion of PD at the SE/PPP interface

The effect of PPP-specific PD closure was examined on root development using an estradiol-inducible line which was constructed based on the LexA-VP16-ER (XVE)-derived *icals3m* system (Vatén *et al*., 2011; Yadav *et al*., 2014; Ross-Elliott *et al.*, 2017). In this system, the expression of *XVE* is driven by the PPP-specific promoter, *cals8,* and the XVE-targeted promoter initiates the transcription of *cals3m,* encoding for a CALS3 mutant protein (Vatén *et al*., 2011). Induction was shown to cause accumulation of callose at PD present at the SE/PPP and PPP/endodermis interfaces (Ross-Elliott *et al*., 2017). Seedlings were placed at 4 days post stratification on either MS media, DMSO or estradiol plates. Root growth was measured at 4h, 8h, 24h and 48h after induction (see Figure 5.2.A and B). There was no significant difference (α=0.05; p-value=0.45) in root growth (in the first 4 hours) between induced and non-induced seedlings (n=40 seedlings for each condition). After 4h, however, the growth of roots in estradiol plates was more than halved compared to the controls. At a rate of less than 50 µm/h, root growth was considered to be arrested. These rates were maintained for the period of observation. Seedlings kept on estradiol plates for 5 days showed a reduced primary root with more lateral roots than the controls (see Figure 5.2.C).

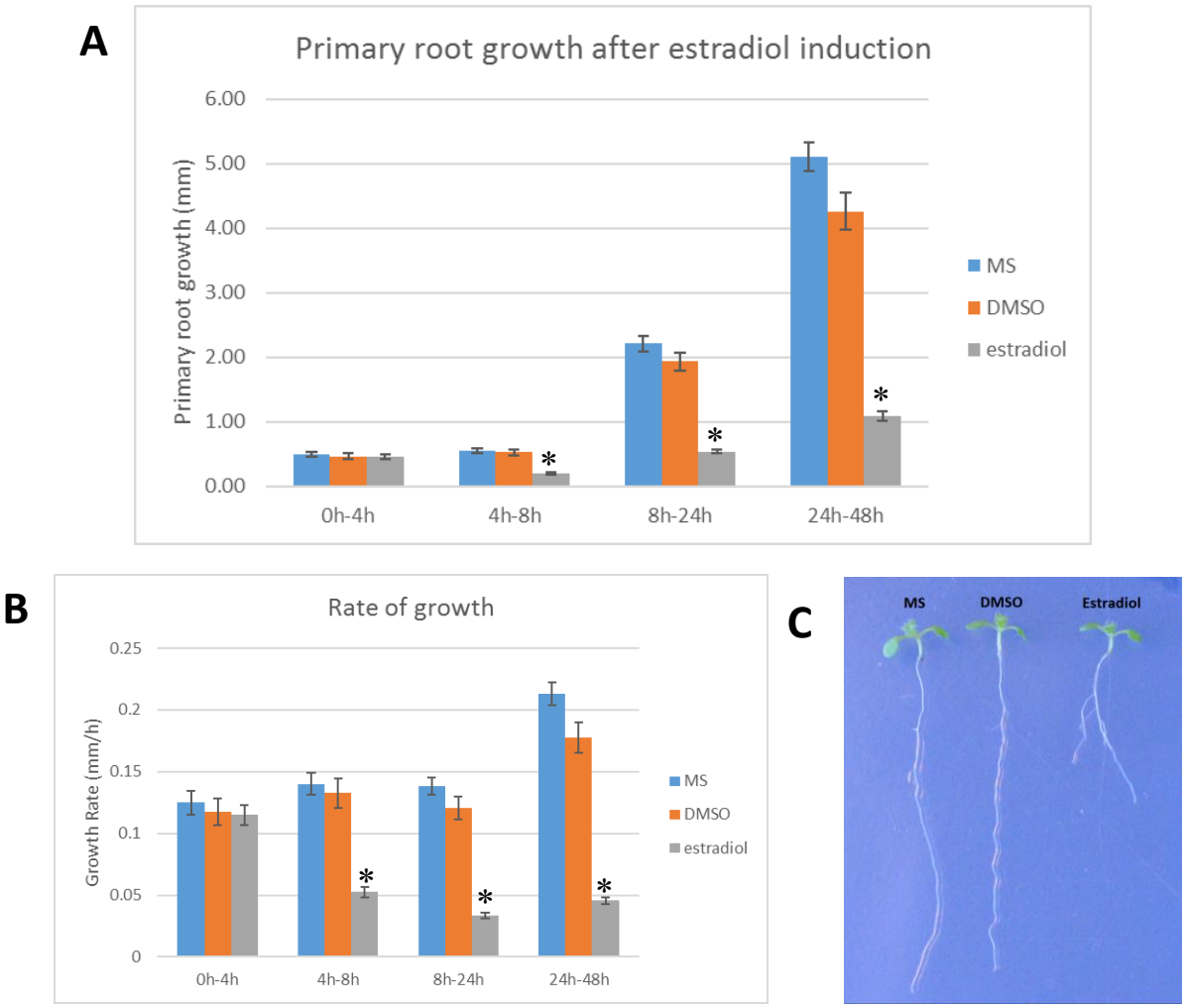

Figure 5.2: A. Measurements of primary root growth of *CalS8*:iCalS3m seedlings at different time point after being placed on estradiol media, MS or DMSO. These data were converted into rate of growth (**B)** Bars indicate Standard Error of the Mean (n=40). Significantly different data (α=0.05; respectively p-value=3.10^{-12}, 10^{-22} and 10^{-28}) are highlighted by a star **C.** seedling left for 5 days on estradiol plates shows a shorter primary root and more lateral roots when compare to the other growth conditions.

5.3.3. Phloem flow is disrupted after occlusion of PD in the PPP

Unloading of assimilates was reported to occur through the SE/CC complex. To test whether CCs could still unload assimilates after the occlusion of PD in the PPP, carboxytetraethylrhodamine (CTER), a red fluorescent phloem-mobile probe developed by Knoblauch *et al*. (2015), was applied to estradiol-induced *CalS8*:iCalS3m seedlings. A 0.2 µl drop of CTER was left to diffuse on one cotyledon of seedlings either growing on MS media (n=5) or that had been induced for 8-10h (n=17). This time point was chosen because of the apparent reduction in root growth after 8h. Translocation was found to be severely impaired between 8h to 10h after induction. The probe was left to translocate 1h after application and observed under a confocal microscope. While all loaded seedlings on MS plates showed an expected unloading pattern, CTER was mainly contained in the stele, with a weak diffusion to the ground tissue (see Figure 5.3.A and B). This occurred for 5 induced seedlings. CTER did not translocate further than half way down the root for 9 other seedlings and 3 displayed a normal unloading pattern. 24h after induction, CTER was applied onto 7 seedlings. After 1h to 1.5h, unloading was observed only in 1 seedling. However, the pattern of unloading looked different to the WT seedlings. CTER was unloaded before the unloading zone and was confined to the stele (see Figure 5.3.C). This might suggest an alternative route for solute transport when the protophloem unloading domain is disrupted.

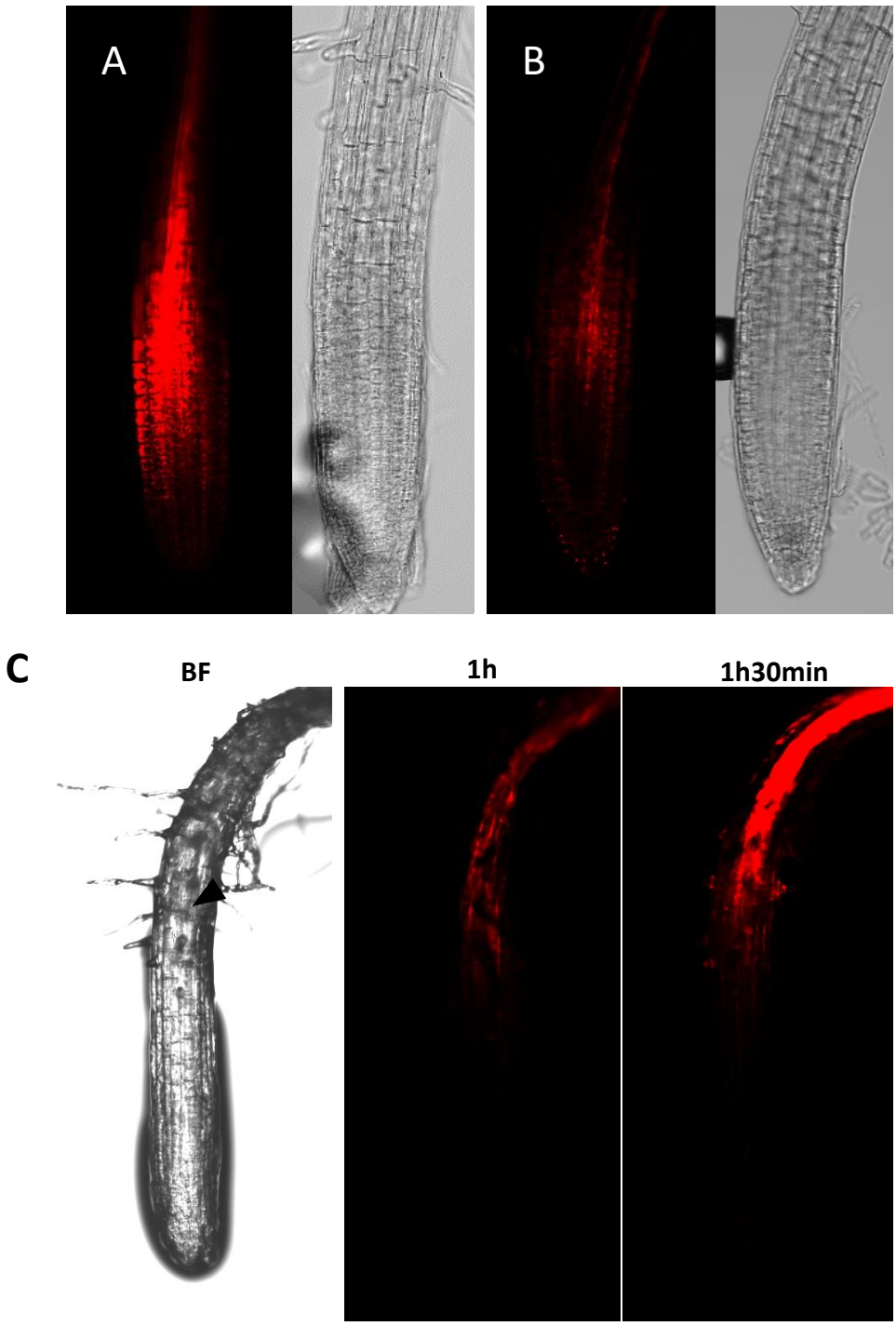

Figure 5.3: Unloading of CTER 1h after application in seedlings left on MS (n=5 out of 5) **(A)** and estradiol (n=5 out of 17) **(B)** plates for 8 to 10h. Restricted movement of the probe is apparent in **B. C.** After 24h of induction, a different unloading pattern could be observed which occurred above the protophloem (arrowhead) after 1h to 1h30 of applicating the probe. (BF: bright field)

5.3.4. The unloading of macromolecules is unaltered in *cals 6,7,8* and *6/8* mutants

The role of callose in defining the PPP unloading domain was investigated using mutants for Callose Synthase 6 (CalS6), CalS7, CalS8 and CalS6/8. *CalS7* is expressed in the phloem. It is essential for the deposition of callose at the pores of sieve elements after wounding or during their maturation (Xie *et al*., 2011). CalS6 is another putative phloem callose synthase expressed in CCs (personal communication with Prof. Helariutta), and CalS8 was shown previously to be PPP-specific (Ross-Elliot *et al*., 2017). The mutants and WT rootstocks were grafted onto scions expressing the ubiquitin-GFP fusion proteins under the *SUC2* promoter. This is a 36kDa fusion protein that is usually restricted to PPP during unloading (Stadler *et al*., 2005b). The pattern of unloading was observed at 10 dag. In all cases the unloading in mutant rootstocks was identical to WT (n=5 for each combination) suggesting that neither of these callose synthases is responsible for the basal SEL in PPP (see Figure 5.4.A-E).

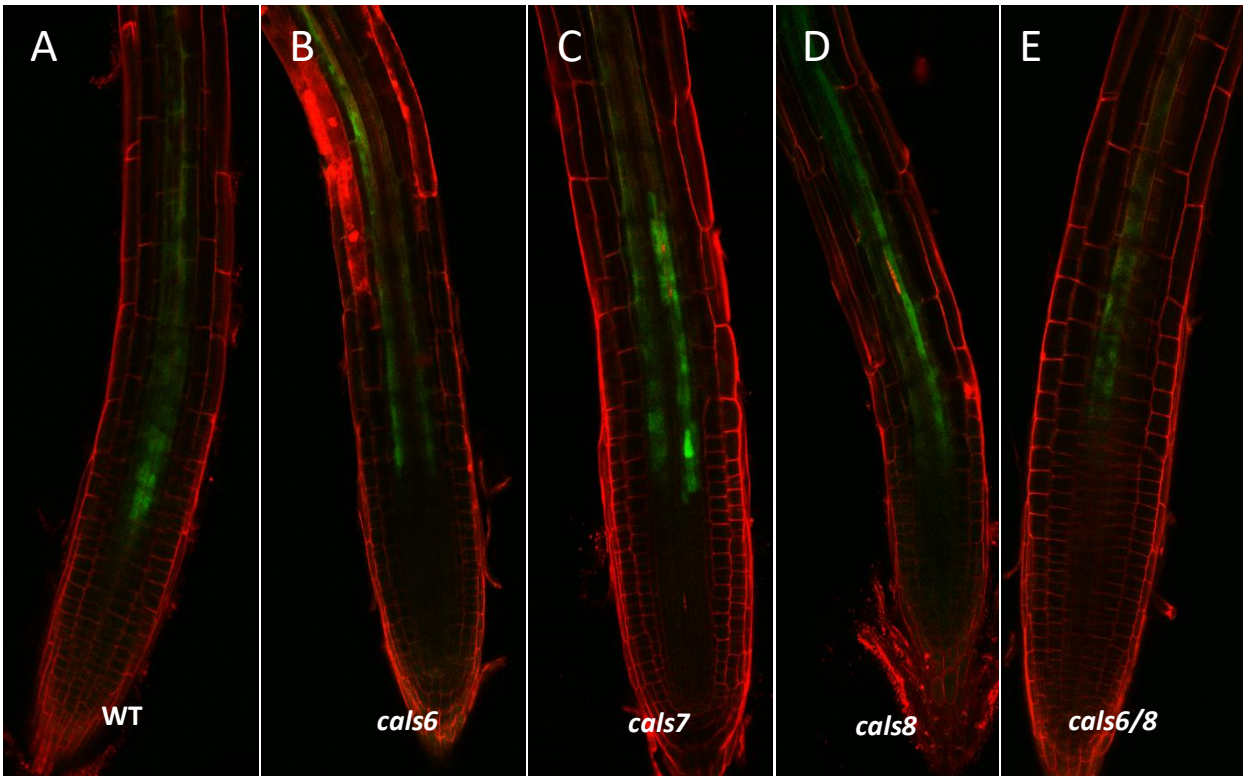

Figure 5.4: Rootstocks of WT **(A)**, *cals6* **(B)**, *cals7* **(C)**, *cals8* **(D)** and *cals6/8* **(E)** grafted onto *AtSUC2*:ubiquitin-GFP scions, observed 10 dag. All rootstocks showed the same unloading pattern, restricted to the PPP.

5.3.5. Solute translocation in *nakr1-1* mutants

A metal binding protein, NaKR1-1, was shown previously to gate the PD of PPPs when expressed as a GFP-fusion protein (Mr 61kDa; Tian *et al*., 2010). It was recently implicated in the unloading of FT-GFP in the shoot apical meristem. In *nakr1-1* mutants, FT-GFP expressed under the *SUC2* promoter could not reach the shoot sink domain and induce flowering, although the protein was present in SEs (Zhu *et al*., 2016). To test the possibility that phloem translocation is compromised in these mutants, as suggested by Tian *et al.* (2010), different phloem probes were applied to the cotyledons of 10-day old *nakr1-1* mutants. These probes i.e. CTER, 8-acetoxypyrene-l,3,6, trisulphonic acid, trisodium salt (HPTS) and esculin, a coumarin glucoside, are thought to load into the phloem using different transport routes (Wright and Oparka, 1996; Knoblauch *et al*., 2015). While the uptake of CTER and HPTS is still not well understood, esculin is actively loaded into the SE/CC complex by the SUC2 transporter (Knoblauch *et al*., 2015). The roots were monitored 1h after loading CTER, which was sufficient for all WT roots to translocate the probe. HPTS and esculin took much longer to translocate and the probes were therefore left to incubate overnight. All the probes used were found to translocate within the root vasculature of the mutants (see Figure 5.5.A). However, the mutants were significantly (p-value=0.04) less efficient than WT at loading and/or translocating the probe HPTS. This might be due to the reduced activity of plasma membrane transporters in *nakr1-1* mutants because of the accumulation of cations (Tian *et al*., 2010). No significant differences were found for the other two probes which might be due to the small size of the samples.

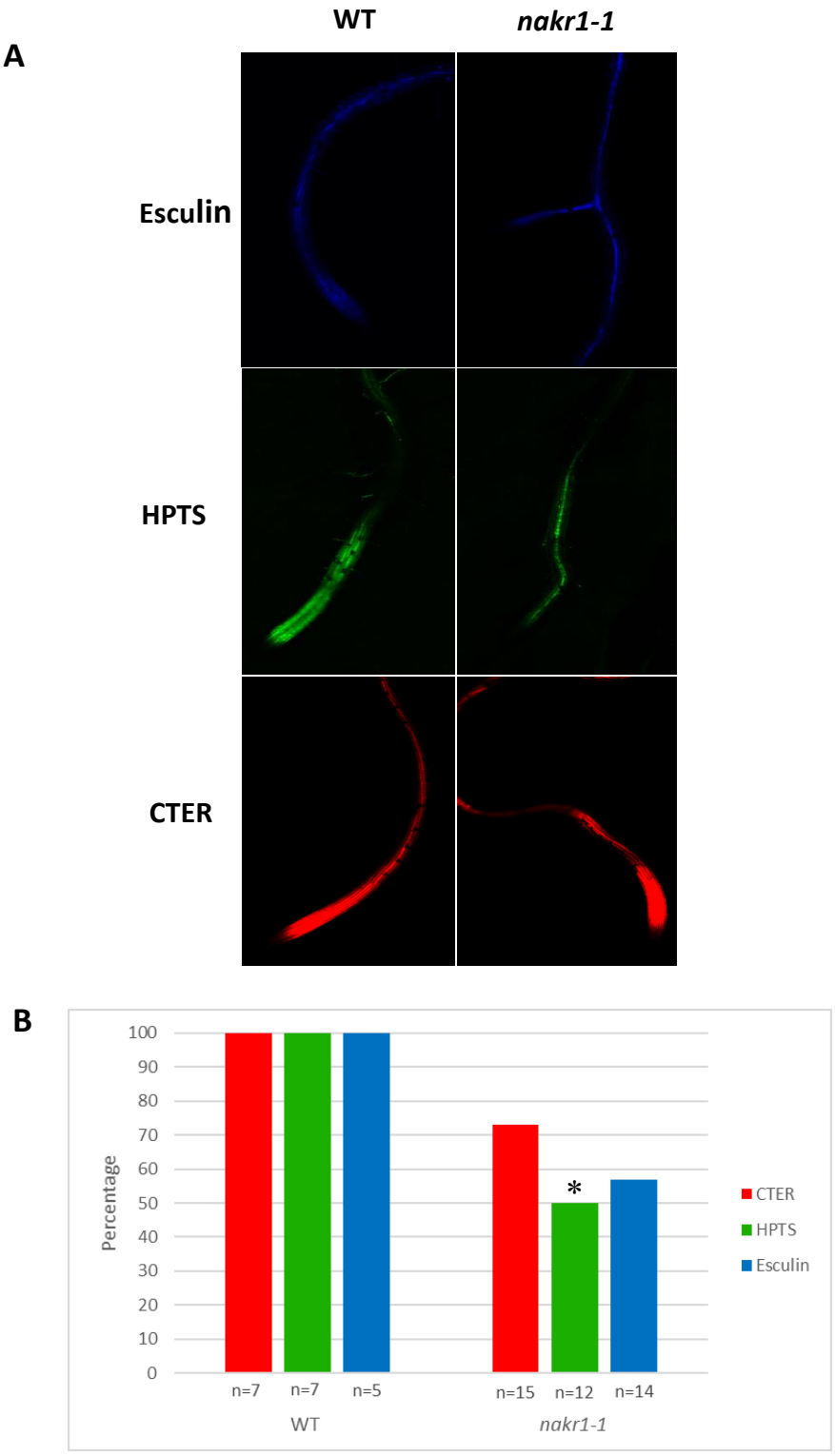

Figure 5.5: A. Translocation of Esculin, HPTS and CTER in both WT and *nakr1-1*. **B.** Percentage of seedlings loaded with a probe that displayed translocation. n indicates the total size of the population tested. Star shows significantly different result (p-value=0.04).

5.3.6. GFP unloading beyond the PPP is restricted in *nakr1-1* rootstocks

The movement of macromolecules in *nakr1-1* sink tissue was assessed by grafting scions expressing *AtSUC2*:GFP onto *nakr1-1* rootstocks. The grafts were monitored between 5 dag to 11 dag. In that timescale, 14 grafts restored the continuity of their phloem, which was confirmed by a GFP signal in the root vasculature. However, only 5 of these grafts were able to resume growth and showed an unloading pattern similar to WT (see Figure 5.6.C). The other 8 grafts did not unload GFP further than the PPPs (see Figure 5.6.A and B). This might indicate a loss of internal pressure in SEs of mutant roots, necessary for 'batch unloading'. Ross-Elliott *et al*. (2017) recently showed that small solutes and macromolecules batch unload from the protophloem into PPP, i.e. they are released in discrete pulses. It might be that 'batch unloading' requires a build-up of pressure at the SE/PPP interface. This might be facilitated by the funnel PD described by Ross-Elliott *et al.* (2017) which would then act as a pressure-driven valve. Alternatively, the conductivity of PD in PPPs might be affected in *nakr1-1*. NaKR1-1 might act as a plant movement protein which, by gating PD for its own transport, might facilitate the transport of smaller macromolecules. It is also unclear whether the grafts that resumed growth did so because WT scions enabled a partial complementation of the mutant phenotype. A rootstock imaged shortly after root growth recovery seemed to have a restricted movement of GFP from the PPP to the endodermis when compared to WT (see Figure 5.6.D-F). Backcrossing *AtSUC2*:GFP into an *nakr1-1* background could identify grafting artefacts from actual restrictions of macromolecule movement into sink tissue.

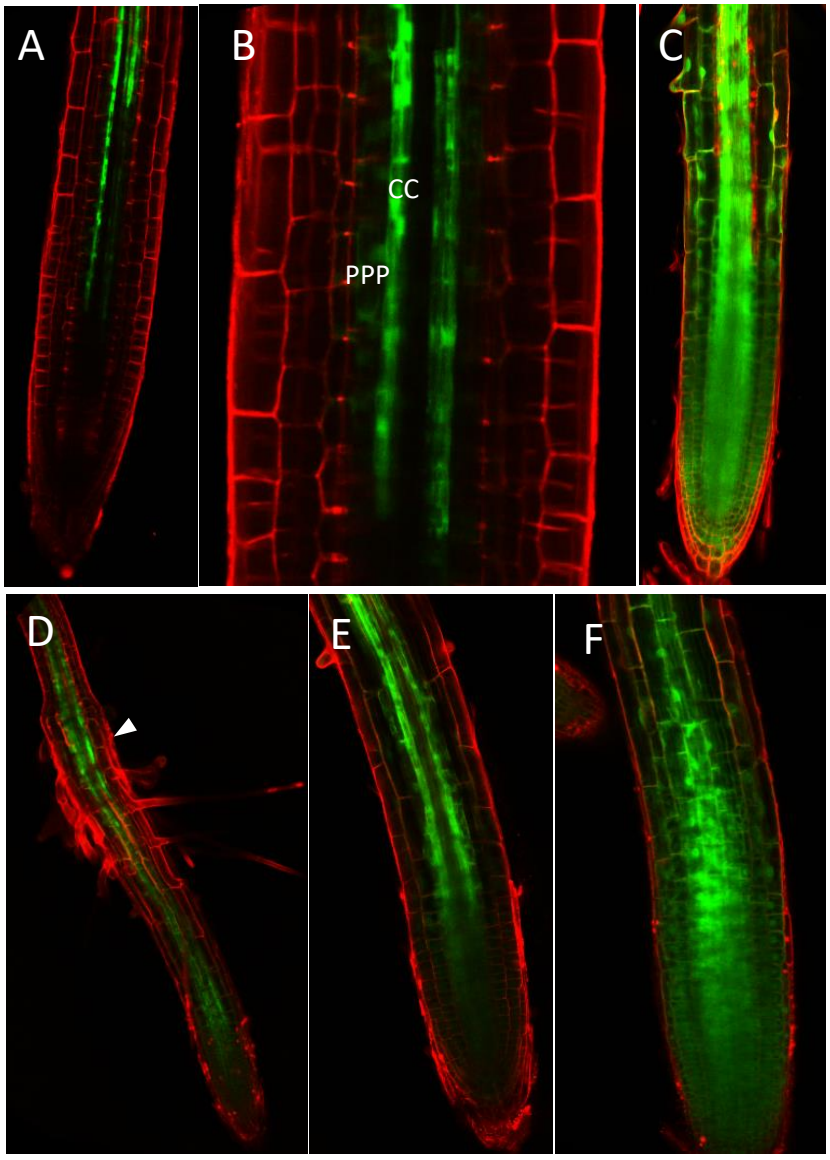

Figure 5.6: A. and **B.** Phenotype displayed by the majority (n=8) of grafts observed (n=14) which were made up of *AtSUC2*:GFP scions and *nakr1-1* rootstock. In these grafts, root growth was stopped as well as macromolecules unloading. Some could resume growth **(C)** showing an unloading pattern similar to WT **(F)** An intermediary stage was observed **(D)** and **(E)** where GFP unloading seemed more retricted when compare to WT **(F)**. The arrowhead in **(D)** indicates where unloading resumed in *nakr1-1* rootstock which caused root hair growth. CC:companion cell; PPP: phloem-pole pericycle.

5.4. Discussion

The *Arabidopsis* primary root is organised in radial cell layers (i.e. epidermis, cortex, endodermis and pericycle) that surround the stele. It is known that pericycle cells can adopt different behaviour depending on their localisation (Parizot *et al*., 2012). For instance, pericycle cells associated with the xylem poles (XPP) are responsive to auxin and can resume cellular division during lateral root formation (Parizot *et al*., 2008). A genome-wide transcriptional analysis has shown that, while the XPP shared a similar expression profile with the protoxylem, the PPP were more associated with the mature phloem, in particular CCs (Parizot *et al*., 2012). The data presented in this chapter corroborate this finding by showing that PPPs are the likely recipient of phloem sap. Macromolecules as large as the aggregates formed by SEOR-YFP (Mr 112 kDa), can reach the PPP where they are degraded (Ross-Elliott *et al*., 2017). PPPs therefore have the vital function of removing potential obstructions from the SE. Indeed, the induced expression of CalS3m in PPP showed that root growth and unloading was arrested and/or hindered when the access to PPP was blocked (see Figure 5.2 and 5.3). EM images have revealed that specialised funnel PD are located at the SE/PPP interface (Ross-Elliott *et al*., 2017). These PPP-specific PD might act as a pressure-driven valve enabling the 'batch unloading' of solutes and macromolecules.

To fulfil the requirement for mass flow, pressure can either be increased in the source and/or reduced in sink tissues (Knoblauch *et al*., 2016). In the root, the conductivity of PPP might therefore be essential for maintaining an appropriate pressure gradient along the flow path. The different vascular callose synthases tested; namely Cals6, 7, and 8, did not seem to regulate the basal SEL of PD in PPP (see Figure 5.4). However, NaKR1-1, a metal binding protein, might increase the

conductivity in PPP by gating PD and enabling macromolecule transport to the endodermis. NaKR1-1 fused to GFP (61 kDa) was non-cell autonomous, and able to travel from its site of expression in CCs to the root unloading domain beyond the PPP (Tian *et al*., 2010). This could increase the SEL of PD, enabling transport of other macromolecules, as demonstrated previously for viral movement proteins and KNOTTED1 (Noueiry *et al*., 1994; Lucas *et al*., 1995). These proteins were shown to gate PD of mesophyll cells, facilitating the transport of microinjected dextrans. In some grafts made from an *AtSUC2*:GFP scion and a *nakr1-1* rootstock, macromolecule unloading seemed to stop, preventing root growth (see Figure 5.6.A and B). Although, this might be due to a grafting artefact, it might explain the lack of movement of FT-GFP to the shoot apical meristem in these mutants (Zhu *et al*., 2016). NaKR1-1 might be necessary for macromolecule unloading in sink tissue. Interestingly, this protein has also been associated with promoting the activity of SUC2 transporters. It might therefore have the concerted action of raising turgor pressure in source tissues while decreasing turgor pressure in sink tissues.

Chapter 6: Conclusions and Future work

The work presented in this thesis was discussed in detail at the end of each of the results chapters. Here, I provide a brief summary of the main findings, together with some suggestions for future work in this field.

The grafting process is a fascinating biological phenomenon which is still poorly understood. The signalling events, leading from cellular recognition to symplasmic recovery, remain unknown. This is due to the technical difficulties associated with the use of large grafted plants (i.e. poor imaging resolution, lack of genetic mutants). Novel techniques have been developed to enable progress in this field (Errea *et al*., 2001; Turnbull *et al*., 2002). For instance, with the advent of *Arabidopsis* micrografting, well characterised mutants and/or cellular-marker lines can be used to identify key components involved in grafting (Turnbull *et al*., 2002; Yin *et al*., 2012; Melnyk *et al*., 2015). In particular, the auxin response of different tissues can be monitored at the graft junction with the use of the auxin-sensitive promoter, *DR5*. From the work I described in Chapter 3, it emerges that auxin might be contained within the stele to optimize cellular division and vascular differentiation. An auxin gradient might develop because of callose deposition at PD. In this respect, it would be useful to study the role of different callose synthases at the graft union. This might be achieved by grafting different callose synthase mutants together. Callose synthases could also contribute significantly to the formation of the symplasmic domain that develops in the callus cells of the stele. In Chapter 3, semi-thin sections of LR-white embedded grafts gave a unique resolution of the graft union, identifying a symplasmic domain with a high SEL (~ 35 kDa) within the callus stele, as well as allowing

unequivocal detection of secondary PD at the graft interface. It also emerges that a specific cell file aligned with the differentiating wound phloem can receive relatively large macromolecules (i.e. aggregates of 112kDa SEOR-YFP). These cells might be differentiating wound-sieve tubes. However, studies on the wound phloem in roots of *Pisum sativum* showed that the secondary opening of plugged sieve pores occurs only in fully mature wound-sieve tubes (Schulz, 1986; 1987). Nucleate wound-sieve tubes are not available for translocation as demonstrated by the restricted symplasmic transport of fluorescein at the wound site (Schulz, 1987). This situation might be different in hypocotyls of *Arabidopsis*. Perhaps some callus cells take on the transient role of clearing up macromolecules that accumulate within the developing wound-sieve tubes to ensure the non-dissipation of turgor pressure. The identity of these cells and their developmental stage could be confirmed by correlative imaging. This technique, developed during this thesis (Bell *et al*., 2013), can link fluorescence localisation (i.e. confocal laser scanning microscopy) to visible subcellular structures (using EM). The type of PD connecting these cells to the differentiating wound-phloem could also be analysed.

In Chapter 3, the possibility was explored of studying the formation of secondary PD using the principles of single cell analysis in microfluidic devices. It gave some promising preliminary results. The culture and fusion of calli with different cellular markers showed that secondary PD formation may be an inherent ability of dedifferentiated callus cells. From my studies, it would appear that callus cells do not require wounding, only physical contact, to initiate the signalling events that lead to the formation of new PD across the cell wall. In Chapter 3, some callus cells, expressing a PD marker, were successfully inserted into a microfluidic device to

observe the formation of secondary PD in single cells. This procedure should be repeated and monitored for longer periods of time, with different media, to test for factors that may influence the development of secondary PD. Eventually, it would be interesting to test cell types from different origins and genetic background for their competence to form secondary PD.

Grafting was also successfully used to study some aspects of macromolecular transport. In Chapter 4, I showed that targeted proteins from a range of subcellular structures could escape CCs and be translocated into the root unloading domain. The bioinformatic and statistical analysis of published datasets (Deeken *et al*., 2008; Batailler *et al*., 2012) suggested that protein size and abundance are the key determinants for allowing transfer of macromolecules between CC and SE. This raises the possibility that gating and/or targeting of PPUs might not be a prerequisite for protein signals to escape into SEs. The systemic movement of FT might illustrate this case. Although FT was reported to require FTIP1-1 for movement into SEs and subsequent translocation to the shoot apical meristem, FT transport to the root apical meristem did not seem to be affected in *ftip1-1* mutants. FT may be retained in certain CCs and this might be rescued by FTIP1-1. CCs are likely to form a varied population of cells with specific genomic expression levels. Their composition might be dependent on the state of the surrounding tissue and this may define which macromolecules are translocated. Interestingly, Corbesier *et al.* (2007) showed that CCs in minor veins had PPUs with a 'native' SEL smaller than the accepted 70 kDa (i.e. < FT-GFP; 47kDa). Expressing GFP fusions of 'putative' phloem chaperones under the promoter of minor vein CC-promoters, such as *GAS1*, may indicate if gating of PPUs can occur in some instances.

The fusion proteins used in Chapter 4 were incorporated into cells immediately adjacent to the protophloem files. These cells were identified in Chapter 5 as the phloem-pole pericycle cells (PPP). These cell files appear to be essential to remove macromolecules from the terminus of the translocation stream. This work, now published as a joint collaboration between a number of groups (Ross-Elliott *et al.*; 2017), showed that macromolecules and small solutes are unloaded in pressure-generated 'batches' into the PPP, mainly through the funnel-shaped PD that connect the PPP with the protophloem files. The induced expression of CalS3m in the PPP caused an arrest in root growth, as well as a restricted unloading of small solutes, pointing out the importance of the PPP for phloem unloading.

The PPP might act as a relay point for signals originally initiated in CCs. It would be interesting to look for proteins that can gate the PD of PPP cells and/or cause a response in the surrounding endodermis. NaKR1-1 might be such a protein. It was reported to facilitate the transport of FT to the shoot apical meristem (Tian *et al*., 2010; Zhu *et al*., 2016). The results obtained in Chapter 5 with grafted *AtSUC2*:GFP scions onto *nakr1-1* rootstocks suggest that NaKR1-1 is important for macromolecular transport, either by increasing the native SEL of PD in the PPP, and hence the conductivity of sink cells, or by raising the internal pressure in SEs, enabling unloading through funnel PD at the SE/PPP interface. NaKR1-1 is a metal binding protein. Shoots of *nakr1-1* mutants display an increase in cations (i.e. Na^+ and K^+) and starch accumulation (Tian *et al*., 2010). It therefore appears to be involved in the activity of SUC2 transporters that are necessary for sucrose loading in the phloem and for maintaining high osmotic pressure in source tissues. The activity of SUC2 is thought to be felt along the length of the translocation stream. In the translocation phloem,

SUC2 might prevent sucrose from constitutively leaking out and causing the dissipation of a pressure gradient (van Bel, 2003). The reduction of SUC2 activity in the rootstock might therefore be enough to cause a drop in the internal pressure necessary for 'batch' unloading into the PPP. Expressing GFP specifically in the PPP of *nakr1-1* mutants might indicate whether the PD SEL is affected in this tissue layer. Interestingly, in *nakr1-1* mutants, FT-GFP movement was shown to be restricted in the shoot apical meristem. Could there be an equivalent of the PPP in the shoot apical meristem that functions in a similar manner? Phloem unloading in sink leaves is thought to occur from class III veins, possibly through CCs, into the mesophyll (Roberts *et al*., 1997). It might be that, at the developing protophloem of the shoot meristem, other phloem cells take on the role of macromolecule unloading? However, this region is particularly hard to image because it is embedded in multiple cell layers. However, semi-thin sections of LR-white embedded tissue may give the resolution necessary to observe the specific cells involved in phloem unloading at the shoot apical meristem, an interesting area for future research.

References

Atkins C.A., Smith P.M. and Rodriguez-Medina C. (2011) Macromolecules in phloem exudates--a review. *Protoplasma*. 248 (1): 165-172.

Banerjee A.K., Chatterjee M., Yu Y., Suh S.G., Miller W.A. and Hannapel DJ. (2006) Dynamics of a mobile RNA of potato involved in a long-distance signalling pathway. *Plant Cell*, 18: 3443–3457.

Batailler B., Lemaître T., Vilaine F., Sanchez C., Renard D., Cayla T., Beneteau J. and Dinant S. (2012) Soluble and filamentous proteins in Arabidopsis sieve elements. *Plant, Cell and Environment*, 35 (7): 1258–1273.

Bell K, Mitchell S, Paultre D, Oparka KJ (2013) Correlative imaging of fluorescent proteins in resin-embedded plant material. *Plant Physiology* 161, 1595-1603

Benitez-Alfonso Y., Faulkner C., Pendle A., Miyashima S. and Helariutta Y. (2013) Symplastic intercellular connectivity regulates lateral root patterning. *Developmental Cell* 26: 136-147

Blackman L.M., Harper J.D.I. and Overall R.L. (1999) Localization of a centrin-like protein to higher plant plasmodesmata. *European Journal of Cell Biology* 78: 297-304

Bloemendal S. and Kück U. (2013) Cell-to-cell communication in plants, animals, and fungi: a comparative review. *Naturwissenschaften* 100:3-19

Boevink P., Oparka K., Santa Cruz S., Martin B., Betteridge A. and Hawes C. (1998) Stacks on tracks: the plant Golgi apparatus traffics on an actin/ER network. *the plant journal*, 15(3): 441–447.

Brown T.A., Fetter R.D., Tkachuk A.N. and Clayton D.A. (2010) Approaches toward super-resolution fluorescence imaging of mitochondrial proteins using PALM. *Methods* 51: 458–463

Brunkard J.O., Runkel A.M. and Zambryski P.C. (2015) The cytosol must flow: intercellular transport through plasmodesmata. *Current Opinion in Cell Biology* 35: 13-20

Calderwood A., Stanislav Kopriva S. and Morris R.J. (2016) Transcript abundance explains mRNA mobility data in Arabidopsis thaliana. *Plant Cell Advance Publication*.

Clough S.J. and Bent A.F. (1998) Floral dip: a simplified method for*Agrobacterium*-mediated transformation of *Arabidopsis thaliana. The Plant Journal* 16: 735–743

Corbesier L., Vincent C., Jang S., Fornara F., Fan Q., Searle I., Giakountis A., Farrona S., Gissot L., Turnbull C. and Coupland G. (2007) FT Protein

Movement Contributes to Long-Distance Signaling in Floral Induction of Arabidopsis. *Science,* 316 (5827): 1030-1033.

Crafts A.S. (1931) Movement of organic materials in plants. *Plant Physiology* 6(1): 1-41

Crane M.M., Clark I.B.N., Bakker E., Smith S. and Swain P.S. (2014) A microfluidic system for studying ageing and dynamic single0cell responses in budding yeasts. PloS ONE 9(6): e100042. Doi:10.1371/journal.pone.0100042

Crawford K.M. and Zambryski P.C. (1999) Phloem transport: Are you chaperoned? *Current Biology* 9:281-285

Crawford K.M. and Zambryski P.C. (2000) Subcellular localization determines the availability of non-targeted proteins to plasmodesmatal transport. *Current Biology,* 10:1032–1040.

Cutler S.R, Ehrhardt D.W., Griffitts J.S. and Somerville C.R. (2000) Random GFP::cDNA fusions enable visualization of subcellular structures in cells of Arabidopsis at a high frequency. *PNAS,* 97 (7): 3718-3723.

Dashevskaya S., Kopito R.B., Friedman R., Elbaum M. and Epel B.L. (2008) Diffusion of anionic and neutral GFP derivatives through plasmodesmata in epidermal cells of Nicotiana benthamiana. *Protoplasma,* 234(1-4):13-23.

Deeken R., Ache P., Kajahn I., Klinkenberg J., Bringmann G. and Hedrich R. (2008) Identification of Arabidopsis thaliana phloem RNAs provides a search criterion for phloem-based transcripts hidden in complex datasets of microarray experiments. *Plant J,* 55(5):746-59.

De Schepper V., De Swaef, Bauweraerts I. and Steppe K. (2013) Phloem transport: a review of mechanisms and controls. *Journal of Experimental Botany,* 64 (16): 4839–4850.

Ding B., Haudenshield J.S., Hull R.J., Wolf S., Beachy R.N. and Lucas W.J. (1992) Secondary plasmodesmata are specific sites of localization of the tobacco mosaic virus movement protein in transgenic tobacco plants. *The Plant Cell* 4: 915-928

Ding B., Turgeon R. and Parthasarathy M.V. (1992) Substructure of freeze-substituted plasmodesmata. *Protoplasma* 69: 28-41

Ehlers K. and Kollmann R. (1996) Formation of branched plasmodesmata in regenerating *Solanum nigrum-protoplasts. Planta* 199: 126-138

Ehlers K. and Kollmann R. (2001) Primary and secondary plasmodesmata: structure, origin, and functioning. *Protoplasma* 216: 1-30

Errea P., Garay L. and Marin J.A. (2001) Early detection of graft incompatibility in apricot (*Prunus armeniaca*) using in vitro techniques. Physiologia Plantarum 112(1): 135-141

Esau K and Thorsch J (1985) Sieve plate pores and plasmodesmata, the communication channels of the symplast: ultrastructural aspects and developmental relations. *American journal of botany*: 1641-1653

Faulkner C., Akman O.E., Bell K., Jeffree C. and Oparka K. (2008) Peeking into Pit Fields: A Multiple Twinning Model of Secondary Plasmodesmata Formation in Tobacco. *The Plant Cell* 20: 1504–1518

Federici F., Dupuy L., Laplaze L., Heisler M. and Haseloff J. (2012) Integrated genetic and computation methods for in planta cytometry. *Nature Methods*, 9: 483–485.

Fernandez-Calvino L., Faulkner C., Walshaw J., Saalbach G., Bayer E., Benitez-Alfonso Y. and Maule A. (2011) Arabidopsis Plasmodesmal Proteome. *PLoS ONE* 6: e18880

Fitzgibbon J., Beck M., Zhou J., Faulkner C., Robatzek S. and Oparka K. (2013) A developmental framework for complex plasmodesmata formation revealed by large-scale imaging of the Arabidopsis leaf epidermis. *The Plant Cell* 25: 25-70

Fitzgibbon J., Bell K., King E. and Oparka K. (2010) Super-resolution imaging of plasmodesmata using three-dimensional structured illumination microscopy. *Plant Physiology* 153: 1453-1463

Friml J., Vieten A., Sauer M., Weijers D., Schwarz H., Hamann T., Offringa R. and Jurgens G. (2003) Efflux-dependent auxin gradients establish the apical-basal axis of Arabidopsis. *Nature* 426:147–153

Froelich D.R., Mullendore D.L., Jensen K.H., Ross-Elliott T.J., Anstead J.A., Thompson G.A., Pélissier H.C. and Knoblauch M. (2011) Phloem Ultrastructure and Pressure Flow: Sieve-Element-Occlusion-Related Agglomerations Do Not Affect Translocation. *The Plant Cell*, 23 (12): 4428-4445.

Fu Z.Q. and Dong X. (2013) Systemic Acquired Resistance: Turning Local Infection into Global Defense. *Annual Review of Plant Biology*, 64: 839-863.

Fuentes I., Stegemann S., Golczyk H., Karcher D. and Bock R. (2014) Horizontal genome transfer as an asexual path to the formation of new species. *Nature* 511: 232-235

Furch A.C.U., van Bel A.J.E., Fricker M.D., Felle H.H., Fuchs M. and Hafke J.B. (2009) Sieve element Ca^{2+} channels as relay stations between remote stimuli and sieve tube occlusion in *Vicia faba*. *The Plant Cell* 21: 2118-2132

Gaupels F. and Ghirardo A. (2013) The extrafascicular phloem is made for fighting. *Frontiers in Plant Science* 4(187): 1-4

Golecki B., Schulz A., Carstens-Behrens U. and Kollmann R. (1998) Evidence for graft transmission of structural phloem proteins or their precursors in heterografts of Cucurbitaceae. *Planta*, 206(4): 630-640

Golecki B., Schulz A. and Thompson G.A. (1999) Translocation of Structural P Proteins in the Phloem. *The Plant Cell* 11(1):127-140

Gould N., Minchin P.E.H. and Thorpe M.R. (2004). Direct measurements of sieve element hydrostatic pressure reveal strong regulation after pathway blockage. *Funct. Plant Biol.* 31: 987–993

Gunning B.E.S. (1978) Age-related and origin-related control of the numbers of plasmodesmata in cell walls of developing *Azolla* roots. *Planta* 143: 181-190

Gurdon C., Svab Z., Feng Y., Kumar D. and Maliga P. (2016) Cell-to-cell movement of mitochondria in plants. *PNAS* 113(12): 3395-3400

Han X., Hyun T.K., Zhang M., Kumar R., Koh E-J., Kang B-H. and Lucas W.J. (2014) Auxin-callose-mediated plasmodesmal gating is essential for tropic auxin gradient formation and signalling. *Developmental Cell* 28: 132-146

Harada T. (2010) Grafting and RNA transport via phloem tissue in horticultural plants. *Scientia Horticulturae* 125: 545–550

Hartig TH (1854) Ueber die quersheidewände zwischen den einzelnen gliedern der siebröhren in *Cucurbita pepo.* Bot. Zeit. 12: 51-54

Haseloff J., Siemering K.R., Prashe D.C., and Hodge S. (1997) Removal of a cryptic intron and subcellular localization of green fluorescent protein are required to mark transgenic Arabidopsis plants brightly. *PNAS*, 94(6): 2122-2127

Hepler P. K. (1982) Endoplasmic Reticulum in the Formation of the Cell Plate and Plasmodesmata. *Protoplasma* 111: 121 - 133

Hofius D., Herbers K., Melzer M., Omid A., Tacke E., Wolf S. and Sonnewald U. (2001) Evidence for expression level-dependent modulation of carbohydrate status and viral resistance by the potato leafroll virus movement protein in transgenic tobacco plants. *Plant J.* 28: 529–543

Hu J., Shibata Y., Voss C., Shemesh T., Li Z., Coughlin M., Kozlov M.M., Rapoport T.A. and Prinz W.A. (2008) Membrane Proteins of the Endoplasmic Reticulum Induce High-Curvature Tubules. *Science* 319: 1247-1250

Hunter P.R., Craddock C.P., Di Benedetto S., Roberts L.M. and Frigerio L. (2007) Fluorescent reporter proteins for the tonoplast and the vacuolar lumen identify a single vacuolar compartment in *Arabidopsis* cells. *Plant Physiology* 145: 1371-1382

Kehr J.(2006) Phloem sap proteins: their identities and potential roles in the interaction between plants and phloem-feeding insects. *J. Exp. Bot.*, 57 (4): 767-774.

Jeffree C. and Yeoman M.M. (1983) Development of intercellular connections between opposing cells in a graft union. *New Phytol*. 93: 491-509

Jekat S.B., Ernst A., von Bohl A., Zielonka S., Twyman R.M., Noll G.A. and Prüfer D. (2013) P-proteins in *Arabidopsis* are heteromeric structures involved in rapid sieve tube sealing. *Frontiers in Plant Science* 4: 1-9

Jorgensen R.A., Atkinson R.G., Forster R.L.S. and Lucas W.J. (1998) An RNA-Based Information Superhighway in Plants. *Science* 279 (5356): 1486-1487

Jones M.G.K. (1976) The origin and development of plasmodesmata. In: Intercellular communication in plants: Studies on plasmodesmata: 81-103, Gunning B.E.S. and Robards A.W., eds. Springer, Berlin Heidelberg New York

Juchaux-Cachau M., Landouar-Arsivaud L., Pichaut J-P., Campion C., Porcheron B., Jeauffre J., Noiraud-Romy N., Simoneau P., Maurousset L. and Lemoine R. (2007) Characterization of AgMaT2, a Plasma Membrane Mannitol Transporter from Celery, Expressed in Phloem Cells, Including Phloem Parenchyma Cells. *Plant Physiology*, 145 (1): 62-74.

Juniper B.E. and Barlow P.W. (1969) The distribution of plasmodesmata in the root tip of maize. *Planta* 89: 352-360

Kempers R., Prior D.A.M., van Bel A.J.E. and Oparka K.J. (1993) Plasmodesmata between sieve element and companion cell of extrafascicular stem phloem of *Cucurbita maxima* permit passage of 3 kDa fluorescent probes. *Plant Journal* 4: 567-575

Kempers R. and van Bel A.J.E. (1997) Symplasmic connections between sieve element and companion cell in the stem phloem of *Vicia faba* L. have a molecular exclusion limit of at least 10 kDa. *Planta* 201: 195-201

Ketelaar T., Allwood E.G., Anthony R., Voigt B., Menzel D. and Hussey P.J. (2004) The Actin-Interacting Protein AIP1 Is Essential for Actin Organization and Plant Development. *Current Biology*, 14 (2): 145-149.

Kim M., Canio W., Kessler S., Sinha N. (2001) Developmental Changes Due to Long-Distance Movement of a Homeobox Fusion Transcript in Tomato. *Science*, 293 (5528): 287-289.

Kim I., Kobayashi K., Cho E. and Zambryski P.C. (2005) Subdomains for transport via plasmodesmata corresponding to the apical–basal axis are established during Arabidopsis embryogenesis. *PNAS* 102: 11945–11950

Kim G., LeBlanc M.L., Wafula E.K., dePamphilis C.W. and Westwood J.H. (2014) Genomic-scale exchange of mRNA between a parasitic plant and its hosts. *Science*, 345(6198): 808-811.

Knoblauch M., Froelich D.R., Pickard W.F. and Peters W.S. (2014) SEORious business: structural proteins in sieve tubes and their involvement in sieve element occlusion. *Journal of Experimental Botany* 65(7): 1879-1893

Knoblauch M, Knoblauch J, Mullendore DM, Savage JA, Babst BA, Beecher SD, Dodgen AC, Jensen KH, Holbrook NM (2016) Testing the Münch hypothesis of long distence phloem transport in plants. eLife http://dx.doi.org/10.7554/eLife.15341

Knoblauch M. and Peters W.S. (2010) Münch, morphology, microfluidics- our structural problem with the phloem. *Plant, Cell and Environment* 33: 1439-1452

Knoblauch M, Vendrell M, de Leau E, Paterlini A, Knox K, Ross-Elliot T, Reinders A, Brockman SA, Ward J, Oparka K (2015) Multispectral Phloem-Mobile Probes: Properties and Applications. Plant Physiology 167: 1211-1220

Knox K., Wang P., Kriechbaumer V., Tilsner J., Frigerio L., Sparkes I., Hawes C. and Oparka K. (2015) Putting the Squeeze on Plasmodesmata: A Role for Reticulons in Primary Plasmodesmata Formation, *Plant Physiology*,168 (4): 1563-1572.

Köhler R.H., Cao J., Zipfel W.R., Webb W.W. and Hanson M.R. (1997) Exchange of Protein Molecules Through Connections Between Higher Plant Plastids. *Science*, 276 (5321): 2039-2042.

Kollmann R. and Glockmann C. (1991) Studies on graft unions III. On the mechanism of secondary formation of plasmodesmata at the graft interface. *Protoplasma* 165: 71-85

Kollmann R., Yang S. and Glockmann C. (1985) Studies on graft unions. II. Continuous and half plasmodesmata in different regions of the graft interface. *Protoplasma* 126: 19-29

Kraner M.E., Link K., Melzer M., Ekici A.B., Uebe S., Tarazona P., Feussner I., Hofmann J. and Sonnewald U. (2017) Choline transporter-like1 (CHER1) is crucial for plasmodesmata maturation in *Arabidopsis thaliana*. *The plant journal* 89(2): 394-406

Lalonde S., Wipf D. and Frommer W.B. (2004) The transport mechanisms for organic forms of carbon and nitrogen between source and sink. *Annual Reviews of Plant Biology* 55: 341-372

Lee K., Choi S., Yang C., Wu H-C. and Yu J. (2013) Autofluorescence generation and elimination: a lesson from glutaraldehyde. *Chem. Commun.* 49: 3028-3030

Lee D. W., Jung C. and Hwanga I. (2013) Cytosolic events involved in chloroplast protein targeting. *Biochimica et Biophysica Acta (BBA),* 1833 (2): 245-252.

Lee J-Y. and Lu H. (2011) Plasmodesmata: the battleground against intruders. *Trends in Plant Science* 16(4): 201-210

Levy A., Erlanger M., Rosenthal M. and Epel B.L. (2007) A plasmodesmata-associated β-1,3-glucanase in Arabidopsis. *The Plant Journal* 49: 669–682

Lifschitz E., Eviatar T., Rozman A., Shalit A., Goldshmidt A., Amsellem Z., Alvarez J.P. and Eshed Y. (2006) The tomato FT ortholog triggers systemic signals that regulate growt and flowering and substitute for diverse environmental stimuli. *PNAS* 103(16): 6398-6403

Lilly S.T., Drummond R.S., Pearson M.N. and MacDiarmid R.M. (2011) Identification and validation of reference genes for normalization of transcripts from virus-infected Arabidopsis thaliana. *Mol Plant Microbe Interact*. 24(3): 294-304

Lin M-K., Belanger H., Y-J. Lee, Varkonyi-Gasic E., Taoka K-I., Miura E., Xoconostle-Cázares B., Gendler K., Jorgensen R.A., Phinney B., Lough T.J. and Lucas W.L. (2007) Flowering Locus T protein may act as the long-distance florigenic signal in the cucurbits. The Plant Cell 19; 1488-1506

Lin M.K., Lee Y.J., Lough T.J., Phinney B.S. and Lucas W.J. (2009) Analysis of the pumpkin phloem proteome provides insights into angiosperm sieve tube function. *Mol Cell Proteomics*, 8(2): 343-356

Liu L., Liu C., Hou X., Xi W., Shen L., Tao Z., Wang Y. and Yu H. (2012) FTIP1 is an essential regulator for florigen transport. PLoS Biol 10(4): e1001313. doi:10.1371/journal.pbio.1001313

Luby-Phelps K., Ning G., Fogerty J. and Besharse (2003) Vizualisation of identified GFP-expressing cells by light and electron microscopy. *The Journal of Histochemistry and Cytochemistry* 51: 271-74

Lucas W.J. (1989) Movement Protein of Tobacco Mosaic Virus Modifies Plasmodesmatal Size Exclusion Limit. *Science* 246: 377-379

Lucas W.J., Bouché-Pillon S., Jackson D.P., Nguyen L., Baker L., Ding B. and Hake S. (1995) Selective trafficking of KNOTTED1 homeodomain protein and its mRNA through plasmodesmata. *Science* 270: 1980-1983

Lucas W.J., Ding B. and van der Schoot C. (1993) Plasmodesmata and the Supracellular Nature of Plants. *New Phytologist*, 125: 435-476

Lucas W.J., Ham B-K. and Kim J-K. (2009) Plasmodesmata – bridging the gap between neighboring plant cells. *Trends in Cell Biology* 19: 495-503

Marques J. P., Dudeck I. and Klösgen R.B. (2003) Targeting of EGFP chimeras within chloroplasts. *Molecular Genetics and Genomics*, 269 (3): 381-387

Martens H.J., Roberts A.G., Oparka K.J. and Schulz A. (2006) Quantification of plasmodesmatal endoplasmic reticulum coupling between sieve elements and companion cells using fluorescence redistribution after photobleaching. *Plant Physiology* 142: 471-480

Mathieu J., Warthmann N., Küttner F. and Schmid M. (2007) Export of FT Protein from Phloem Companion Cells Is Sufficient for Floral Induction in Arabidopsis. *Current Biology,* 17 (12): 1055–1060.

Maule A. (2008) Plasmodesmata: structure, function and biogenesis. *Current Opinion in Plant Biology* 11(6): 680-686

May T. and Soll J. (2000) 14-3-3 proteins form a guidance complex with chloroplast precursor proteins in plants. *The Plant Cell* 12: 53-63

Melnyk C.W., Schuster C., Leyser O. and Meyerowitz E.M. (2015) A developmental framework for graft formation and vascular reconnection in Arabidopsis thaliana. *Current Biology* 25: 1306-1318

Molnar A., Melnyk C.W., Bassett A., Hardcastle T.J., Dunn R. and Baulcombe D.C. (2010) Small Silencing RNAs in Plants Are Mobile and Direct Epigenetic Modification in Recipient Cells. *Science,* 328 (5980): 872-875

Moore R. (1984) A Model for Graft Compatibility-Incompatibility in Higher Plants. *American Journal of Botany* 71: 752-758

Moore R. (1984) The Role of Direct Cellular Contact in the Formation of Compatible Autografts in *Sedum telephoides. Annals of Botany* 54: 127-133

Mudge K., Janick J., Scofield S. and Goldschimdt E.E. (2009) A history of grafting. *Horticultural Reviews* 35: 437-493

Mullendore D.L., Windt C.W., Van As H. and Knoblauch M. (2010) Sieve tube geometry in relation to phloem flow. *The Plant Cell* 22 (3): 579-593

Mulo P. (2011) Chloroplast-targeted ferredoxin-NADP+ oxidoreductase (FNR): Structure, function and location. *Biochimica et Biophysica Acta (BBA) – Bioenergetics,* 1807 (8): 927–934.

Münch E (1930) Die Stoffbewegung in der Pflanze. Jena, Germany: Fischer

Niklas K.J. (2014) The evolutionary-developmental origins of multicellularity. *American Journal of Botany* 101(1): 6-25

Noueiry A.O., Lucas W.J. and Gilbertson R.L. (1994) Two proteins of a plant DNA virus coordinate nuclear and plasmodesmatal transport. *Cell* 76 (5): 925-932

Paultre DSG, Gustin M-P, Molnar A, Oparka KJ (2016) Lost in transit: long-distance trafficking and phloem unloading of protein signals in *Arabidopsis* homografts. *The Plant Cell* :tpc.00249.2016

Pina A. and Errea P. (2005) A review of new advances in mechanism of graft compatibility–incompatibility. *Scientia Horticulturae* 106: 1–11

Pina A., Errea P., Schulz A. and Martens H.J. (2009) Cell-to-cell transport through plasmodesmata in tree callus cultures. *Tree Physiology* 29: 809–818

Ormenese S., Bernier G. and Périlleux C. (2006) Cytokinin application to the shoot apical meristem of *Sinapis alba* enhances secondary plasmodesmata formation. *Planta* 224: 1481–1484

Oparka K.J. (1990) What is phloem unloading? *Plant Phys.* 94: 393-396

Oparka K.J. (2004) Getting the message across: how do plant cells exchange macromolecular complexes? *Trends in Plant Science* 9: 33-41

Oparka K., Duckett C., Prior D. and Fisher D. (1994) Real-time imaging of phloem unloading in the root tip of Arabidopsis. The Plant Journal 6: 759-766

Oparka K.J. and Roberts A.G. (2001) Plasmodesmata. A Not So Open-and-Shut Case. *Plant Physiology* **125**: 123–126

Oparka K.J. and Santa Cruz S. (2000) The great escape: phloem transport and unloading of macromolecules. *Annu. Rev. Plant Phys. Plant Mol. Biol.* 51: 323-347

Oparka K.J. and Turgeon R. (1999) Sieve Elements and Companion Cells—Traffic Control Centers of the Phloem. *The Plant Cell*, 11 (4): 739-750

Overall R.L., Wolfe J. and Gunning B.E.S. (1982) Intercellular Communication in *Azolla* Roots: I. Ultrastructure of Plasmodesmata. *Protoplasma* 111: 134-150

Overall R.L. and B1ackman L. (1996) A model of the macromolecular structure of plasmodesmata. *Trends in plant science* 1: 307-311

Palevitz B.A. and Hepler P. K. (1985) Changes in dye coupling of stomatal cells of *Allium* and *Commelina* demonstrated by microinjection of Lucifer yellow. *Planta* 164: 473-479

Parizot B., Laplaze L., Ricaud L., Boucheron-Dubuisson E., Bayle V., Bonke M., De Smet I., Poethig S.R., Helariutta Y., Haseloff J., Chriqui D., Beeckman T. and Nussaume L. (2008) Diarch symmetry of the vascular bundle in Arabidopsis root encompasses the pericycle and is reflected in distich lateral root initiation. *Plant Physiology* 146:140-148

Parizot B., Roberts I., Raes J., Beeckman T. and De Smet I. (2012) *In silico* analyses of pericycle cell populations reinforce their relation with associate vasculature in *Arabidopsis*. *Phil. Trans. R. Soc. B* 367: 1479-1488

Pyke K., Zubko M.K. and Day A. (2000) Marking cell layers with spectinomycin provides a new tool for monitoring cell fate during leaf development. *Journal of Experimental Botany* 51(351): 1713-1720

Radford J.E. and White R.G. (1998) Localization of a myosin-like protein to plasmodesmata. *The Plant Journal* 14: 743-750

Reichelt S., Knight A.E., Hodge T.P., Baluska F., Samaj J., Volkmann D. and Kendrick-Jones J. (1999) Characterization of the unconventional myosin VIII in plant cells and its localization at the post-cytokinetic cell wall. *The Plant Journal* 19: 555-567

Robards A. W. (1971) The Ultrastructure of Plasmodesmata. *Protoplasma* 72: 315-323

Robards A. W. (1968) A New Interpretation of Plasmodesmatal Ultrastructure. *Planta* (Berl.) 82: 200-210

Roberts A.G., Santa Cruz S., Roberts I.M., Prior D.A., Turgeon R. and Oparka K.J. (1997) Phloem unloading in sink leaves of Nicotiana benthiamiana: comparison of a fluorescent solute with a fluorescent virus. The Plant Cell 9: 1381-1396

Ross-Elliott T.J., Jensen K.H., Haaning K.S., Wager B.M., Knoblauch J., Howell A.H., Mullendore D. L., Monteith A.G., Paultre D., Yan D., Otero-Perez S., Bourdon M., Sager R., Lee J-Y., Helariutta Y., Knoblauch M. and Oparka K.J. (2017) Phloem unloading in Arabidopsis roots is convective and regulated by the phloem-pole pericycle. *eLife*: 10.7554/eLife.24125

Ruiz-Trillo I., Burger G., Holland P.W.H., King N., Lang B.F., Roger A.J. and Gray M.G. (2007) The origins of multicellularity: a multi-taxon genome initiative. Trends in Genetics 23 (3): 113-118

Schulz A. (1986) Wound phloem in transition to bundle phloem in primary roots of *Pisum sativum* L. II. The plasmatic contact between wound-sieve tubes and regular phloem. *Protoplasma* 130: 27-40

Schulz A. (1987) Sieve-element differentiation and fluoresceine translocation in wound-phloem of pea roots after complete severance of the stele. *Planta* 170: 289-299

Schulz A. (2017) Long-Distance Trafficking: Lost in Transit or Stopped at the Gate? *Plant cell* 29(3): 426-430

Seagull R.W. (1983) Differences in the frequency and disposition of plasmodesmata resulting from root cell elongation. *Planta* 159: 497-504

Seguí-Simarro J.M., Austin J.R., White E.A. and Staehelin L.A. (2004) Electron Tomographic Analysis of Somatic Cell Plate Formation in Meristematic Cells of Arabidopsis Preserved by High-Pressure Freezing. *The Plant Cell* 16: 836–856

Simpson C., Thomas C., Findlay K., Bayer E. and Maule A.J. (2009) An Arabidopsis GPI-Anchor Plasmodesmal Neck Protein with Callose Binding Activity and Potential to Regulate Cell-to-Cell Trafficking. *The Plant Cell* 21: 581–594

Sjolund RD (1997) The Phloem Sieve Element: A River Runs through It. *Plant Cell* 9: 1137-1146

Spiegelman Z., Golan G. and Wolf S. (2013) Don't kill the messenger: Long-distance trafficking of mRNA molecules. *Plant Science*, 213: 1–8.

Stadler R., Lauterbach C. and Sauer N. (2005a) Cell-to-Cell Movement of Green Fluorescent Protein Reveals Post-Phloem Transport in the Outer Integument and Identifies Symplastic Domains in Arabidopsis Seeds and Embryos. *Plant Physiology*, 139 (2): 701-712.

Stadler R., Wright K.M., Lauterbach C., Amon G., Gahrtz M., Feuerstein A., Oparka K.J. and Sauer N. (2005b) Expression of GFP-fusions in Arabidopsis companion cells reveals non-specific protein trafficking into sieve elements and identifies a novel post-phloem domain in roots. *The Plant Journal* 41: 319-331

Stegemann S. and Bock R. (2009) Exchange of genetic material between cells in plant tissue grafts. *Science* 324(5927): 649-651

Stegemann S., Keuthe M., Greiner S. and Bock R. (2012) Horizontal transfer of chloroplast genomes between plant species. *PNAS* 109: 2434–2438

Tamaki S., Matsuo S., Wong H.L., Yokoi S. and Shimamoto K. (2007) Hd3a Protein Is a Mobile Flowering Signal in Rice. *Science* 316 (5827): 1033-1036**Tetyuk O., Benning,U.F. and Hoffmann-Benning S**. (2013) Collection and Analysis of Arabidopsis Phloem Exudates Using the EDTA-facilitated Method. *J. Vis. Exp.* 80: e51111, doi:10.3791/51111

Thieme C.J., Rojas-Triana M., Stecyk E., Schudoma C., Zhang W.,Yang L., Miñambres M., Walther D., Schulze W.X., Paz-Ares J., Scheible W-R. and Kragler F. (2015) Endogenous Arabidopsis messenger RNAs transported to distant tissues. *Nature Plants*, 1: 1-8

Thomas C.L., Bayer E.M., Ritzenthaler C., Fernandez-Calvino L. and Maule A.J. (2008) Specific targeting of a plasmodesmatal protein affecting cell-to-cell communication. *PLOS*

Tian H., Baxter I.R., Lahner B., Reinders A., Salt D.E. and Ward J.M. (2010) Arabidopsis NPCC6/NaKR1 is a phloem mobile metal binding protein necessary for phloem function and root meristem maintenance. *Plant Cell* 22(12): 3963-3979

Tilsner J., Amari K. and Torrance L. (2011) Plasmodesmata viewed as specialised membrane adhesion sites. *Protoplasma* 248: 39–60

Turnbull C.G.N., Booker J.P. and Leyser H.M.O. (2002) Micrografting techniques for testing long-distance signalling in Arabidopsis. *The Plant Journal* 32: 255–262

van Bel A.J.E. (1996) Interaction between sieve element and companion cell and the consequences for photoassimilate distribution. Two structural hardware frames with associated physiological software in dicotyledons? *Journal of Experimental Botany* 47: 1129-1140

van Bel A.J.E. (2003) The phloem, a miracle of ingenuity. *Plant, Cell and Environment* 26: 125-149

van Bel A.J.E. and Knoblauch M. (2000) Sieve element and companion cell: the story of the comatose patient and the hyperactive nurse. *Functional Plant Biology* 27: 477-487

van der Schoot C., Dietrich M.A., Marc Storms M., Verbeke J.A. and Lucas W.J. (1995) Establishment of a cell-to-cell communication pathway between separate carpels during gynoecium development. *Planta* 195: 450-455

Vatén A., Dettmer J., Wu S., Stierhof Y-D., Miyashima S., Yadav S.R., Roberts C.J., Campilho A., Bulone V., Lichtenberger R., Lehesranta S., Mähönen A.P., Kin J-Y., Jokitalo E., Sauer N., Scheres B., Kakajima K., Carlsbecker A., Gallagher K.L. and Helariutta Y. (2011) Callose biosynthesis regulates symplastic trafficking during root development. *Developmental Cell* 21: 1144-1155

Watanabe S., Punge A., Hollopeter G., Willig K.I., Hobson R.J., Davi M.W., Hell S.W. and Jorgensen E.M. (2011) Protein localization in electron micrographs using fluorescence microscopy. *Nature Methods* 8: 81-85

Wetmore R.H. and Rier J.P. (1963) Experimental induction of vascular tissue in callus of angiosperm. *American Journal of Botany* 50: 418-430

White R.G., Badelt K., Overall R.L. and Vesk M. (1994) Actin associated with plasmodesmata. *Protoplasma* 180: 169-184

Wright K.M. and Oparka K.J. (1996) The fluorescent probe HPTS as a phloem-mobile, symplastic tracer: an evaluation using confocal laser scanning microscopy. Journal of Experimental Botany 47: 439-445

Wu H., Liu W., Tu Q., Song N., Li L., Wang J. and Wang J. (2011) Culture and chemical-induced fusion of tobacco mesophyll protoplasts in a microfluidic device. *Microfluidic Nanofluid* 10: 867-876

Xie B., Wang X., Zhu M., Zhang Z. and Hong Z. (2011) *CalS7* encodes a callose synthase responsible for deposition in the phloem. *The Plant Journal* 65: 1-14

Xoconostle-Cázares B., Xiang Y., Ruiz-Medrano R., Wang H-L., Monzer J., Yoo B-C., McFarland K.C., Franceschi V.R. and Lucas W.J. (1999) Movement

protein that potentiates transport of mRNA into the phloem. *Science* 283: 94-98

Yadav S.R., Yan D., Sevilem I. and Helariutta Y. (2014) Plasmodesmata-mediated intercellular signaling during plant growth and development. *Front Plant Sci*. 5:1-7

Yin H., Yan B., Sun J., Jia P., Zhang Z., Yan X., Chai J., Ren Z., Zheng G. and Liu H. (2012) Graft-union development: a delicate process that involves cell-cell communication between scion and stock for local auxin accumulation. *Journal of Experimental Botany* 63: 4219–4232

Zambryski P. and Crawford K. (2000) Plasmodesmata: Gatekeepers for Cell-to-Cell Transport of Developmental Signals in Plants. *Annu. Rev. Cell Dev. Biol*. 16: 393–421

Zeevaart J.A.D. (2006) Florigen Coming of Age after 70 Years. *The Plant Cell* 18: 1783-1789

Zhang W., Thieme C.J., Kollwig G., Apelt F., Yang L., Winter N., Andresen N., Walther D. and Kragler F. (2016) tRNA-related sequences trigger systemic mRNA transport in plants. *The Plant Cell* 28: 1237-1249

Zhang B., Tolstikov V., Turnbull C., Hicks L.M. and Fiehn O. (2010) Divergent metabolome and proteome suggest functional independence of dual phloem transport systems in cucurbits. PNAS 107: 13532-13537

Zhu Y., Liu L., Shen L. and Yu H. (2016) NaKR1 regulates long-distance movement of Flowering Locus T in Arabidopsis. *Nature plants* 2: 1-10